THE
PROCEEDINGS
OF
THE PHYSICAL SOCIETY

Section B

VOL. 64, PART 10 — 1 October 1951 — No. 382 B

CONTENTS

Price to non-members 10*s*. net, by post 6*d*. extra. Annual subscription: £5 5*s*.
Composite subscription for both Sections A and B: £9 9*s*.

Published by
THE PHYSICAL SOCIETY
1 Lowther Gardens, Prince Consort Road, London S.W.7

PROCEEDINGS OF THE PHYSICAL SOCIETY

The *Proceedings* is now published monthly in two Sections.

Papers for publication in the *Proceedings* should be addressed to the Hon. Papers Secretary, Dr. H. H. Hopkins, at the Office of the Physical Society, 1 Lowther Gardens, Prince Consort Road, London S.W.7. Telephone : KENsington 0048, 0049.

Detailed Instructions to Authors were included in the February 1948 issue of the *Proceedings*; separate copies can be obtained from the Secretary-Editor.

PHYSICAL SOCIETY SPECIALIST GROUPS

OPTICAL GROUP

The Physical Society Optical Group exists to foster interest in and development of all branches of optical science. To this end, among other activities, it holds meetings about five times a year to discuss subjects covering all aspects of the theory and practice of optics, according to the papers offered.

COLOUR GROUP

The Physical Society Colour Group exists to provide an opportunity for the very varied types of workers engaged on colour problems to meet and to discuss the scientific and technical aspects of their work. Five or six meetings for lectures and discussions are normally held each year, and reprints of papers are circulated to members when available. A certain amount of committee work is undertaken, and reports on Defective Colour Vision (1946) and on Colour Terminology (1948) have already been published.

LOW TEMPERATURE GROUP

The Low Temperature Group was formed to provide an opportunity for the various groups of people concerned with low temperatures—physicists, chemists, engineers, etc.—to meet and become familiar with one another's problems. The group seeks to encourage investigations in the low temperature field and to assist in the correlation and publication of data.

ACOUSTICS GROUP

The Acoustics Group was formed to meet the long-felt need for a focus of acoustical studies in Great Britain. The scope includes the physiological, architectural, psychological and musical aspects of acoustics as well as the fundamental physical studies on intensity transmission and absorption of sound. The Group achieves its object by holding discussion meetings, by the circulation of reprints and by arranging symposia on selected acoustical topics.

Further information may be obtained from the Offices of the Society:
1 LOWTHER GARDENS, PRINCE CONSORT ROAD, LONDON S.W.7.

THE PROCEEDINGS OF
THE PHYSICAL SOCIETY

Section B

VOL. 64, PART 10 1 October 1951 No. 382 B

Some Phenomena of the Upper Atmosphere

BY SYDNEY CHAPMAN*
Queen's College, Oxford

Presidential Address, delivered 2nd May 1951; *MS. received* 21*st May* 1951

ABSTRACT. The height distribution of the atmosphere depends on the temperature and the mean molecular weight of the air; recent progress in our knowledge of these two quantities will be reviewed, the main sources of information being outlined. The motions (winds and tides) in the upper atmosphere will similarly be considered.

The main gross uncertainty regarding composition at high levels relates to the proportion of atomic nitrogen present. Besides the major constituents that chiefly determine the mean molecular weight, there are important rare constituents, such as ozone, sodium and hydroxyl, which reveal their presence by their absorption or emission spectra; and there are others whose presence can be inferred from theirs.

The composition of the atmosphere changes by escape from the top (hydrogen and helium) and, by addition, from below (e.g. helium and carbon dioxide) and, as shown by the auroral spectrum, from above (hydrogen); cosmic rays also both add to the atmosphere and produce changes of composition by nuclear reactions.

Near the magnetic equator there are important ionospheric phenomena not yet fully explored and explained. Among these one of the most interesting is the abnormal intensification of electric current flow, specially notable over Huancayo in Peru.

§ 1. INTRODUCTION

EVEN a slight acquaintance with the history of thought suggests that the human mind generally thinks too simply of matters on which it has little knowledge; the phrase *omne ignotum pro simplici* might often describe the position. This is well illustrated in the science of the atmosphere. After Torricelli had invented the barometer and Pascal had shown that the barometric pressure decreases with height according to the weight of the intervening air, even so great a man as Halley was ready to think that the atmosphere was substantially understood. In the eighteenth and nineteenth centuries balloonists found that in the free air, as well as on mountains, the air temperature decreases with height. The decrease was associated with the strong convection present in the air at low levels, being about half the adiabatic rate characteristic of thorough mixing. It was generally tacitly assumed that this decrease continued, so that the atmosphere would have a finite height.

* Professor Chapman was elected President for the period 1949–51, but owing to his absence in America during 1950–51 he was only able to hold this office for one year, and the Presidential Address had to be postponed.

But early this century Teisserenc de Bort * found by kite measurements that above about 10 km. in our latitudes the upward decrease of temperature ceases, and may be followed by a slight upward increase. The layers below and above this level of change of temperature gradient were called the troposphere and stratosphere, and the level itself was called the tropopause.

When de Bort's discovery gained general acceptance, opinion swung round to the conception of a static stratosphere, in which the temperature was controlled mainly by radiative processes, and remained constant at all greater heights. This conception led also to the inference that the gases of the atmosphere settled out by relative diffusion, so that the proportion of the heavier constituents decreased steadily upwards, and ultimately the lightest gases predominated. Calculations on this basis were made as to the height distribution of the pressure and density in the air, both as a whole and for each constituent separately; but by 1920 or so there were questioning voices, as regards the constancy of temperature, and also as to the diffusive separation.

There was indeed already ample evidence that in the atmosphere much goes on that is not comprised in so simple a philosophy.

§ 2. THE COMPLEXITY OF THE UPPER ATMOSPHERE

Even in the eighteen-eighties Balfour Stewart had inferred that somewhere high in the atmosphere the air is rendered electrically conducting by solar radiation, and that electrical currents flow there, which are induced by the dynamo action of the motion of the air across the earth's magnetic field—whose variations observed at the earth's surface formed the basis of these remarkable inferences.

Before the first World War Marconi's success in radio telegraphy over great distances led Heaviside and Kennelly to reach anew the conclusion that the upper atmosphere is ionized; and in the nineteen-twenties Appleton, and Breit and Tuve, by new methods of radio research, wonderfully confirmed these inferences, and added numerical substance to them. They and their successors have since contributed a wealth of complicated facts about the upper atmosphere, in the region named by Watson-Watt the ionosphere—facts gained by that most penetrating of all our present means of atmospheric exploration, the radio transmitter and receiver.

But Nature unaided also shows that the upper atmosphere is not simple. Meteors continually shoot into it and appear as transient falling stars; a few of them leave trails that endure for minutes, or even for an hour or more, in rare cases. These trails almost always become contorted as they fade, and thus indicate clearly the presence of non-uniform winds, at levels of 70 to 100 km. and more.

During the first World War the sound of gunfire in Flanders was heard here in London, and since then many experiments have been made with artificial explosions to investigate such abnormal propagation of sound to zones beyond the distance at which the sound usually ceases to be heard. It became clear that the abnormal sound came down from above, and indicated a downward deflection of waves originally travelling upwards. This implies the presence of a region, at a height estimated at about 40 km., in which sound travels more rapidly than in

* At the time of printing, Professor Chapman's papers had not arrived from America; it was therefore impossible to insert bibliographic references in the text in the normal manner. These references, however, are listed at the end of the article.

the air at ground level. One fantastic interpretation of this was that the air in this region consists of hydrogen; but the most complete quiescence in the stratosphere could not enable diffusion to render hydrogen predominant at that level.

The now accepted alternative explanation is that the air in the said region is hotter than near the ground. But it was on the basis of a theory of meteors and their luminosity that Lindemann and Dobson first definitely concluded that there is an upward increase of temperature above de Bort's isothermal layer.

For a higher level, at about 100 km., near the lower limit of aurorae, Vegard found evidence in the auroral band spectrum for a much lower temperature, of the same order as at the tropopause. For a time this seemed doubtfully compatible with the ideas of Lindemann and Dobson, but support for both views came during the nineteen-thirties from an unexpected source—the study of the daily variations of the barometer.

§3. ATMOSPHERIC TIDES AND THE TEMPERATURE DISTRIBUTION

Laplace, who first developed Newton's tidal theory in its application to the atmosphere, was also the first to seek to determine the lunar atmospheric tide from the barometric observations. After more than a century of effort in this direction, the distribution of the lunar air tide over the earth is now fairly well ascertained. Substantially it is in phase with the moon, that is, the air is heaped up twice daily, raising the barometric column, when the moon is on or near the meridian of observation or the opposite meridian. But the whole range of pressure thus produced is very small—only about a tenth of a millimetre of mercury—and, whereas the sea-tides are controlled by the moon and only modified by the sun, the moon makes only a minor contribution to the air tide. The chief daily barometric variation is solar semi-diurnal, with maxima at about 10 a.m. and 10 p.m., and minima at 4 a.m. and 4 p.m.; this variation has a range of about 2 mm. at the equator, about fifteen times as great as the lunar air tide.

The reason for this peculiar reversal of tidal predominance as between the sun and the moon, and the seas and the atmosphere, was first suggested by Kelvin in 1882, but it was not substantially established until half a century later. G. I. Taylor and C. L. Pekeris then confirmed Kelvin's idea by showing that the atmosphere can have more than one mode of free travelling wave of tidal type, and that one of these can reasonably be supposed to have a period of almost exactly 12 solar hours. If this is so, the solar tide—to which the sun's thermal action contributes about equally with its gravitational attraction—can be magnified about a hundred times by resonance, whereas the lunar tide, whose period is 25 minutes longer, will be much less magnified. Taylor's proof that more than one free mode of such oscillation can exist enabled this resonant property to be reconciled with the observed speed of propagation of the great waves of air pressure sent round the world—more than once—by the volcanic explosion of Krakatoa, and with that of the smaller waves set up by the great Siberian meteorite. This reconciliation was possible only if the atmosphere had a certain type of thermal structure, involving a temperature maximum in the stratosphere, and above it an upward decrease to another minimum.

Above the level of this minimum temperature the air is thought to become progressively hotter with increasing height, at least up to the F2 layer, where temperatures of the order 1,000° or 1,500° K. may exist. This view is based on several independent lines of radio evidence.

Thus the current conception of the temperature distribution is as shown i
Figure 1, in which the details are to be regarded as diagrammatic, not quantitative
as regards both height and temperature. A nomenclature appropriate to thi
distribution is also indicated (modifying slightly some suggestions of my own

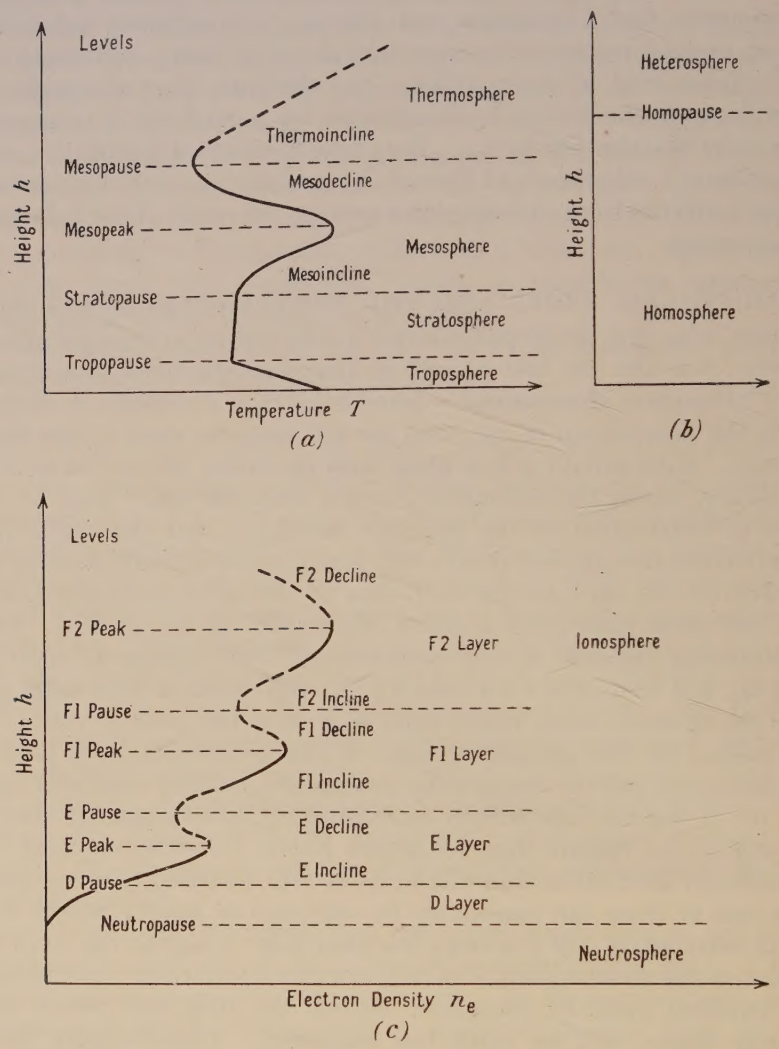

Figure 1. Atmospheric nomenclature in relation to (*a*) the temperature distribution, (*b*) t
composition (cf. § 6), and (*c*) the ionization or the electron density. *Pause* refers to the
of a layer or region, *peak* to the *level of maximum* of temperature or electron density, *incl*
to a region in which one or other of these quantities is *increasing* upwards, *decline* to a regi
of upward *decrease*. The nomenclature is provisional, and international agreement on t
or some modification of it is being discussed.

§ 4. THE SCALE HEIGHT

The height distribution of the air density and pressure is, by and larg
determined by the equation of static equilibrium $dp = -\rho g\, dh$, which connec
the decrement of pressure dp with the increment of height dh, and with t
density ρ and gravitational acceleration g. As $p = \boldsymbol{k}nT$, where $\boldsymbol{k}$ denot

Boltzmann's constant and n the number-density (or number of molecules per unit volume), and $\rho = n\bar{m}$, where $\bar{m}$ is the mean molecular mass,

$$\frac{dp}{p} = -\frac{\bar{m}g}{\boldsymbol{k}T}dh = -\frac{dh}{H},$$

if $H = \boldsymbol{k}T/\bar{m}g = \boldsymbol{R}T/\bar{M}g$, where $\boldsymbol{R}$ denotes the gas-constant $8{\cdot}3 \times 10^7$, and $\bar{M}$ the mean (chemical) molecular *weight*. Thus, if H were constant, the variation of pressure with height would be given by $p/p_0 = e^{-h/H}$, where p_0 is the value of p at zero height; actually H, now called the 'scale height', is not constant, because T and g vary with height; so also does $\bar{m}$ in certain ranges of height. The variation of g is known: $g/g_0 = a^2/(a+h)^2$, where g_0 denotes the ground value of g, and a the earth's radius; over the range of height now of interest in atmospheric physics, which is at least up to 300 km., the variation of g is not negligible; the reduction at 300 km. is 8·8%.

To calculate p and ρ as functions of height it is further necessary to know T and $\bar{m}$. Paneth has shown that at the ground $\bar{m}$ is constant all over the earth within very narrow limits, although in certain regions notable amounts of helium enter the atmosphere from the ground. The mixing action of the winds will maintain this uniformity of composition at least up to the tropopause. Throughout the troposphere, and indeed throughout most of the stratosphere, the process of diffusive separation is very slow.

§ 5. THE CHEMICAL COMPOSITION OF THE UPPER ATMOSPHERE

Not long before the second World War E. Regener and Paneth obtained samples of air, by means of balloons, from the layer from 20 to 25 km. height, in order to find whether there is any appreciable diffusive separation of the constituents in that region. Their results in different ways agreed in indicating a slight separation; Regener found a small reduction in the proportion of oxygen, one of the heavier constituents, and Paneth found a small but larger increase in the proportion of helium.

Since the war intense efforts have been made in the United States to extend the range of direct investigation of the upper atmosphere by means of rockets, partly German V2's and partly new American types. On account especially of the high speed of the rockets and the low air density, the problems of measurement and investigation are extremely difficult, but the difficulties are being attacked with great energy and skill. Among the chief government agencies concerned in this work are the U.S. Naval Research Laboratory, the U.S. Army Signal Corps, and the Air Force Geophysical Research Directorates. One of the many projects undertaken is the collection of air samples from great heights. The University of Michigan, under contract with the U.S. Army Signal Corps, has obtained many such samples. Some of them, taken at a height of rather more than 60 km., and analysed at the University of Durham by Prof. Paneth and his colleagues, have shown that the helium content of the air there is not appreciably different from that at the ground. This and other evidence obtained in the same analyses is in conflict with the pre-war results from the 20–25 km. levels, which at the time were accepted as reliable; the discrepancy has not been explained, and unless this can be done it seems to call for further investigation of balloon samples of air, which should now be obtainable from 40 km. or even higher. As regards the high-level conclusions, they have been challenged by some published results for the ratio of $^{14}N^{15}N$ nitrogen molecules to the main

$^{14}N^{14}N$ type, from the same samples; the determinations, made by mass spectrograph, gave a perceptible reduction of the proportion of the rarer isotope, as compared with the ratio at the ground. But further mass spectrograph determinations from the same samples do not confirm these published results (see Hagelbarger *et al.* 1951).

At present, therefore, the balance of evidence indicates that the mean molecular weight $\bar{M}$ of the air remains constant up to at least 60 or 65 km. Work is actively proceeding to obtain samples by rockets from still greater heights. New problems of sampling will arise at the levels, about 100 km. and above, where, there is good reason to believe, the oxygen is partly dissociated into atoms. These may oxidize the entry tube and containing vessel, and in any case the atomic oxygen cannot be brought down to the ground in atomic form. It may be advisable to place in the entry tube some substance that will absorb the atomic but not the molecular oxygen, so that they may be distinguishable and separately measurable when the vessel is recovered. Accurate values of the O_2/O ratio at different levels in the ionosphere would be of great interest to atmospheric and radio physicists.

§ 6. PHOTOCHEMICAL ACTION

Besides the opposing influences of mixing and diffusion, respectively tending to maintain and to alter the composition of the air, there is the important influence of the solar radiation absorbed at different heights, which also tends to modify the composition. One constituent whose presence is due to such photochemical action is ozone, which cuts off the solar spectrum at the ultra-violet end. The total amount is of the order 3 atmo-millimetres, that is to say, if all the ozone in any vertical column of air were collected at the bottom of the column, at normal temperature and pressure, its thickness would be about 3 mm. This ozone is distributed with a concentration which increases upwards from the ground up to about 35 km., above which the concentration decreases. Though ozone is a rather stable gas in the conditions of the free atmosphere, the chemical processes responsible for its formation and destruction are clearly more rapid than the mixing action of turbulence, which continually tries to blur out the gradients of concentration. Similarly in the ionosphere the ionized layers and the atomic oxygen region are able to maintain themselves against the tendency of both mixing and diffusion to modify their distribution.

I have lately suggested the name *turbosphere* for the region from the ground upwards in which mixing is more powerful than diffusion. The upper boundary of the turbosphere, which will of course be only roughly defined, may similarly be called the *turbopause*. Above this level the composition of the air, and consequently the value of $\bar{M}$, definitely changes; but owing to photochemical action (chiefly the dissociation of oxygen) $\bar{M}$ may change appreciably at levels below the turbopause. The level at which $\bar{M}$ ceases to be approximately constant may be called the *homopause*, the upper boundary of the *homosphere*, the region in which $\bar{M}$ can be treated as constant. The overlying region may be called the *heterosphere*. Heterospheric air is materially different from the homospheric air we know, and not only as regards small constituents like ozone, which, though of great interest and importance in many respects, are too rare to modify $\bar{M}$ appreciably. Theory is not yet able to assign levels to the turbopause and homopause, which must be determined by observation (directly or inferentially); so also must we rely on observation for the value of $\bar{M}$ for heterospheric air. If the

ratio of nitrogen to total oxygen by mass remains the same in the heterosphere as at the ground, complete dissociation of the oxygen would reduce $\overline{M}$ from 29·1 to 23·8.

Thus on account of $\overline{M}$ and g, the scale height H, which at the ground is about 8 km., may be increased at, say, 300 km. height by about one-third. The change of temperature with height, however, has much more influence upon H.

§ 7. THE MEASUREMENT OF TEMPERATURE AT HIGH LEVELS

It is very far from easy to measure the temperature in the upper air, even with instruments carried by balloons, on account of the low density of the air (and especially by day in the sunshine); but this can now be done, up to heights of over 40 km., by the new large neoprene balloons used by the U.S. Army Signal Corps. Above this level, measurements have been made by means of rockets, whose rapid motion and disturbing influence makes the determination of temperature from them a most difficult technical problem. Several different ways of doing it have been tried by our American colleagues; one of the most promising is by the measurement of the conical angle of the shock wave extending from the nose of the rocket, in conjunction with the Taylor–Maccoll theory of the wave. Another method uses grenades ejected from the rocket at successive heights. They explode in the free air, and the time of travel of the sound wave to the ground is measured. In this way the mean temperature of the air between the levels of successive explosions can be determined.

These and other methods used are in fairly early stages of development, and it is still uncertain whether the differences between their results are due to real differences in the air temperature distribution on different occasions, or to undiscovered errors affecting one or more of the methods. The results, which will not be given here, have been compared with the tentative 'standard' atmosphere specified a few years ago by the U.S. National Advisory Committee on Aeronautics (N.A.C.A.); the main conclusion is that between about 30 and 70 km. the direct observations indicate rather lower temperatures.

It would be highly advantageous if reliable methods were available to determine the air temperature distribution up to great heights by ground-based observations, such as radio physicists use to explore the ionosphere. One such method, already mentioned, namely the observation of anomalous sound propagation from explosions, has been much used in America in recent years, also in India and elsewhere. But its height range is limited, very great preparations are required, and the results are affected by high-level winds and are difficult to interpret unless the propagation is known to be very nearly symmetrical in all directions.

Another method of much promise, for places where the night sky is often cloudless and the air clear, is the observation of the light scattered from a powerful well focused modulated searchlight beam. This method is being actively developed at the Geophysical Institute of the University of Alaska; the preliminary results give the temperature up to about 60 km., though they must be critically examined and if possible checked by some independent method before final acceptance.

The temperature of the stratopause, somewhat below 100 km., has not yet been measured *in situ* with proven accuracy. Above that level radio measurements suggest values of the scale height and of the collision frequency which

imply that in the upper ionosphere the air is spread out in a manner corresponding to temperatures that increase to high values.

The bulge in the temperature graph for the stratosphere is reasonably attributed to absorption of solar radiation there by ozone; but the theory of the heat balance in the upper atmosphere is still rudimentary. D. R. Bates, in a paper recently presented to this Society, has studied the energy balance in the ionosphere; he finds it difficult to explain why the air there is as hot as it is generally supposed to be. He suggests that there may be an unsuspected supply in energy of ionization of some quickly recombining constituent, which does not contribute appreciably to the observed ionization (itself still in many respects not understood).

§8. WINDS AT HIGH LEVELS

I have referred to winds in the upper atmosphere, as shown by the deformation of meteor trails. Only rarely are these trails sufficiently extensively and reliably observed to give values of the wind at various points. The most remarkable case known to me is that of 23rd February 1909, for which J. E. Clark collected and discussed a large number of observations from both sides of the English Channel; it lasted for over two hours. The main difficulty in deriving wind results from such occurrences is their unexpectedness and the fewness of reliable and constant observers. D. R. Bates has suggested that it may be possible by means of rockets to lay a trail of sodium vapour in the upper atmosphere, which may be luminous and remain sufficiently long for the determination of the wind, giving, in fact, the equivalent of a long-enduring meteor trail at a predetermined place and time. It is hoped that this experiment will ere long be made in America. If successful, it should also throw important light on the photochemistry of the upper atmosphere.

However, wind determinations from meteor trails have been made by radar methods by Manning and his colleagues at Stanford University, though the method gives (by Doppler effect) only the line of sight component of the wind. In Australia, in this country and in America it has been found possible to determine ionospheric winds by the motion of irregularities in the ionosphere.

The lunar tidal currents in the various ionospheric layers have also been extensively studied, following the pioneer work of Appleton and Weekes. Both the vertical tidal motion and the associated changes of electron density have been considered, but the data do not lend themselves easily to the determination of the horizontal tidal motion.

§9. ATMOSPHERIC EMISSION SPECTRA

Recent years have seen great progress in the exploration and interpretation of the spectra of the airglow (formerly known as the light of the night or twilight sky) and the aurora. Besides the main lines and bands contributed by atomic oxygen and molecular nitrogen, there are others that reveal the presence of rare but interesting constituents such as atomic sodium, seen in the night airglow (and enhanced at twilight, apparently by ultra-violet excitation); its continued luminosity throughout the night is still not yet definitely explained. Last year saw a very important addition to our knowledge of these rare constituents, when Meinel of the Yerkes Observatory showed, with the aid of Herzberg, that the infra-red radiation near 10,400 A. (which is of exceptionally high intensity, and was formerly supposed by some writers to be due to atomic nitrogen), is emitted

by hydroxyl, OH. An important study of the reactions associated with the OH molecules in the upper atmosphere has been made by D. R. Bates and M. Nicolet, who have estimated the amount and distribution of this gas and of the associated gases H, H_2, and H_2O at high levels.

The degree of dissociation of nitrogen in the ionosphere is at present a controversial question; my own opinion continues to be that there is very little atomic nitrogen at least up to and including the F2 peak. This opinion is based on the observation of the band spectrum of the nitrogen molecule in sunlit aurorae up to much higher levels, 800 or even 1,000 km.

§ 10. THE ENTRY OF SOLAR HYDROGEN INTO THE ATMOSPHERE

The past year has brought another spectral discovery of intense interest, also by Meinel, though foreshadowed by Gartlein and Vegard. This is the observation of highly Doppler-displaced lines of atomic hydrogen in the auroral spectrum, when looking nearly along the auroral rays. The maximum displacements are to the ultra-violet, and indicate the downward passage of hydrogen atoms with speeds exceeding 3,000 km/sec. This affords the most direct proof yet available for the corpuscular theory of magnetic storms and aurorae, for which the previous evidence, though strong, was indirect. There is still much obscurity as to auroral theory, but it seems probable that the hydrogen atoms thus observed to enter the atmosphere travelled from the sun with a decidedly lower speed, 1,000 or 1,500 km/sec., and in the form of stripped atoms, namely protons, in company with equal numbers of electrons and smaller numbers of atoms and ions of the minor constituents of the solar atmosphere (as first proposed in this connection by the present Lord Cherwell). Near the earth the protons are in some way accelerated and guided along the earth's lines of force to enter the atmosphere in auroral latitudes. In their passage through the air the protons ionize and dissociate and excite the air molecules and atoms, and occasionally themselves capture an electron, which completes the hydrogen atom, and enables it to make its presence and motion known by its radiation and Doppler effect. This discovery certainly opens an exciting and very important new chapter in auroral research.

§ 11. NUCLEAR CHEMISTRY AND THE ATMOSPHERE

Another new phase of atmospheric physics now being developed is the influence of cosmic rays on the atmosphere. The ionization they produce is unimportant compared with that due to solar radiation, but the rays cause nuclear reactions and changes of isotopic ratio in the atmospheric gases which are of great interest.

A somewhat analogous topic is the addition of gases to the atmosphere from the ground, particularly the products of radioactive decay. Tatel has recently estimated the age of the atmosphere on the basis of the abundance of the radioactive potassium isotope ^{40}K in the earth, and the amount in the atmosphere of the decay product ^{40}A, an isotope of argon.

§ 12. IONOSPHERIC VARIATIONS

Turning again to higher levels, radio exploration has shown that the ionosphere has a normal régime of daily varying ionization in layers ionized mainly by solar radiation. But occasionally this régime is disturbed, perhaps only for an hour or so, as in radio fadeouts, or for a day or a few days, as in the much more intense

disturbances known as ionospheric storms. In extreme storms the F layer rapidly rises and seems to disappear into outer space, whereafter a new F layer may be re-created at the normal level within an hour or two. If this simple interpretation of the radio records is correct, there may be loss of air to free space outside the earth at a rate which, though operating only for short times at long intervals, may be more important than the continual slow leakage of fast-moving atoms and molecules usually alone considered in the theory of escape of planetary atmospheres. The latter, however, suffices to explain the absence of a hydrogen layer at great heights, and also the loss of most of the helium that has entered the atmosphere from radioactive transformations within the earth's crust during its long history.

§ 13. ELECTRIC CURRENTS: THE AURORAL ELECTROJET

I do not possess the knowledge required to give even an outline of the course of an ionospheric storm; instead I will devote my remaining minutes to some remarks on the electric currents that flow in the ionosphere as revealed by the geomagnetic variations at the earth's surface.

Figure 2. Atmospheric electric current systems responsible for the daily magnetic variations: for the equinoxes (*a*) and for the June solstice (*b*). In each case the left-hand diagram shows the current system as viewed from the sun, and therefore flowing over the sunlit hemisphere; and the right hand diagram shows the current flow over the night hemisphere. The earth is shown with the north pole uppermost. The lines shown are lines of current flow, and between adjacent lines the flow is 10,000 amperes.

There is a regular régime for these currents, as shown by the regular daily magnetic variations, in which both the sun and moon play a part. The magnetic data clearly indicate the form and intensity, but not the height, of the current-sheet. Figure 2 shows the system of currents associated with the solar daily magnetic variation, as viewed from the sun or, for the night hemisphere, from an imaginary anti-sun. At times of magnetic and ionospheric storms, however, the normal régime is disturbed by the addition of a much more intense system of currents very differently distributed over the earth, as shown in Figure 3, as seen from the sun and from above the north pole. This system differs from that of Figure 2, (i) in being as intense over the night as over the day hemisphere, (ii) in being most intense in the polar regions instead of over the middle belt of the earth, and (iii) in being exceptionally concentrated along the line of the auroral zone. By analogy with the jet streams discovered in the upper atmosphere by meteorologists in recent years, I suggest that such a concentration of electric current be called an *electrojet*.

§ 14. THE EQUATORIAL ELECTROJET

But this auroral electrojet is no longer the only one known. The regular régime on quiet days also includes an electrojet, though it is not shown on Figure 2, which is based on an analysis of magnetic data made in 1918. Four

years later the Department of Terrestrial Magnetism of the Carnegie Institution of Washington founded a new magnetic observatory at Huancayo in Peru, on the magnetic equator, which is there 12° south of the geographical equator. It soon appeared that at this station the daily variation of horizontal force H was abnormally great, with a range of the order 100γ instead of 30 or 40γ as elsewhere near the equator. In 1948 the International Association for Terrestrial Magnetism and Electricity appointed a Committee to investigate over what range of latitude this abnormality extended. The daily variation of H has now been measured at several low latitudes along meridians in Africa, India and America. The most extensive set of observations is due to Dr. A. A. Giesecke, Director of the Huancayo Observatory. His results show that the abnormality covers a range

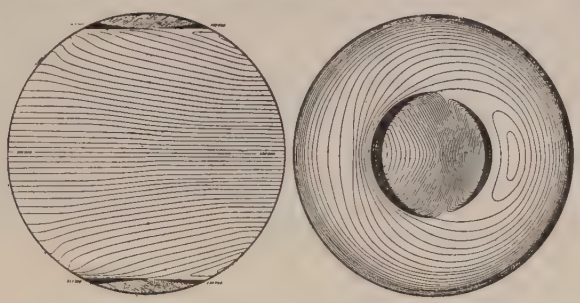

Figure 3. The atmospheric current system that could produce the surface magnetic field during a magnetic storm. As in Figure 2, the lines are lines of current flow spaced at 10,000 amperes apart. The left-hand diagram shows the system as viewed from the sun; the flow over the night hemisphere is similar. The right-hand diagram shows the system as viewed from above the north pole. The part of the system consisting of the auroral electrojets and the flow over the polar caps within the auroral zones is really situated in the atmosphere, the part between the zones may correspond to currents not actually flowing in the atmosphere.

of only about 10° of latitude. It is not difficult to infer from this that the abnormality at Huancayo—paralleled also elsewhere on or near the magnetic equator—is due to an equatorial electrojet, which grows in intensity from dawn to about 11 a.m. local time, and then decreases again. This is superposed on the normal current flow already illustrated. The electrojet must have a return flow, probably both to the north and south, and it will also induce currents in the earth. The field observed at the earth's surface includes the effects of all these currents, and is certain to be much more spread out than the electrojet itself, which probably has a width of only about 2° or 3°, like the auroral electrojet. It must also cause abnormalities in the daily variations of the vertical force and declination at stations to the north and south of those that show the abnormality in H, and the study of these further irregularities will enable us to determine the height and intensity of the electrojet. It seems to me that both Bombay and Manila show this abnormality in vertical force. The Magnetic Association meets again this year, and it is to be expected that plans for further work on this interesting phenomenon of the upper atmosphere will be made.

§ 15. CONCLUSION

In conclusion, I hope I have shown by this discursive survey of many phenomena, ranging widely both in time and subject, that the field of upper atmospheric physics is one that rests on many techniques of observation, touches many branches of physics, chemistry and mathematics, and is in the full tide of active progress.

REFERENCES

General References

Detailed bibliographies on topics included in the above Address may be found in the following :

American Meteorological Society, *Compendium of Meteorology*, in the press.

Bates, D. R., 1949, *Mon. Not. R. Astr. Soc.*, **109**, 215.

Chapman, S., and Bartels, J., 1940, *Geomagnetism* (Oxford : University Press).

Gassiot Committee, 1943, *Rep. Prog. Phys.*, **9**, 1 (London : Physical Society); 1948, *The Emission Spectra of the Night Sky and Aurora* (London : Physical Society).

Joint Discussion of the Chemical, Physical and Royal Meterorological Societies, 1937, *Quart. J.R. Met. Soc.*, **63**.

Mitra, S. K., 1948, *The Upper Atmosphere* (Calcutta : Royal Asiatic Society of Bengal).

Recent Papers

Bates, D. R., 1950, *J. Geophys. Res.*, **55**, 345.

Bates, D. R., and Nicolet, M., 1950, *J. Geophys. Res.*, **55**, 301.

Chackett, K. A., Paneth, F. A., and Wilson, E. J., 1950, *J. Atmos. Terr. Phys.*, **1**, 49.

Chapman, S., 1950, *J. Geophys. Res.*, **55**, 395; 1951, *Arch. Met. Geophys. Bioklim.*, in the press.

Gartlein, C. W., 1948, *Int. Assoc. Terr. Mag. Elec.* (*Oslo*), Document T124; 1948, *Phys. Rev.*, **74**, 1208; 1950, *Trans. Amer. Geophys. Un.*, **31**, 18; 1951 *Phys. Rev.*, **81**, 463.

Giesecke, A. A., 1951, *J. Geophys. Res.*, in the press.

Hagelbarger, D. W., Loh, L. T., Neill, H. W., Nichols, M. H., and Wenzel, E. A., 1951, *Phys. Rev.*, **82**, 107.

Havens, R., Koll, R., and Lagow, H., 1950, *Pressures and Temperatures in the Earth's Upper Atmosphere*, Naval Research Laboratory Report, March 1950 ; 1951, *J. Geophys. Res.*, in the press.

Manning, L. A., Villard, O. G., Jr., and Peterson, A. M., 1950, *Proc. Inst. Radio Engrs., N.Y.*, **38**, 977.

McQueen, J. H., 1950, *Phys. Rev.*, **80**, 100.

Meinel, A. B., 1951, *Astrophys. J.*, **113**, 50.

Tatel, H. E., 1950, *J. Geophys. Res.*, **55**, 329.

A General Formula for the Conductivity of a Gas containing Free Electrons

By L. G. H. HUXLEY

Department of Physics, University of Adelaide

Communicated by Willis Jackson; *MS. received* 30*th January* 1951, *and in amended form* 23*rd April* 1951

ABSTRACT. This paper contains a general discussion of electron drift in gases according to the method of free paths in which a fallacy contained in some earlier treatments is avoided. A general formula is derived for drift velocity in an electric field which is an arbitrary function of the time, and from it formulae for drift velocities in the following special cases of importance are deduced : drift in a constant electric field, in an alternating sinusoidal field, in a constant electric field with an applied magnetic field, in an alternating electric field with an applied magnetic field. Formulae for the electrical conductivity of an electron-laden gas follow from those for the drift velocities. Applications of the formulae to ionospheric and other studies are mentioned.

§ 1. INTRODUCTION

In this paper a general formula is derived for the drift velocity of the centroid of a group of electrons moving through a gas in a uniform electric field which is an arbitrary function of the time. In order to extend the generality and usefulness of the treatment it is supposed that a constant and uniform magnetic field is also present.

The current density and conductivity of the gas are then obtained immediately from the drift velocity.

Special cases of the general formula possess a wide range of application, as for instance in the theory of the electrical conductivity of metals and semiconductors, of the conductivity and permittivity of an electron-laden gas, of the propagation of electromagnetic waves in an ionized atmosphere and of the Hall effect. The general formula, and the special cases implicit in it, are derived by a correct application of the method of free paths which avoids an error which is often made in the derivation of formulae for drift velocities by this method.

§ 2. NOMENCLATURE AND SUMMARY OF FORMULAE

It is convenient in this section to define the chief symbols employed throughout the paper and to give a summary of some of the formulae to be derived in later sections.

2.1. *List of Chief Symbols*

A bar above a symbol or expression denotes its mean value taken with respect to the agitational speeds U. $\mathbf{W}$ = drift velocity, $\mathbf{i}_1, \mathbf{i}_2, \mathbf{i}_3$ = coordinate unit vectors, $\mathbf{U} = U\mathbf{u}$ = agitation velocity of an electron, l = mean free path of an electron (supposed to be independent of U), $\rho = e/m$ = the specific charge of an electron (e is treated in formulae as a positive quantity, that is to say the value $e = -4{\cdot}8 \times 10^{-10}$ E.S.U. would be used in substitution). $\mathbf{B}_0$ = a uniform and constant magnetic field, $\omega = -\gamma\rho B_0$ (γ is a constant determined by the system of electric units employed. Its value in the chief three systems is given in the table in the Appendix; since ρ is negative, ω is positive for electrons), $\boldsymbol{\Omega} = -\gamma\rho\mathbf{B}_0$ (the gyro-angular velocity, $|\Omega| = \omega$), p = an angular velocity of an alternating electric field, $\nu = U/l$ = collisional frequency at speed U, $\bar{\nu} = \overline{U}/l$, t = time measured from the instant of application of the electric field $\mathbf{E}(t)$.

Other symbols are introduced in the course of the discussion.

2.2. *Formulae for Drift Velocities*

It will be shown later that the velocity of drift of the centroid of a group of a large number of electrons in an electric field $\mathbf{E}(t) = \mathbf{i}_1 X(t) + \mathbf{i}_2 Y(t) + \mathbf{i}_3 Z(t)$ which as an arbitrary function of the time is expressible in the form

$$\mathbf{W} = \frac{d}{dt}\overline{[\mathbf{S}_1 + \mathbf{S}_2 + \mathbf{S}_3 + \mathbf{S}_4]}, \qquad \ldots\ldots(1)$$

in which the quantities $\mathbf{S}_k$ ($k = 1, 2, 3$, or 4) are displacements which are defined in the sequel. It proves to be the case that the displacements $\mathbf{S}_3$ and $\mathbf{S}_4$ contribute only terms that are evanescent with increasing t and that the persisting terms in $\mathbf{W}$ are derived from $\mathbf{S}_1$ or $\mathbf{S}_2$ or both. We are therefore usually chiefly concerned with $\mathbf{S}_1$ and $\mathbf{S}_2$ and it is convenient to state the formulae for them only.

Let the electric field be $\mathbf{E}(t) = \mathbf{i}_1 X(t) + \mathbf{i}_2 Y(t) + \mathbf{i}_3 Z(t)$ and let the applied magnetic field be $\mathbf{B}_0 = \mathbf{i}_3 B_0$, that is to say its direction is that of the Oz coordinate axis.

Let the components of $\mathbf{E}(t)$ normal to $\mathbf{B}_0$ be combined into a complex quantity $E_N(t)=X(t)+jY(t)$, then as will be shown, the components of the displacements $\mathbf{S}_1$ and $\mathbf{S}_2$ are to be obtained from the following formulae:

$$S_{1x}+jS_{1y}=\rho\nu\int_0^t \exp(-\nu\eta)\left\{\int_0^\eta\left[\int_0^{\eta-g} E_N(t-g-h)\exp(j\omega h)\,dh\right]dg\right\}d\eta \qquad \ldots\ldots(2)$$

$$S_{1z}=\rho\nu\int_0^t \exp(-\nu\eta)\left\{\int_0^\eta\left[\int_0^{\eta-g} Z(t-g-h)\,dh\right]dg\right\}d\eta \qquad \ldots\ldots(3)$$

$$S_{2x}+jS_{2y}=\rho\nu^2\int_0^t \exp(-\nu\eta)\left[\int_0^{t-\eta}\left\{\int_0^\eta\left(1-\frac{\exp j\omega g}{3}\right)\left[\int_0^{\eta-g} E_N(\tau+\eta-g-h)\times\exp(j\omega h)\,dh\right]dg\right\}d\tau\right]d\eta \qquad \ldots\ldots(4)$$

$$S_{2z}=\tfrac{2}{3}\rho\nu^2\int_0^t \exp(-\nu\eta)\left[\int_0^{t-\eta}\left\{\int_0^\eta\left[\int_0^{\eta-g} Z(\tau+\eta-g-h)\,dh\right]dg\right\}d\tau\right]d\eta \qquad \ldots\ldots(5)$$

In these formulae the symbols ρ, ν, ω, t, E_N and Z have the meanings given to them in §§2.1 and 2.2, whereas h, g, τ and η are dummy variables.

It is to be noticed that, according to equations (3) and (5) the components of $\mathbf{W}$ parallel to $\mathbf{B}_0$ are independent of $\mathbf{B}_0$ since ω does not appear in these formulae, and that (3) and (5) are special cases of (2) and (4) with $\omega=0$.

It is important to note that in deriving these formulae it is assumed that the mean speed of agitation $\overline{U}$ of the electrons and the distribution of the speeds U do not change appreciably during the interval t. Thus the formulae are applicable to the following situations: drift in a field such that the ratio (field strength/gas pressure) is small so that the electrons effectively retain their thermal agitation energies; drift in a steady field $\mathbf{E}(t)=$ constant after a time t such that the mean agitational energy $\frac{1}{2}m\overline{U^2}$ of the electrons is constant; drift under an alternating field whose frequency $p/2\pi$ is sufficiently great in comparison with the time constant of decay of the energy $\frac{1}{2}m\overline{U^2}$ (when the field is removed) that the fluctuation of $\frac{1}{2}m\overline{U^2}$ about its mean value during a cycle of the alternating field is relatively negligible.

Because the general formulation is of less immediate practical use than some of the special cases that are implicit in it, we proceed to give in summary the formulae for the drift velocities $\mathbf{W}$ in some of these special cases which have a practical interest.

2.3. *Summary of Particular Instances of Electron Drift*

The following special formulae are derived from equations (1) to (5).

(*a*) *Drift in a uniform and constant electric field* $\mathbf{E}(t)=$ *constant* $=\mathbf{E}$ *with no applied magnetic field* $\mathbf{B}_0$.

If in the general equations we put $\mathbf{E}(t)=$ constant, $\omega=0$, it will be seen that the terms that are not evanescent as t increases give (see the end of sub-section 3.2),

$$\mathbf{W}=\tfrac{2}{3}\mathbf{E}\rho l(\overline{U^{-1}}), \qquad \ldots\ldots(6)$$

a well-known formula (Lorentz 1916, Becker 1933, Townsend 1936).

The formula, more often than not, is given incorrectly in the literature, with the factor 2/3 replaced by unity. The factor $(\overline{U^{-1}})$ is the mean of the reciprocals of the speeds U.

If the number of electrons per unit volume is n, the current density $\mathbf{J}$ and electrical conductivity are given by $\mathbf{J}=\sigma\mathbf{E}=\frac{2}{3}(ne^2/m)l(\overline{U^{-1}})\mathbf{E}$.

(*b*) *Drift in a uniform sinusoidal electric field with* $B_0=0$ (Huxley 1937 b)

Put $\omega=0$, $X=E_0\cos pt$, $Y=E_0\sin pt$, whence $E_N=E_0\exp(jpt)$. Then

$$W=W_x+jW_y$$

$$=\frac{2}{3}\rho E_0\left[\overline{\frac{\nu}{\nu^2+p^2}\left\{1+\frac{p^2}{\nu^2+p^2}\right\}}-j\,\overline{\frac{p}{\nu^2+p^2}\left\{\frac{1}{2}+\frac{p^2}{\nu^2+p^2}\right\}}\right]\exp(jpt)$$

$$=\frac{2}{3}\frac{\rho E_0}{p}[\overline{\phi(x)}-j\overline{\psi(x)}]\exp(jpt), \qquad \ldots\ldots(7)$$

where $x=\nu/p$ and

$$\phi(x)=\frac{x}{1+x^2}\left[1+\frac{1}{1+x^2}\right];\quad \psi(x)=\frac{1}{1+x^2}\left[\frac{1}{2}+\frac{1}{1+x^2}\right]. \qquad \ldots\ldots(8)$$

It follows that
$$W_x=\frac{2}{3}\frac{\rho E_0}{p}[\overline{\phi(x)}\cos pt+\overline{\psi(x)}\sin pt]. \qquad \ldots\ldots(9)$$

When $\bar{\nu}\gg p$, $x\gg 1$, $\overline{\phi(x)}\to\overline{(1/x)}=p/\nu=pl(\overline{U^{-1}})$, $\overline{\psi(x)}\to 0$, and the formula for W_x agrees with formula (6) as it should. When $\bar{\nu}\ll p$, $x\ll 1$, $\overline{\phi(x)}\to 0$, $\overline{\psi(x)}\to 3/2$,

$$W_x\to(\rho E_0/p)\sin pt, \qquad \ldots\ldots(10)$$

a formula which is derived immediately from the equation of motion of a free electron and the condition $(\overline{\mathbf{U}})=0$.

(*c*) *Drift in a uniform and constant electric field* $\mathbf{E}$ *with an applied magnetic field* $\mathbf{B}_0$ (Huxley 1937 a, Townsend 1937, 1947).

Put $\mathbf{B}_0=\mathbf{i}_3B_0$, $\omega=-\rho B_0$, $E_N=X+jY=$ constant. Then the general formulae give

$$W_x+jW_y=\tfrac{2}{3}\rho\frac{E_N}{\omega}[\overline{\phi(y)}+j\overline{\psi(y)}], \qquad \ldots\ldots(11)$$

in which $y=\nu/\omega$ and $\phi(y)$ and $\psi(y)$ are the same as the functions that appear in equation (7) but with x replaced by y. It is evident from the general equations that W_z is obtained from equation (6) with $|E|$ replaced by Z.

The formulae for W_x, W_y and W_z are therefore

$$\left.\begin{aligned}W_x&=\tfrac{2}{3}(\rho/\omega)[X\overline{\phi(y)}-Y\overline{\psi(y)}]\\ W_y&=\tfrac{2}{3}(\rho/\omega)[X\overline{\psi(y)}+Y\overline{\phi(y)}]\\ W_z&=\tfrac{2}{3}\rho Zl(\overline{U^{-1}})\end{aligned}\right\} \qquad \ldots\ldots(12)$$

(*d*) *Drift in a rotating electric field with an applied magnetic field normal to the electric field.*

Let $\mathbf{B}_0=\mathbf{i}_3B_0$, $\mathbf{E}=\mathbf{i}_1X+\mathbf{i}_2Y$, $X=E_0\cos pt$, $Y=E_0\sin pt$, $E_N=E_0\exp(jpt)$. With these postulates, the general formulae give

$$W_x+jW_y=\tfrac{2}{3}\rho E_0\left[\frac{1}{\nu-j(\omega-p)}\left\{1-\frac{j(\omega-p)}{\nu-j(\omega-p)}\right\}\right]\exp(jpt). \qquad \ldots\ldots(13)$$

That is to say

$$W_x+jW_y=\tfrac{2}{3}\rho E_0\left[\frac{\nu}{\nu^2+(\omega-p)^2}\left\{1+\frac{(\omega-p)^2}{\nu^2+(\omega-p)^2}\right\}\right.$$
$$\left.+j\frac{(\omega-p)}{\nu^2+(\omega-p)^2}\left\{\frac{1}{2}+\frac{(\omega-p)^2}{\nu^2+(\omega-p)^2}\right\}\right]\exp(jpt). \qquad \ldots\ldots(14)$$

It is convenient to introduce the symbols

$$\left.\begin{aligned} F[(\omega-p),\nu] &\equiv \frac{\nu}{\nu^2+(\omega-p)^2}\left\{1+\frac{(\omega-p)^2}{\nu^2+(\omega-p)^2}\right\} \\ f[(\omega-p),\nu] &\equiv \frac{(\omega-p)}{\nu^2+(\omega-p)^2}\left\{\frac{1}{2}+\frac{(\omega-p)^2}{\nu^2+(\omega-p)^2}\right\} \end{aligned}\right\} \quad \ldots\ldots(15)$$

then $$W_x+jW_y=\tfrac{2}{3}\rho E_0\{F[(\omega-p),\nu]+jf[(\omega-p),\nu]\}\exp(jpt). \quad \ldots\ldots(16)$$

If instead of an electric field $E_X=E_0\exp(jpt)$ which rotates about $\mathbf{B}_0$ in a positive sense, we consider the oppositely rotating field $E_X=E_0\exp(-jpt)$, then it is necessary only to replace p by $-p$ in (14), (15) and (16) in order to find (W_x+jW_y); that is to say, in this field,

$$W_x+jW_y=\tfrac{2}{3}\rho E_0\{F[(\omega+p),\nu]+jf[(\omega+p),\nu]\}\exp(-jpt). \quad \ldots\ldots(17)$$

(*e*) *Drift in a uniform sinusoidal electric field with a magnetic field* $\mathbf{B}_0$ (Huxley 1937 b (incomplete treatment), 1940).

$\mathbf{B}_0=\mathbf{i}_3B_0$, $\mathbf{E}=\mathbf{i}_1X$, $X=E_0\cos pt$, $Z=Z_0\cos(pt+\beta)$. The field X can be resolved into a pair of oppositely rotating fields as follows:

$$E=(E_0/2)[\exp(jpt)+\exp(-jpt)],$$

whence, from (16) and (17)

$$\begin{aligned} W_x+jW_y=\tfrac{2}{3}\rho\tfrac{1}{2}E_0[&\{F[(\omega-p),\nu]+jf[(\omega-p),\nu]\}\exp(jpt) \\ &+\{F[(\omega+p),\nu]+jf[(\omega+p),\nu]\}\exp(-jpt)]. \quad \ldots\ldots(18) \end{aligned}$$

In order to obtain compact expressions for W_x, W_y and W_z we further extend the symbolism as follows:

$$\left.\begin{aligned} S[\omega,p,\nu] &\equiv F[(\omega+p),\nu]+F[(\omega-p),\nu] \\ s[\omega,p,\nu] &\equiv f[(\omega+p),\nu]+f[(\omega-p),\nu] \\ D[\omega,p,\nu] &\equiv F[(\omega+p),\nu]-F[(\omega-p),\nu] \\ d[\omega,p,\nu] &\equiv f[(\omega+p),\nu]-f[(\omega-p),\nu]. \end{aligned}\right\} \quad \ldots\ldots(19)$$

It follows from (18) and (7) that

$$\left.\begin{aligned} W_x &= \tfrac{1}{3}\rho E_0[S\cos pt+d\sin pt] \\ W_y &= \tfrac{1}{3}\rho E_0[s\cos pt-D\sin pt] \\ W_z &= \tfrac{2}{3}\rho Z_0[F(p,\nu)\cos(pt+\beta)+f(p,\nu)\sin(pt+\beta)]. \end{aligned}\right\} \quad \ldots\ldots(20)$$

In the more general case in which $X=X_0\cos pt$, $Y=Y_0\cos(pt+\alpha)$, $Z=Z_0\cos(pt+\beta)$ and are represented in the notation of complex quantities as $X=X_0\exp(jpt)$, $Y=Y_0\exp(jpt+\alpha)$, $Z=Z_0\exp(jpt+\beta)$, then

$$\left.\begin{aligned} W_x &= \tfrac{1}{3}\rho\{[S-jd]X-[s+jD]Y\} \\ W_y &= \tfrac{1}{3}\rho\{[s+jD]X+[S-jd]Y\} \\ W_z &= \tfrac{2}{3}\rho Z\{F(p,\nu)-jf(p,\nu)\} \end{aligned}\right\} \quad \ldots\ldots(21)$$

the real parts of W_x, W_y and W_z being the physical components of the drift velocity.

The matrix of the complex conductivity of the gas is

$$\|\sigma\|=\begin{Vmatrix} \sigma_{xx} & \sigma_{xy} & 0 \\ \sigma_{yx} & \sigma_{yy} & 0 \\ 0 & 0 & \sigma_{zz} \end{Vmatrix} \quad \ldots\ldots(22)$$

in which

$$\left.\begin{aligned}\sigma_{xx}&=(ne^2/3m)(S-jd)=\sigma_{yy}\\ \sigma_{yx}&=-\sigma_{xy}=(ne^2/3m)(s+jD)\\ \sigma_{zz}&=(2ne^2/3m)[F(p,\nu)-jf(p,\nu)].\end{aligned}\right\} \quad \ldots\ldots\ldots(23)$$

The current density is

$$\begin{Bmatrix} J_x \\ J_y \\ J_z \end{Bmatrix} = \|\sigma\| \begin{Bmatrix} X \\ Y \\ Z \end{Bmatrix}. \quad \ldots\ldots(24)$$

It remains to deduce the general formulae (1) to (5) of sub-section 2.2.

§ 3. THE METHOD OF FREE PATHS AND THE THEORY OF DRIFT VELOCITY OF ELECTRONS

3.1. *General Assumptions*

In the more rigorous discussions of the motions of free electrons among molecules of a gas it is best to suppose that electrons and molecules interact as point centres of force. The forces are supposed to be of relatively short range so that for the greater portion of its life an electron moves in rectilinear motion, except when it approaches a molecule which deflects it through some angle whose magnitude is determined by the precise circumstances of the encounter. Formulae for the diffusion coefficient and drift velocity of electrons based on this picture of electron motion, although theoretically satisfying, suffer in practice from analytical complexity and an element of uncertainty concerning the precise laws of force that operate between electrons and molecules of various gases.

In the method of free paths a simplified situation is envisaged in which the electrons move among the molecules in random agitational motion along paths which comprise a succession of straight segments (when the magnetic field $\mathbf{B}_0$ is absent) with discontinuous changes of direction between adjacent segments. The lengths of the straight segments or free paths are distributed at random according to the law that the proportion of a large number of free paths that exceeds s in length is $\exp(-s/l)$, where l is the mean free path.

The directions of the free paths are supposed to be distributed at random in space, that is, the agitational velocities of the electrons are distributed at random with respect to direction. The mathematical expression of the assumption of chaotic agitational motion is the following:

Let the velocity of agitation of an electron at any instant be

$$U=\mathbf{i}_1U_x+\mathbf{i}_2U_y+\mathbf{i}_3U_z,$$

then

$$\left.\begin{aligned}\overline{U_x^2}=\overline{U_y^2}=\overline{U_z^2}&=\overline{U^2}/3\\ \overline{U_xU_y}=\overline{U_xU_z}=\overline{U_yU_z}&=0\\ \overline{U_x}=\overline{U_y}=\overline{U_z}&=0,\end{aligned}\right\} \quad \ldots\ldots(25)$$

where the average is taken over any large number of free paths described at speed U.

Thus electrons and molecules are regarded as particles with dimensions negligible in comparison with the mean free path. They collide as rigid bodies bounded by fixed geometrical surfaces.

In order to preserve the chaotic character of the agitational motion it is not necessary to postulate any particular shape for the molecules. They may be regarded as spheres, regular or irregular polyhedra or as bounded by smooth

surfaces of arbitrary form. Provided the axes of inertia of the irregular bodies are directed at random the chaotic agitational motion of the electrons will be preserved. It is obvious that this indifference of the method of free paths to the form of the molecules renders it impossible for the method to provide information about the mean energy lost by an electron in collisions with molecules. The method however when used to interpret the results of experiments on the diffusion and drift of electrons permits this quantity to be assessed.

If the mean cross section presented by a molecule to an electron is A and if n is the number of molecules per unit volume, then the mean free path is $l=1/nA$. It is often convenient to consider the molecules to be spheres of radius $a=(A/\pi)^{1/2}$.

According to the method of free paths the mechanism of electron drift through a gas under an applied electric field $\mathbf{E}$ is the following: Since the field $\mathbf{E}$ exerts a force $\mathbf{E}e$ on each electron the free paths are, in general, no longer straight because each electron receives a small displacement in the course of a free path. The vector sum of such displacements for all the electrons of a group taken over many free paths is not zero, but is in general a function of the time. The centroid of the group is therefore displaced in time, and the time rate of change of the vector joining centroid and some fixed point is the required drift velocity. Thus the procedure for finding the drift velocity $\mathbf{W}$ requires an accurate vector summation of the elementary vector displacements caused by the field $\mathbf{E}$ in the course of the free paths.

3.2. *Derivation of Formulae for Drift Velocities—General Method*

It is convenient first to suppose the magnetic field $\mathbf{B}_0$ to be absent. In the absence of an applied electric or magnetic field the path of an electron between successive collisions with molecules is a straight line traversed at constant speed U. In a time of flight η the distance travelled is $s=\eta U$. When the electron moves in an electric field $\mathbf{E}$ its path in general is curved and in a time of free flight η, not terminated in a collision, the distance traversed is different from $s=\eta U$. Thus, in the

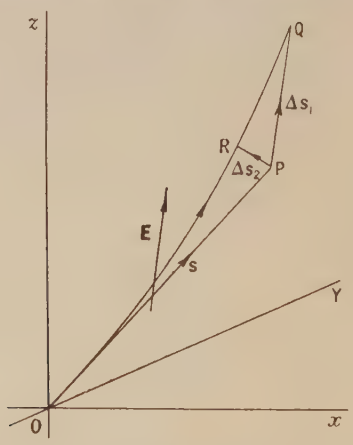

Figure, $\mathrm{OP}=\mathbf{s}$ represents the vector displacement $\mathbf{s}=\eta\mathbf{U}$ when $\mathbf{E}$ the applied field is zero. When $\mathbf{E}$ is not zero the path is curved and in time η the electron reaches the point Q. Thus the additional displacement effected by the field $\mathbf{E}$ in time η is $\Delta\mathbf{s}_1$. It is easy to obtain a general expression for $\Delta\mathbf{s}_1$ when the electric field is an arbitrary function $\mathbf{E}(t)$ of the time.

The vector equation of motion of the electron is $d^2\mathbf{r}/dt^2=\rho\mathbf{E}(t)$, where $\mathbf{r}$ is the vector displacement from O and $\rho=e/m$.

Double integration of the equation of motion gives

$$\mathrm{OQ}=\mathbf{r}(\eta)=\eta\mathbf{U}+\rho\int_{\tau}^{\tau+\eta}\left[\int_{\tau}^{g}\mathbf{E}(h)\,dh\right]dg, \qquad \ldots\ldots(26)$$

in which τ is the time at which the electron passes through the origin at velocity $\mathbf{U}$ in the direction OP. Since $\mathrm{OP}=\mathbf{s}=\eta\mathbf{U}$ it follows that

$$\mathrm{PQ}=\Delta\mathbf{s}_1=\rho\int_{\tau}^{\tau+\eta}\left[\int_{\tau}^{g}\mathbf{E}(h)\,dh\right]dg. \qquad \ldots\ldots(27)$$

It is again stressed that $\Delta\mathbf{s}_1$ is the displacement effected by $\mathbf{E}(t)$ in a specified time of flight. This, however, is not the only type of elementary displacement effected by $\mathbf{E}(t)$ that we are required to consider.

It is important to note that the effect of the field $\mathbf{E}$ is to curve the free paths but not to alter the mean value of the free paths described at speed U nor the distribution of their lengths about the mean which still conforms to the law that the proportion of a large group which exceeds a length s is $\exp(-s/l)$.

Thus, we are also concerned with the problem of finding the displacement $\Delta\mathbf{s}_2$ due to $\mathbf{E}(t)$ when the length of the free path is previously specified to be s.

Thus, whereas in the calculation of $\Delta\mathbf{s}_1$ the interval η is the same for the distorted and undistorted paths, in the calculation of $\Delta\mathbf{s}_2$ the lengths of the distorted and undistorted free paths are the same, but the time of flight is different for each.

We shall suppose in all cases that the displacements $\Delta\mathbf{s}_1$ and $\Delta\mathbf{s}_2$ are small compared with the undistorted displacements $s=\mathrm{OP}$.

Reference to the Figure shows that the displacement $\Delta\mathbf{s}_2$ is PR which for small displacements is effectively normal to OP. The distorted free path is OR.

There is an evident geometrical relationship between $\Delta\mathbf{s}_1$, $\Delta\mathbf{s}_2$ and $\mathbf{U}=U\mathbf{u}$ ($\mathbf{u}$ is unit vector parallel to $\mathbf{U}$):

$$\Delta\mathbf{s}_2=\Delta\mathbf{s}_1-(\mathbf{u}.\Delta\mathbf{s}_1)\mathbf{u}. \qquad \ldots\ldots(28)$$

Thus, in the example shown in the Figure if the time of flight along the free path $\mathrm{OP}=s$ when $\mathbf{E}=0$ is η, then that along the curved path OR of length s when $\mathbf{E}\neq 0$ is $(\eta-\Delta\eta)$, where $\Delta\eta=\mathrm{RQ}/U=\mathrm{PS}/U=(\mathbf{u}.\Delta\mathbf{s}_1)/U$.

Thus the effect of $\mathbf{E}$ is to alter the speed of the particle in the direction of $\mathbf{U}$ without adding to its displacement in this direction since that is already prescribed to be s to the first order of small quantities. The only displacement produced by $\mathbf{E}(t)$ is $\Delta\mathbf{s}_2$ as shown. Failure to recognize the distinction between $\Delta\mathbf{s}_1$ and $\Delta\mathbf{s}_2$ has led to erroneous formulae in many previous treatments.

Of interest for what follows, is the mean value of $\Delta\mathbf{s}_2$ taken over all possible directions of the velocity with free paths of prescribed and fixed length s. Let the vectors $\Delta\mathbf{s}_1$, $\Delta\mathbf{s}_2$, $\mathbf{U}$ and $\mathbf{u}$ be expressed in terms of their components and the unit vectors $\mathbf{i}_1$, $\mathbf{i}_2$ and $\mathbf{i}_3$ with respect to a cartesian system of coordinates, as follows:

$$\Delta\mathbf{s}_1=\mathbf{i}_1\Delta x_1+\mathbf{i}_2\Delta y_1+\mathbf{i}_3\Delta z_1, \qquad \Delta\mathbf{s}_2=\mathbf{i}_1\Delta x_2+\mathbf{i}_2\Delta y_2+\mathbf{i}_3\Delta z_2,$$

$$\mathbf{U}=\mathbf{i}_1U_x+\mathbf{i}_2U_y+\mathbf{i}_3U_z, \qquad \mathbf{u}=\mathbf{i}_1\frac{U_x}{U}+\mathbf{i}_2\frac{U_y}{U}+\mathbf{i}_3\frac{U_z}{U},$$

also, $\mathbf{E}=\mathbf{i}_1X+\mathbf{i}_2Y+\mathbf{i}_3Z$. In terms of components, equation (28) becomes

$$\begin{aligned}\Delta\mathbf{s}_2&\equiv\mathbf{i}_1\Delta x_2+\mathbf{i}_2\Delta y_2+\mathbf{i}_3\Delta z_2\\&=\Delta\mathbf{s}_1-(U_x\Delta x_1+U_y\Delta y_1+U_z\Delta z_1)(\mathbf{i}_1U_x+\mathbf{i}_2U_y+\mathbf{i}_3U_z)/U^2\\&=\mathbf{i}_1\left[\Delta x_1\left(1-\frac{U_x^2}{U^2}\right)-\frac{U_xU_y+U_xU_z}{U^2}\right]+\mathbf{i}_2\left[\Delta y_1\left(1-\frac{U_y^2}{U^2}\right)-\frac{U_yU_x+U_yU_z}{U^2}\right]\\&\quad+i_3\left[\Delta z_1\left(1-\frac{U_z^2}{U^2}\right)-\frac{U_zU_x+U_zU_y}{U^2}\right].\end{aligned}$$

In averaging $\Delta\mathbf{s}_2$ over all possible values of U_x, U_y and U_z with fixed U we use equations (25) and obtain

$$(\overline{\Delta\mathbf{s}_2}) = \tfrac{2}{3}[\mathbf{i}_1\Delta x_1 + \mathbf{i}_2\Delta y_1 + \mathbf{i}_3\Delta z_1] = \tfrac{2}{3}\Delta\mathbf{s}_1, \qquad \ldots\ldots(29)$$

whence, using (27),

$$(\overline{\Delta\mathbf{s}_2}) = \tfrac{2}{3}\rho\int_\tau^{\tau+\eta}\left[\int_\tau^g E(h)\,dh\right]dg, \qquad \ldots\ldots(30)$$

where $\eta = s/U$.

We proceed to derive a general expression for the drift velocity $\mathbf{W}$ under a field $\mathbf{E}$ in the absence of a magnetic field. Let the speeds U of the electrons be distributed according to some law that the number of electrons in a large group N whose speeds are not less than U but do not exceed $(U+dU)$ at any instant is $N_U\,dU = Nf(U)\,dU$. The mean collisional frequency of an electron is

$$\bar{\nu} = \bar{U}/\bar{l}, \text{ where } \bar{l} = \int_0^\infty lf(U)\,dU \quad \text{and} \quad \bar{U} = \int_0^\infty Uf(U)\,dU.$$

It is convenient to neglect the dependence of mean free path upon the speed U and to suppose that l is the same as $\bar{l}$. We write, therefore,

$$\bar{\nu} = \int_0^\infty \frac{U}{l}f(U)\,dU = \int_0^\infty \nu f(U)\,dU, \qquad \text{where} \quad \nu = U/l.$$

The number of collisions made by the N electrons per second is

$$N\bar{\nu} = \int_0^\infty \nu N f(U)\,dU = \int_0^\infty N_U\nu\,dU.$$

Thus the group of N electrons may be considered to comprise sub-groups $N_U\,dU = Nf(U)\,dU$, in which the electrons move at a fixed speed U and with a collisional frequency $\nu = U/l$.

The number of collisions within an elementary interval of time $d\tau$ is $N\bar{\nu}\,d\tau = d\tau\int_0^\infty N_U\nu\,dU$, consequently the number of free paths originating in this interval in which the initial speed lies between U and $(U+dU)$ is $d\tau\,\nu N_U\,dU$. Suppose the field $\mathbf{E}$ to be applied at time $\tau = 0$. We proceed to find the sum of the displacements due to $\mathbf{E}$ along all free paths that exist during an extended interval $0 \leqslant \tau \leqslant t$.

Of the $\nu N_U\,dU\,d\tau$ free paths that begin within the elementary interval $d\tau$ at time τ, some are not terminated within the chosen interval, that is they continue for time η such that $\tau+\eta \geqslant t$. The remainder terminate in collisions which occur at or before time t, that is to say $\tau+\eta \leqslant t$.

First consider the former type of free path, for which $\tau+\eta \geqslant t$. The number of such free paths is $\nu N_U\,dU\,d\tau\exp[-\nu(t-\tau)]$. The mean displacement produced by the applied field $\mathbf{E}$ in these unterminated paths at time t is given by equation (28), that is,

$$\Delta\mathbf{s}_1 = (\Delta\mathbf{s}_1) = \rho\int_\tau^t\left[\int_\tau^g \mathbf{E}(h)\,dh\right]dg. \qquad \ldots\ldots(31)$$

The sum of these displacements for all possible initial intervals $d\tau$ that fall within the large interval $0 \leqslant \tau \leqslant t$ is

$$\mathbf{S}_1(N_U\,dU) = (N_U\,dU)\nu\int_0^t \Delta\mathbf{s}_1\exp[-\nu(t-\tau)]\,d\tau$$

$$= (N_U\,dU)\rho\nu\int_0^t \exp[-\nu(t-\tau)]\left\{\int_\tau^t\left[\int_\tau^g \mathbf{E}(h)\,dh\right]dg\right\}d\tau, \qquad \ldots\ldots(32)$$

where $\mathbf{S}_1$ is the coefficient of $(N_U\,dU)$.

We require also the sum of the displacements along free paths of the latter type, that is along free paths originating in an interval $d\tau$ at time τ but terminating before time $\tau=t$, that is to say the duration η of the free path is such that $\tau+\eta\leqslant t$.

According to equations (29) and (30) the mean displacement along such a path is

$$(\Delta\mathbf{s}_2)=\tfrac{2}{3}\rho\int_\tau^{\tau+\eta}\left[\int_\tau^g \mathbf{E}(h)\,dh\right]dg. \qquad \ldots\ldots(33)$$

The number of free paths starting within $d\tau$ at time τ and persisting for times which exceed η but do not exceed $\eta+d\eta$ is $N_U\,dU\nu^2\exp(-\nu\eta)\,d\eta\,d\tau$.

Since terminated free paths of duration η are distributed at random over the interval $0\leqslant\tau\leqslant t-\eta$, it follows that the sum of the displacements due to $\mathbf{E}$ in such free paths is

$$N_U\,dU\nu^2\exp(-\nu\eta)\,d\eta\int_0^{t-\eta}\overline{(\Delta\mathbf{s}_2)}\,d\tau,$$

where $\overline{(\Delta\mathbf{s}_2)}$ is defined in equation (33).

It remains to sum over the range $0\leqslant\eta\leqslant t$ of permissible durations η that fall within the interval $0\leqslant\tau\leqslant t$. The sum of these displacements is

$$\mathbf{S}_2(N_U\,dU)=(N_U\,dU)\tfrac{2}{3}\rho\nu^2\int_0^t\exp(-\nu\eta)\left[\int_0^{t-\eta}\left\{\int_\tau^{\tau+\eta}\left(\int_\tau^g\mathbf{E}(h)\,dh\right)dg\right\}d\tau\right]d\eta. \qquad \ldots\ldots(34)$$

The equation serves to define $\mathbf{S}_2$.

It remains to consider displacements along free paths that start before time $\tau=0$ but persist into or beyond the interval $0\leqslant\tau\leqslant t$.

The number of free paths that begin within an interval $d\tau'$ at time τ' earlier than time $\tau=0$ but are not terminated before time $\tau=0$ is

$$N_U\,dU\int_0^\infty\exp(-\nu\tau')\,d\tau'=N_U\,dU.$$

The number of free paths being traversed at time $\tau=0$ that continue beyond the end of the interval $\tau=t$ is $N_U\,dU\exp(-\nu t)$, and the sum of the displacements due to $\mathbf{E}$ in these paths at time t is

$$N_U\,dU(\Delta\mathbf{s}_1)\exp(-\nu t)=\mathbf{S}_3(N_U\,dU), \qquad \ldots\ldots(35)$$

where $(\Delta\mathbf{s}_1)$ is as defined in equation (31) but with $\tau=0$.

The number of the $N_U\,dU$ paths whose durations are not less than η but do not exceed $\eta+d\eta$, when η is such that $0\leqslant\eta\leqslant t$, is $N_U\,dU\exp(-\nu\eta)\,d\eta$, and the sum of the displacements along all such paths terminated before time $\tau=t$ is

$$N_U\,dU\nu\int_0^t\overline{(\Delta\mathbf{s}_2)}\exp(-\nu\eta)\,d\eta=\mathbf{S}_4(N_U\,dU), \qquad \ldots\ldots(36)$$

where $\overline{(\Delta\mathbf{s}_2)}$ is defined in equation (33).

It follows that the sum of the displacements along free paths of all types traversed at speed U up to time t is

$$(N_U\,dU)\mathbf{S}=(N_U\,dU)[\mathbf{S}_1+\mathbf{S}_2+\mathbf{S}_3+\mathbf{S}_4], \qquad \ldots\ldots(37)$$

where $\mathbf{S}_1$, $\mathbf{S}_2$, $\mathbf{S}_3$ and $\mathbf{S}_4$ are defined in equations (32), (34), (35) and (36).

The sum of all the displacements due to $\mathbf{E}$ for all free paths and the whole range of speeds U is

$$\int_0^\infty\mathbf{S}N_U\,dU=N\int_0^\infty\mathbf{S}f(U)\,dU=N\bar{\mathbf{S}}. \qquad \ldots\ldots(38)$$

This equation serves to define the mean displacements $\mathbf{S}$ of an electron of the group. If at time $\tau=0$ the centroid of the group of N electrons is at the origin of coordinates, then at time t the centroid is at the end of the vector

$$\mathbf{R}_0=\bar{\mathbf{S}} \qquad \ldots\ldots(39)$$

and the drift velocity $\mathbf{W}$ at time t is

$$\mathbf{W}=\frac{d\mathbf{R}_0}{dt}=\frac{d\bar{\mathbf{S}}}{dt}=\frac{d}{dt}\overline{[\mathbf{S}_1+\mathbf{S}_2+\mathbf{S}_3+\mathbf{S}_4]}. \qquad \ldots\ldots(40)$$

The terms $d(\bar{\mathbf{S}}_3)/dt$ and $d(\bar{\mathbf{S}}_4)/dt$ are evanescent and become unimportant as t becomes large.

The first two terms in the square brackets in equation (40) not only yield evanescent contributions to $\mathbf{W}$ but also give the steady state value of $\mathbf{W}$, which is what is most commonly required. Since the formulae for the displacements $\mathbf{S}_k$ $(k=1, 2, 3, 4)$ are distributed within the discussion it is useful to display them as a group:

$$\begin{aligned}
\mathbf{S}_1&=\rho\nu\int_0^t\exp[-\nu(t-\tau)]\left\{\int_\tau^t\left[\int_\tau^g\mathbf{E}(h)\,dh\right]dg\right\}d\tau,\\
\mathbf{S}_2&=\tfrac{2}{3}\rho\nu^2\int_0^t\exp(-\nu\eta)\left[\int_0^{t-\eta}\left\{\int_\tau^{\tau+\eta}\left(\int_\tau^g\mathbf{E}(h)\,dh\right)dg\right\}d\tau\right]d\eta,\\
\mathbf{S}_3&=\rho\exp(-\nu t)\int_0^t\left[\int_0^g\mathbf{E}(h)\,dh\right]dg,\\
\mathbf{S}_4&=\tfrac{2}{3}\rho\nu\int_0^t\exp(-\nu\eta)\left\{\int_0^\eta\left[\int_0^g\mathbf{E}(h)\,dh\right]dg\right\}d\eta.
\end{aligned}$$

In practice the formulae are given a more convenient form by making suitable changes in the dummy variables so that every lower limit of integration is zero. They are thus equivalent to

$$\left.\begin{aligned}
\mathbf{S}_1&=\rho\nu\int_0^t\exp(-\nu\eta)\left\{\int_0^\eta\left[\int_0^{\eta-g}\mathbf{E}(t-g-h)\,dh\right]dg\right\}d\eta,\\
\mathbf{S}_2&=\tfrac{2}{3}\rho\nu^2\int_0^t\exp(-\nu\eta)\left[\int_0^{t-\eta}\left\{\int_0^\eta\left(\int_0^{\eta-g}\mathbf{E}(\tau+\eta-g-h)dh\right)dg\right\}d\tau\right]d\eta,\\
\mathbf{S}_3&=\rho\exp(-\nu t)\int_0^t\left[\int_0^g\mathbf{E}(h)\,dh\right]dg,\\
\mathbf{S}_4&=\tfrac{2}{3}\rho\nu\int_0^t\exp(-\nu\eta)\left\{\int_0^\eta\left[\int_0^g\mathbf{E}(h)\,dh\right]dg\right\}d\eta.
\end{aligned}\right\} \qquad \ldots\ldots(41)$$

Formulae (41) are the same as formulae (2), (3), (4) and (5) when $\omega=0$. To illustrate their use, put $\mathbf{E}(t)=$ constant in equations (41). Then

$$\begin{aligned}
\mathbf{S}_1&=\rho\mathbf{E}\left[\frac{1}{\nu^2}-\frac{\nu}{2}\frac{d^2}{d\nu^2}\left\{\frac{\exp(-\nu t)}{\nu}\right\}\right],\\
\mathbf{S}_2&=\tfrac{2}{3}\rho\nu^2\mathbf{E}\,\tfrac{1}{2}\left[t\frac{d^2}{d\nu^2}\left\{\frac{1-\exp(-\nu t)}{\nu}\right\}-\frac{d^3}{d\nu^3}\left\{\frac{1-\exp(-\nu t)}{\nu}\right\}\right],\\
\mathbf{S}_3&=\frac{\rho\mathbf{E}t^2}{2}\exp(-\nu t),\\
\mathbf{S}_4&=\frac{\rho\nu\mathbf{E}}{9}\frac{d^3}{d\nu^3}\left\{\frac{\exp(-\nu t)-1}{\nu}\right\}.
\end{aligned}$$

The terms independent of t vanish in equation (40) and those containing the factor $\exp(-\nu t)$ still retain it after differentiation, and are evanescent as t increases.

The only term in $\underline{\mathbf{W}}$ which is not evanescent derives from $\mathbf{S}_2$. Thus when t is large, $\mathbf{W} \to \frac{2}{3}\rho\mathbf{E}(1/\nu) = \frac{2}{3}\rho\mathbf{E}l(\overline{U^{-1}})$ as stated in equation (6).

It remains to derive the general formulae for drift in the presence of a magnetic field $\mathbf{B}_0$.

3.3. *Electron Drift in the Presence of a Steady Magnetic Field*

It is important to obtain formulae for the drift velocity $\mathbf{W}$ when electrons move through a gas in the presence of a constant and uniform magnetic field $\mathbf{B}_0$.

It is necessary first to derive expressions for the elementary displacements $\Delta\mathbf{s}_1$ (in a specified time η) and $\Delta\mathbf{s}_2$ (in a specified length of path s) as defined in §3.2.

The equation of motion of an electron in free flight at velocity $\mathbf{V}$ is $m d\mathbf{V}/dt = e[\mathbf{E} + \gamma(\mathbf{V} \times \mathbf{B}_0)]$ which may be written

$$d\mathbf{V}/dt + (\mathbf{V} \times \boldsymbol{\Omega}) = \rho\mathbf{E}, \qquad \ldots\ldots(42)$$

in which $\rho = e/m$, $|\Omega| = \omega = -\gamma\rho B_0$ (e positive); that is to say, ω is positive for electrons. The constant γ is defined in the Appendix.

Choose the direction of B_0 to be that of the axis Oz; let

$$\mathbf{E}(t) = \mathbf{i}_1 X(t) + \mathbf{i}_2 Y(t) + \mathbf{i}_3 Z(t).$$

Equation (42) resolves into

$$\ddot{x} + \omega\dot{y} = \rho X, \qquad \ddot{y} - \omega\dot{x} = \rho Y, \qquad \ddot{z} = \rho Z. \qquad \ldots\ldots(43)$$

If $\chi = (x + jy)$ then it follows from equations (43) that

$$\ddot{\chi} - j\omega\dot{\chi} = \rho[X + jY] = \rho E_N, \qquad \ddot{z} = \rho Z. \qquad \ldots\ldots(44)$$

Equations (44) are equivalent to

$$d/dt\,[\dot{\chi}\exp(-j\omega t)] = \rho[\exp(-j\omega t)]E_N, \qquad \ddot{z} = \rho Z. \qquad \ldots\ldots(45)$$

At time $t = \tau$ we suppose that $\chi = 0$, $z = 0$, $\dot{\chi}(\tau) = {}_0U_x + j\,{}_0U_y = U_N \exp(i\alpha)$, and $\dot{z} = {}_0U_z$. Integrate each side of equation (45) between the limits τ and g to find

$$\left.\begin{aligned} \dot{\chi}(g) = V_x + jV_y &= \exp(j\omega g)\int_\tau^g [\exp(-j\omega h)]E_N(h)\,dh \\ &\quad + U_N \exp j\{\omega(g-\tau) + \alpha\}, \\ V_z = \dot{z} &= \rho\int_\tau^g Z(h)\,dh + {}_0U_z. \end{aligned}\right\} \qquad \ldots\ldots(46)$$

It is convenient to change the limits of integration and to write equations (46) in the equivalent form

$$\left.\begin{aligned} \dot{\chi}(g) = V_x + jV_y &= \rho\int_0^{g-\tau} \exp(j\omega h)E_N(g-h)\,dh \\ &\quad + U_N \exp j\{\omega(g-\tau) + \alpha\}, \\ \dot{z}(g) = V_z &= \rho\int_0^{g-\tau} Z(g-h)\,dh + {}_0U_z. \end{aligned}\right\} \qquad \ldots\ldots(47)$$

Thus the orbital velocities at time g are

$$\left.\begin{aligned} V_x &= U_N \cos[\omega(g-\tau)+\alpha] + \rho \int_0^{g-\tau} [X(g-h)\cos\omega h - Y(g-h)\sin\omega h]\,dh = U_x + v_x, \\ V_y &= U_N \sin[\omega(g-\tau)+\alpha] + \rho \int_0^{g-\tau} [X(g-h)\sin\omega h + Y(g-h)\cos\omega h]\,dh = U_y + v_y, \\ V_z &= {}_0U_z + \rho \int_0^{g-\tau} Z(g-h)\,dh = U_z + v_z, \end{aligned}\right\} \quad \ldots\ldots(48)$$

where $\mathbf{v} = \mathbf{i}_1 v_x + \mathbf{i}_2 v_y + \mathbf{i}_3 v_z$ is the additional velocity due to the applied field **E**. A further integration of equations (45) gives the following expressions for the displacements of the electron from time τ to $(\tau+\eta)$. These are

$$\begin{aligned} \chi(\tau+\eta) &= \rho \int_\tau^{\tau+\eta} \left[\int_0^{g-\tau} \exp(j\omega h) E_N(g-h)\,dh \right] dg + \frac{U_N[\exp(j\omega\eta)-1]\exp(j\alpha)}{j\omega}, \\ &= \rho \int_0^{\eta} \left[\int_0^{\eta-g} \exp(j\omega h) E_N(\tau+\eta-g-h)\,dh \right] dg + \frac{U_N \exp(j\alpha)[\exp(j\omega\eta)-1]}{j\omega}, \\ z(\tau+\eta) &= \rho \int_0^{\eta} \left[\int_0^{\eta-g} Z(\tau+\eta-g-h)\,dh \right] dg + \eta U_z. \end{aligned} \quad \ldots\ldots(49)$$

Since all values of the angle α are equally probable and the mean value $\overline{U_z}$ is zero, it follows that the mean displacement along a free path in a specified interval of time from τ to $(\tau+\eta)$ is $\Delta\mathbf{s}_1 = \mathbf{i}_1\Delta s_{1x} + \mathbf{i}_2\Delta s_{1y} + \mathbf{i}_3\Delta s_{1z}$, where

$$\left.\begin{aligned} \Delta s_{1x} &= \rho \int_0^{\eta} \left[\int_0^{\eta-g} \{X(\tau+\eta-g-h)\cos\omega h - Y(\tau+\eta-g-h)\sin\omega h\}\,dh \right] dg, \\ \Delta s_{1y} &= \rho \int_0^{\eta} \left[\int_0^{\eta-g} \{X(\tau+\eta-g-h)\sin\omega h + Y(\tau+\eta-g-h)\cos\omega h\}\,dh \right] dg, \\ \Delta s_{1z} &= \rho \int_0^{\eta} \left[\int_0^{\eta-g} Z(\tau+\eta-g-h)\,dh \right] dg, \end{aligned}\right\} \quad (50)$$

$$\text{whence} \quad (\Delta s_{1x} + j\Delta s_{1y}) = \rho \int_0^{\eta} \left[\int_0^{\eta-g} E_N(\tau+\eta-g-h)\exp(j\omega h)\,dh \right] dg, \quad \ldots(51)$$

where $E_N = (X+jY)$. In order to derive formulae for the displacements $\Delta\mathbf{s}_2 = \mathbf{i}_1\Delta s_{2x} + \mathbf{i}_2\Delta s_{2y} + \mathbf{i}_3\Delta s_{2z}$ which occur during a free path of specified length s it is first necessary to obtain an expression for the alteration in the time of flight along the path s caused by the field **E**. The tangential speed ds/dt of an electron along a free path is given by

$$\left(\frac{ds}{dt}\right)^2 = V_x^2 + V_y^2 + V_z^2 = (U_x+v_x)^2 + (U_y+v_y)^2 + (U_z+v_z)^2 = U^2 + 2\mathbf{U}\cdot\mathbf{v} + v^2, \quad \ldots\ldots(52)$$

in which the velocities **U** and **v** are defined in equations (48).

It is assumed that the field components X, Y and Z are not of sufficient strength to make the velocity **v** comparable at any point of a free path with the initial agitational velocity **U**, consequently the term v^2 in equation (52) is discarded as a small quantity of the second order of magnitude. With this restriction it follows from (52) that

$$ds/dt \simeq U + (\mathbf{U}\cdot\mathbf{v})/U. \quad \ldots\ldots(53)$$

The length of free path traversed from the instant of collision at time τ up to time $(\tau+\eta)$ is

$$s \simeq \eta U + \int_\tau^{\tau+\eta} \frac{\mathbf{U}\cdot\mathbf{v}}{U}\,dg. \quad \ldots\ldots(54)$$

When the field **E** is zero the time required to describe a helical free path of length s at constant speed U is $\eta = s/U$, but when **E** is not zero the path of length s is described in a different time, $\eta' = \eta - \Delta\eta$. An approximate expression for $\Delta\eta$ follows immediately from equation (54), which may be written

$$\eta' \simeq \frac{s}{U} - \int_\tau^{(\tau+s/U)} \frac{\mathbf{U}.\mathbf{v}}{U^2}\,dg = \eta - \Delta\eta, \quad \text{i.e.} \quad \Delta\eta \simeq \int_\tau^{(\tau+s/U)} \frac{\mathbf{U}.\mathbf{v}}{U^2}\,dg. \qquad \ldots\ldots(55)$$

Thus, whereas the displacement $\Delta\mathbf{s}_1$, whose components are given in equations (50) and (51), is that which is effected in time $\eta = s/U$, the displacement over the path length s is effected in time $\eta - \Delta\eta$. Thus $\Delta\mathbf{s}_2 = \Delta\mathbf{s}_1 - \Delta\eta\, d(\Delta\mathbf{s}_1)/d\eta - \Delta\eta\, U(\tau+\eta)$. The term $\Delta\eta\, d(\Delta\mathbf{s}_1)/d\eta$ depends upon squares and products of the field components X, Y and Z and is therefore of the second order of small quantities. It follows that at time $g = \tau + \eta$

$$\Delta\mathbf{s}_2 = \Delta\mathbf{s}_1 - \Delta\eta\, U(\tau+\eta) = \Delta\mathbf{s}_1 - \frac{U(\tau+\eta)}{U^2}\int_\tau^{\tau+\eta} \mathbf{U}.\mathbf{v}\,dg. \qquad \ldots\ldots(56)$$

The mean displacement $(\overline{\Delta\mathbf{s}_2})$ effected along free paths s for all initial directions of the velocity **U** is

$$\overline{\Delta\mathbf{s}_2} = \Delta\mathbf{s}_1 - \left[\frac{U(\tau+\eta)}{U^2}\int_\tau^{\tau+\eta} \mathbf{U}.\mathbf{v}\,dg\right]. \qquad \ldots\ldots(57)$$

The velocities **U** and **v** are defined in equations (48). Thus, at time g

$$U_x = U_N \cos[\omega(g-\tau)+\alpha] = {}_0U_x \cos\omega(g-\tau) - {}_0U_y \sin(g-\tau),$$
$$U_y = U_N \sin[\omega(g-\tau)+\alpha] = {}_0U_x \sin\omega(g-\tau) + {}_0U_y \cos\omega(g-\tau),$$
$$U_z = {}_0U_z.$$

It follows that the second term in (57) is the sum of terms containing the products ${}_0U_x\,{}_0U_y$, ${}_0U_x\,{}_0U_z$, ${}_0U_y\,{}_0U_z$ as coefficients which vanish in the mean. There are also coefficients $({}_0U_x/U)^2$, $({}_0U_y/U)^2$, $({}_0U_z/U)^2$ each of which has, according to equation (11), the same average value of 1/3.

When these facts are noted it will be found that equations (57) and (47) and (50) lead to the following expressions for the components of the vector displacement $\overline{\Delta\mathbf{s}_2}$:

$$\left.\begin{aligned}
\overline{\Delta\mathbf{s}_{2x}} &= \rho\left[\int_0^\eta \left\{\left(1-\frac{\cos\omega g}{3}\right)\int_0^{\eta-g}[X(\tau+\eta-g-h)\cos\omega h\right.\right.\\
&\quad \left. - Y(\tau+\eta-g-h)\sin\omega h]\,dh\right\}dg - \left\{\frac{\sin\omega g}{3}\int_0^{\eta-g}[X(\tau+\eta-g-h)\sin\omega h\right.\\
&\quad \left.\left. + Y(\tau+\eta-g-h)\cos\omega h]\,dh\right\}dg\right],\\
\overline{\Delta\mathbf{s}_{2y}} &= \rho\left[\int_0^\eta \left\{\frac{\sin\omega g}{3}\int_0^{\eta-g}[X(\tau+\eta-g-h)\cos\omega h - Y(\tau+\eta-g-h)\sin\omega h]\,dh\right.\right.\\
&\quad + \left(1-\frac{\cos\omega g}{3}\right)\int_0^{\eta-g}[X(\tau+\eta-g-h)\sin\omega h\\
&\quad \left.\left. + Y(\tau+\eta-g-h)\cos\omega h]\,dh\right\}dg\right],\\
\overline{\Delta\mathbf{s}_{2z}} &= \tfrac{2}{3}\rho\int_0^\eta\left[\int_0^{\eta-g} Z(\tau+\eta-g-h)\,dh\right]dg.
\end{aligned}\right\} \qquad \ldots\ldots(58)$$

The vectors $\mathbf{S}_1$, $\mathbf{S}_2$, $\mathbf{S}_3$ and $\mathbf{S}_4$ are derived from $\Delta\mathbf{s}_1$ and $\overline{\Delta\mathbf{s}_2}$ by the same procedure as that employed in § 3.2. We find, corresponding to equations (41), that the components of $\mathbf{S}_1$ and $\mathbf{S}_2$ are given by equations (2) to (5) in § 2.2. The formulae for the displacements $\mathbf{S}_3$ and $\mathbf{S}_4$ are not stated because they contribute evanescent terms only to $\mathbf{W}$.

Although only elementary analysis is required, the derivation of the formulae for the particular instances from the general formulae, as discussed in § 2.3, is somewhat tedious.

§ 4. APPLICATIONS OF FORMULAE

4.1. *Magnetic Deflection of an Electron Stream*

In formulae (12) put $Y=Z=0$; then $W_x=(2\rho/3\omega)X\overline{\phi(y)}$; $W_y=(2\rho/3\omega)X\overline{\psi(y)}$; thus $W_y/W_x=\overline{\psi(y)}/\overline{\phi(y)}$. When $y^2=(\nu/\omega)^2\gg 1$, $\overline{\phi(y)}\to(1/y)$, $\overline{\psi(y)}\to\frac{1}{2}(1/y^2)$ and $W_y/W_x\to\frac{1}{2}\omega\overline{(1/\nu^2)}/\overline{(1/\nu)}=-\frac{3}{4}(\gamma B_0/X)W\overline{(U^{-2})}/\overline{(U^{-1})}^2$, where W is given by (6). A method for testing these formulae has been described (Huxley and Zaazou 1949).

4.2. *Hall Coefficient*

Let a current flow in a rectangular lamina lying in the xOy plane and whose edges are parallel to the axes Ox and Oy. Suppose the current to flow parallel to Ox and let $\mathbf{B}_0$ be directed along Oz. Since no steady current can flow in the direction $\pm$Oy, it follows that W_y in equations (12) is zero. Thus $Y=-X\overline{\psi(y)}/\overline{\phi(y)}$ and $W_x=(2\rho/3\omega)X\overline{\phi(y)}[1+(\overline{\psi(y)}/\overline{\phi(y)})^2]$. The current density is $\mathbf{J}=ne\mathbf{W}$ and the Hall coefficient

$$R=\frac{Y}{J}=-\frac{3\omega\overline{\psi(y)}}{ne\rho[\overline{\psi(y)}^2+\overline{\phi(y)}^2]}.$$

When, as in a metal, $y=\nu/\omega\gg 1$, this formula shows that

$$R\to 0{\cdot}75[\overline{(U^{-2})}/\overline{(U^{-1})}]\gamma B_0/ne.$$

When the speeds U are distributed according to Maxwell's law then $R\to 1{\cdot}175\gamma B_0/ne$, a standard formula.

4.3. *The Mean Power communicated by a High-Frequency Electric Field to an Electron in a Steady State of Motion in a Gas*

The mean power given to an electron is $w=\frac{1}{2}e\,\mathrm{Re}\,[XW_x^*+YW_y^*+ZW_z^*]$, where asterisks denote the conjugate of the complex quantity. It follows from equations (21) that (Huxley 1949)

$$w=(e^2/6m)[(X_0^2+Y_0^2)S+2X_0Y_0D\sin\alpha+2F(p,\nu)Z_0^2]. \quad \ldots\ldots(59)$$

For instance, if the electric field rotates with constant amplitude about the Oz axis (parallel to $\mathbf{B}_0$) then $X_0=Y_0=E_0$; $Z_0=0$; $\sin\alpha=\pm 1$. Thus from (59), with $\sin\alpha=+1$,

$$w_{\mathrm{ord}}=\frac{e^2E_0}{3m}[S+D]=\frac{2}{3}\frac{e^2}{m}E_0^2F[(\omega+p),\nu],$$

and with $\sin\alpha=-1$,

$$w_{\mathrm{extraord}}=\frac{e^2E_0^2}{3m}[S-D]=\frac{2}{3}\frac{e^2}{m}E_0^2F[(\omega-p),\nu].$$

If $Y=0$ and $\beta=0$ (plane polarized field) $w=(e^2/3m)[\frac{1}{2}SX_0^2+F(p,\nu)Z_0^2]$. When, in addition, $\mathbf{B}_0=0$ $(\omega=0)$, $w=(e^2/3m)F(p,\nu)[X_0^2+Z_0^2]$. These results are of interest for wave propagation in the ionosphere.

4.4. *The Refraction and Absorption of Electromagnetic Waves in an Ionized Medium*

In order to illustrate how the theoretical formulae for the conductivity of an electron gas in a high-frequency field finds an application in the study of the propagation of electromagnetic waves it suffices to consider the simple problem in which the applied magnetic field $\mathbf{B}_0$ is absent. (A more general discussion has been given by Huxley (1940).)

According to equations (7) the conductivity with no constant magnetic field is a complex quantity of the form

$$\sigma = a - jb, \qquad \ldots\ldots(60)$$

where, according to equations (8) and (9),

$$a = \frac{2}{3}\frac{Ne^2}{m}\frac{1}{p}\overline{\phi(x)}, \qquad b = \frac{2}{3}\frac{Ne^2}{m}\frac{1}{p}\overline{\psi(x)}, \qquad \ldots\ldots(61)$$

in which N is the number of electrons per unit volume. Since we require Maxwell's equations of the electromagnetic field they are here stated in general terms valid for any particular system of self-consistent units. In this notation the equations read

$$\left.\begin{array}{ll} \operatorname{curl}\mathbf{E} = -\gamma\dot{\mathbf{B}}, & \operatorname{curl}\mathbf{H} = \gamma(\dot{\mathbf{D}}+\mathbf{J}) = \gamma(\dot{\mathbf{D}}+\sigma\mathbf{E}), \\ \operatorname{div}\mathbf{D} = \rho, & \operatorname{div}\mathbf{B} = 0, \end{array}\right\} \qquad \ldots\ldots(62)$$

with $\mathbf{B} = \mu_0 K_m \mathbf{H}$; $\mathbf{D} = \epsilon_0 K_e \mathbf{E}$.

The values of the constants γ, ϵ_0 and μ_0 are determined by the particular system of units adopted, as is explained in the Appendix. K_m is the magnetic permeability and K_e the dielectric constant. In this notation the Poynting vector is

$$\mathbf{P} = (\mathbf{E}\times\mathbf{H})/\gamma. \qquad \ldots\ldots(63)$$

In (62) put $K_m = 1$; $\rho = 0$; $\mathbf{J} = \sigma\mathbf{E}$, and suppose $\mathbf{E}$ and $\mathbf{H}$ to be the fields of a plane sinusoidal wave train. It follows that

$$\operatorname{curl}\mathbf{H} = (j\gamma p\epsilon_0)\left(1+\frac{\sigma}{jp\epsilon_0}\right)\mathbf{E} = \gamma\epsilon_0\left(1-\frac{j\sigma}{p\epsilon_0}\right)\dot{\mathbf{E}} = \gamma\epsilon_0 K_e'\dot{\mathbf{E}}, \qquad \ldots\ldots(64)$$

where

$$K_e' = (1 - j\sigma/p\epsilon_0), \qquad \ldots\ldots(65)$$

is an equivalent dielectric constant.

The phase velocity in a vacuum is $c = 1/[\gamma(\epsilon_0\mu_0)^{1/2}]$ whereas that in the medium is $v = 1/[\gamma(\epsilon_0\mu_0 K_e')^{1/2}]$. The refractive index of the medium is therefore

$$n' = n - jc\kappa/p = (K_e')^{1/2} = (1 - j\sigma/\epsilon_0 p)^{1/2}. \qquad \ldots\ldots(66)$$

Since $(\mu_0)^{1/2}H = (\epsilon_0 K_e)^{1/2}E$, it follows that

$$H = (\epsilon_0/\mu_0)^{1/2}(n - jc\kappa/p)E. \qquad \ldots\ldots(67)$$

The absorption coefficient is κ, consequently if $E = E_0\exp(-\kappa s)\exp[jp(t-ns/c)]$ then $H = E_0(\epsilon_0/\mu_0)^{1/2}(n^2 + c^2\kappa^2/p^2)^{1/2}\exp(-\kappa s)\exp[jp(t-ns/c) - j\alpha]$, where $\tan\alpha = (c\kappa/np)$. Put $\sigma = (a - jb)$ in (66) to obtain

$$n^2 - (c\kappa/p)^2 = 1 - b/\epsilon_0 p, \qquad 2nc\kappa/p = a/\epsilon_0 p. \qquad \ldots\ldots(68)$$

When $\kappa\lambda/2\pi$ is small compared with unity, that is to say the wave is not strongly absorbed, it follows from (68) that $n^2 \simeq 1 - b/\epsilon_0 p$. Furthermore, if the wave is

travelling in a region in which the refractive index n is not greatly different from unity, that is the region does not reflect the wave, then $\kappa \simeq a/(2\epsilon_0 c)$. It follows from the definitions of a and b given in equations (61) that in these circumstances

$$n^2 = 1 - (2Ne^2/3m)(1/p^2)\overline{\psi(x)}, \qquad \kappa = (Ne^2/3m\epsilon_0 c)(1/p)\overline{\phi(x)}$$

when $$\bar{x} = \bar{\nu}/p \ll 1\,; \quad \overline{\psi(x)} \to 3/2\,; \quad \overline{\phi(x)} \to 2\bar{x} = (2/p)\bar{\nu} = 2\overline{U}/lp.$$

The refractive index is then given by the standard formula

$$n^2 \simeq 1 - Ne^2/(\epsilon_0 mp^2), \qquad \text{but} \qquad \kappa \simeq (2\bar{\nu}Ne^2/3\epsilon_0 mcp^2). \quad \ldots\ldots (69)$$

The usual formula for κ is, however, $\kappa = Ne^2\bar{\nu}/(2\epsilon_0 mcp^2)$, that is to say it makes κ too small by a factor of 3/4. Formulae (69) apply to the F region of the ionosphere when $p/2\pi \simeq 3 \times 10^6$ c/s. or greater.

Next suppose $\bar{x} = \bar{\nu}/p \simeq 1$. $\phi(x)$ is a maximum at $x = 0{\cdot}78$, its value also being 0·78. Since $\phi(1) = 0{\cdot}75$ and $\phi(0{\cdot}5) = 0{\cdot}72$, the maximum is flat and $\phi(x)$ does not change markedly in the range $0{\cdot}5 \leqslant x \leqslant 1$. In this range κ is virtually independent of x and is approximately represented by

$$\kappa = 0{\cdot}25Ne^2/(\epsilon_0 mp). \qquad \ldots\ldots (70)$$

The usual formula adopted for κ is $\kappa = (Ne^2/2\epsilon_0 mcp)[x/(1+x^2)]$. The function $x/(1+x^2)$ attains its maximum value of 0·5 at $x = 1$, consequently, according to this formula, near $x = 1$ κ is approximately represented by $\kappa = 0{\cdot}25Ne^2/(\epsilon_0 mp)$, which is the same as (70). It may be concluded that the usual formulae for κ are not seriously in error when $\bar{x} = \bar{\nu}/p \simeq 1$, as for instance in the E region of the ionosphere.

4.5. *The Complex Dielectric Constant of an Ionized Gas*

Equation (65) is the formula for the complex dielectric constant of an electron-laden gas. The formula is equivalent to

$$\begin{aligned} K_e' &= 1 + (b/p\epsilon_0) - j(a/p\epsilon_0) \\ &= 1 + (2Ne^2/3m)(1/p^2\epsilon_0)\overline{\phi(x)} - j[(2Ne^2/3m)(1/p^2\epsilon_0)]\overline{\psi(x)}, \qquad \ldots\ldots (71) \end{aligned}$$

in which $x = \nu/p = U/(lp)$ and ϕ and ψ are defined in equation (8).

§ 5. CONCLUSION

The theoretical investigations presented in this paper, of the drift velocities of electrons in various circumstances, reveal an underlying unity in the subject which was hitherto lacking. What were previously a collection of apparently independent formulae are now seen to be particular examples of one comprehensive general formula covering the subject of drift velocities of electrons in direct or sinusoidal electric fields accompanied or unaccompanied by a permanent magnetic field.

APPENDIX

The constants ϵ_0, μ_0 and γ enter electrical theory as follows: The two coulomb laws (ϵ_0 and μ_0) are

$$F = q_1 q_2/(4\pi\epsilon_0 K_e r^2), \qquad F = m_1 m_2/(4\pi\mu_0 K_m r^2),$$

in which K_e is the dielectric constant and K_m the magnetic permeability. It is the custom to write $\epsilon = \epsilon_0 K_e$, $\mu = \mu_0 K_m$.

The constant γ enters through law of the equivalent shell: $\chi=\gamma\mu i=\gamma\mu_0 K_m i$, where χ is the strength of the uniform shell equivalent to the current loop i.

A single relationship exists between the constants in any absolute self-consistent system of units: $\gamma^2\epsilon_0\mu_0=1/c^2$, where c is the velocity of light in a vacuum. Thus, if so preferred, γ may be eliminated in favour of c.

The values of ϵ_0, μ_0 and γ in the three principal systems of units are the following:

System	ϵ_0	μ_0	γ	c (approx.)	$\gamma^2\mu_0$	$\gamma\mu_0$
Gaussian	$1/4\pi$	$1/4\pi$	$4\pi/c$	3×10^{10}	$4\pi/c^2$	$1/c$
E.M.U.	$1/4\pi c^2$	$1/4\pi$	4π	3×10^{10}	4π	1
Rationalized M.K.S.	$10^7/4\pi c^2$ $\simeq 1/(36\pi\times10^9)$	$4\pi\times10^{-7}$	1	3×10^8	$4\pi\times10^{-7}$	$4\pi\times10^{-7}$

It should be noted that induction $\mathbf{B}$ in general or in M.K.S. units is not the same physical quantity as induction $\mathbf{B}'$ (say) in gaussian or electromagnetic units. The former is $\mathbf{B}=\mu\mathbf{H}=\mu_0 K_m\mathbf{H}$; the latter is $\mathbf{B}'=K_m\mathbf{H}$, thus $\mathbf{B}=\mu_0\mathbf{B}'$. Since μ_0 in general possesses physical dimensions, $\mathbf{B}$ and $\mathbf{B}'$ are not the same physical quantity. Similarly $\mathbf{D}=\epsilon\mathbf{E}=\epsilon_0 K_e\mathbf{E}=\epsilon_0\mathbf{D}'$. The gyro-angular velocity $\boldsymbol{\Omega}=\mathbf{i}_3\omega$, employed in the representation of drift in the presence of an applied magnetic field $\mathbf{B}_0$, is $\boldsymbol{\Omega}=-\gamma\rho\mathbf{B}_0$, i.e. $\omega=-\gamma\rho B_0$. The general formula for the Lorentz force is $F=\gamma e[\mathbf{V}\times\mathbf{B}_0]$.

REFERENCES

Becker, R., 1933, *Theorie der Elektrizitat* (Leipzig : Teubner), p. 205.

Huxley, L. G. H., 1937 a, *Phil. Mag.* (7), **23**, 210; 1937 b, *Ibid.*, **23**, 442; 1940, *Ibid.*, **29**, 313; 1949, *Proc. Roy. Soc.* A, **196**, 427.

Huxley, L. G. H., and Zaazou, A. A., 1949, *Proc. Roy. Soc.* A, **196**, 402.

Lorentz, H. A., 1916, *Theory of Electrons* (Leipzig : Teubner), p. 273.

Townsend, J. S., 1915, *Electricity in Gases* (Oxford : University Press), p. 100; 1936, *Phil. Mag.* (7), **22**, 145; 1937, *Ibid.*, **23**, 880; 1947, *Electrons in Gases* (London : Hutchinson's Scientific and Technical Publications), p. 15.

Particular instances of the general problem have been discussed by :

Margenau, H., 1946, *Phys. Rev.*, **69**, 508.

Cahn, J. H., 1949, *Phys. Rev.*, **75**, 838.

GENERAL REFERENCES

Cobine, J. D., 1941, *Gaseous Conductors* (New York : McGraw-Hill).

Healey, R. H., and Reed, J. W., 1941, *The Behaviour of Slow Electrons in Gases* (Amalgamated Wireless (Australasia) Ltd.).

Loeb, L. B., 1939, *Fundamental Processes in Electrical Discharge in Gases* (New York : Wiley and Sons).

Townsend, J. S., 1947, *Electrons in Gases* (London : Hutchinson's Scientific and Technical Publications).

The Refractive Indices and Dielectric Constants of Air and its Principal Constituents at 24,000 Mc/s.

By L. ESSEN and K. D. FROOME
Electricity Division, National Physical Laboratory, Teddington, Middlesex

Communication from the National Physical Laboratory; *MS. received 3rd May* 1951

ABSTRACT. The refractive indices of air and its principal constituents have been measured at a frequency of 24,000 Mc/s. with a precision comparable with that obtained in the optical range. The method is based on the measurement of the resonant frequency of a cavity resonator first when it is filled with the gas and then when it is evacuated. The source of oscillations used is a Pound-stabilized velocity-modulated oscillator, and its frequency is measured by reference to a high harmonic of a quartz standard, with a precision of 1 part in 10^8. The cavity is provided with a tuning plunger, which changes the resonant frequency through a range of about 10 Mc/s., and is calibrated to an accuracy of within 1 kc/s.

Most of the measurements were made by the frequency-change method and the plunger was used in a narrow region only for a precise setting to resonance. It is possible by a larger movement of the plunger to compensate for the whole frequency change due to the removal of the gas and thus to work at a fixed frequency.

The following results were obtained for $(n-1)10^6$ where n is the refractive index at 0°c., 760 mm. Hg: dry CO_2-free air, $288{\cdot}15\pm0{\cdot}1$; nitrogen, $294{\cdot}1\pm0{\cdot}1$; oxygen, $266{\cdot}4\pm0{\cdot}2$; argon, $277{\cdot}8\pm0{\cdot}2$; carbon dioxide, 494 ± 1; and the value for water vapour at 20°c., 10 mm. Hg pressure was $60{\cdot}7\pm0{\cdot}1$.

The dielectric constants can be calculated from the relationship $\mu\epsilon=n^2$, where μ is the magnetic permeability and ϵ the dielectric constant, the values of $(\mu-1)10^6$ being taken as 0·4 for air, 1·9 for oxygen and zero for the other gases.

Accurate formulae are given for obtaining the refractive index of moist air at different atmospheric conditions, and are reduced to the following simple formula which is applicable for normal atmospheric conditions:

$$(n_{t,p}-1)10^6=\frac{103{\cdot}49}{T}p_1+\frac{177{\cdot}4}{T}p_2+\frac{86{\cdot}26}{T}\left(1+\frac{5748}{T}\right)p_3,$$

where p_1, p_2, p_3 are the partial pressures of dry air, carbon dioxide and water vapour, t is the temperature in degrees c., and $T=273+t$ is the absolute temperature. A value of $1{\cdot}839\pm0{\cdot}002\times10^{-18}$ e.s.u. was derived for the dipole moment of the water vapour molecule.

§ 1. INTRODUCTION

There are several different branches of work in the radio-frequency field which require a more accurate value of the refractive index of air than is so far available.

Precision radar, for example, has reached a stage of development at which the accuracy is limited by uncertainties in the value of the correction which must be applied to allow for the effect of the atmosphere. An accurate value is also required for a microwave interferometer which is being developed at the National Physical Laboratory for the measurement of length. The present operating frequency of the instrument is 24,000 Mc/s. and the measurements described here have therefore been made at this frequency, although the method could be used at any frequency in the microwave region.

No previous determinations appear to have been made at 24,000 Mc/s., although there are a number at lower microwave frequencies and at low radio frequencies. As shown in the discussion later, none of these has the precision required for the present application and, moreover, they diverge by considerably

more than the limits given by the authors. The values of refractive index obtained for dry air by extrapolation from the dispersion formulae established by the most reliable optical measurements also differ appreciably, and it is not certain that the effect of the resonant absorption by oxygen in the millimetre band can be altogether ignored, and therefore that extrapolation is completely valid.

The most convenient method at microwave frequencies is the measurement of the change in the resonant frequency of a cavity when filled with the gas under test and then evacuated. Then for gases which do not absorb microwaves heavily ($k \ll n$)

$$n-1=(f_v-f_g)/f_g=(\mu\epsilon)^{1/2}-1 \quad \ldots\ldots(1)$$

where n is the refractive index of the gas, μ the magnetic permeability, ϵ the dielectric constant, k the absorption coefficient, f_v the resonant frequency of the cavity when evacuated and f_g the resonant frequency of the cavity when filled with the gas.

The original aim was to measure $n-1$ with an accuracy of at least 1 part in 1000 and since $n-1$ itself is only 3×10^{-4} the precision of the resonant setting must be about 1 part in 10^7, although the absolute value of resonant frequency is not so important. One method giving the necessary sensitivity has been used by Crain (1948) and others. Two cavities, one containing the gas, control the frequencies of two oscillators in the manner described by Pound (1947), and the heterodyne beat frequency between them is measured. The cavity containing the gas is then evacuated and the change in the beat frequency determined. This technique though beautifully simple is open to several objections. In the first place, any change in the frequency of the comparison oscillator during the measurements causes a direct error in f_v-f_g, and to overcome this uncertainty in the work described here the comparison oscillator was dispensed with and the frequency measurements made absolutely in terms of a quartz standard. A second and probably more serious source of error arises from the fact that a Pound-stabilized oscillator is not controlled at exactly the resonant frequency of the cavity and the point of control varies with the setting of other components in the circuit. The operation may not be at the same point for the two different frequencies f_v and f_g. The absolute frequency measurements made here enabled the effect of circuit changes to be studied in some detail. It was found that the modulating crystal diode used in the control circuit was particularly sensitive to frequency. For a fixed setting of the cavity the frequency of control could be changed by as much as 1 part in 10^4 for extreme circuit conditions and direct measurements of refractive index by this method indicated that errors of 1 part in 10^6 (in n) could readily occur. It was decided therefore to connect the cavity in a separate circuit and to use the Pound circuit merely as a source of oscillations.

A number of other very sensitive methods of using cavity resonators have been designed for detecting small changes of refractive index but they have not been used for absolute measurements with the required accuracy.

§ 2. EXPERIMENTAL ARRANGEMENT

The 24,000 Mc/s. (K band) oscillator in Figure 1 is controlled in a Pound circuit by a cavity resonator (not shown) which is provided with a micrometer adjustment for making small changes of frequency. The hybrid junction ('magic T') A is a part of this circuit and the usable power output is transmitted

through an attenuator towards a second hybrid junction B. At B it is divided into two equal parts, one going towards the measuring cavity resonator and the other towards a load and matching stub. The fully absorbing load is equivalent to a perfectly matched cavity at resonance. The tuning stub can be made to represent the mismatch of the cavity including the reflection from the window, which

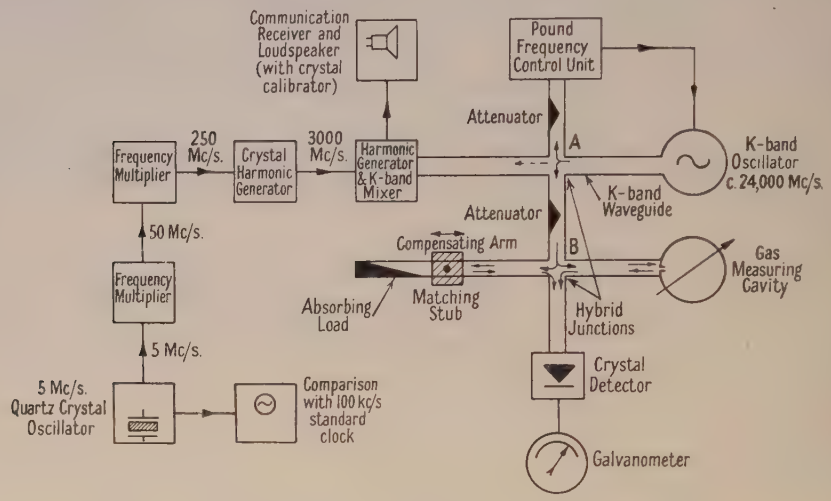

Figure 1. Diagram of cavity bridge and frequency comparator.

isolates it from the waveguide circuit and enables it to be evacuated or filled with the gas under test. The waves returning from the stub and from the cavity are again divided at the junction, a part returning towards the oscillator and a part entering the detector arm. Hence the output from the crystal detector is proportional to the vector sum of the two reflected waves. The matching stub is first fully withdrawn and the cavity tuned by adjustment of a small plunger attached to a micrometer to give a minimum deflection; the penetration of the stub is then gradually increased and its position adjusted until the minimum obtained by tuning the cavity is very near to zero. This corresponds to the true resonant condition of the cavity. Other conditions for zero deflection can be obtained with further penetration of the stub but the true resonant condition is likely to give the greatest stability and reproducibility of setting. The stub is situated at nearly the same electrical distance from the junction as the cavity (owing to the properties of the hybrid junction the distances should in fact differ by $\lambda/8$ for the zero current condition) and the balance is therefore obtained at the true resonant setting of the cavity for a considerable range of frequencies.

The waveguide bridge arrangement enables a very high sensitivity to be obtained. The power entering junction B is such that with the cavity detuned a galvanometer deflection equivalent to 10,000 scale divisions is obtained and a deviation from the minimum of 0·1 division can be detected.

A small amount of radiation, which enters the fourth arm of junction A due to a slight mismatch of the padding attenuators, is used for the frequency measurement. It is mixed in a crystal diode with an output of 3,000 Mc/s. obtained as shown from a harmonic of a 250 Mc/s. output derived by multiplication from a 5 Mc/s. quartz oscillator. The frequency of the quartz oscillator is set

exactly at its nominal value by reference to the N.P.L. standard quartz clock. The power at 250 Mc/s. is about 2 watts and this is applied to a crystal diode (a selected CV 247) which is connected across a tunable length of waveguide. The harmonic at 3,000 Mc/s. is selected and taken from the guide through a short length of coaxial cable to a second crystal diode (a selected VX 4026) connected across the waveguide carrying the small output from the K-band oscillator. This crystal acts as both harmonic producer and mixer. The heterodyne beat at about 9 Mc s. produced between the eighth harmonic of the 3,000 Mc/s. output and the K-band oscillator is detected in a sensitive communication receiver. The receiver possesses an internal quartz calibrator which can be used for the measurement of the beat frequency or for the setting of this frequency to an exact multiple of 0·1 Mc/s. by adjustment of the K-band oscillator.

If the frequency multiplying stages are carefully designed to be free from phase modulation the purity of the beat note heard in the receiver gives an indication of the degree of stabilization attained by the Pound controlled circuit. It was found that the note could be set to below 200 c/s.—or better than 1×10^{-8} of the operating frequency—and that any gradual drift, due mainly to the temperature change of the cavity in the Pound circuit, could be readily followed. It was thus possible to maintain the frequency of the oscillator to within 1×10^{-8} of the desired value during a set of measurements.

§ 3. DESIGN AND CALIBRATION OF THE CAVITY

One of the two cavities used for measuring the gas is shown in Figure 2. They are made from invar, the inner walls being silver or copper plated. The H_{017} mode of resonance is used in the larger cavity and a groove is cut in the

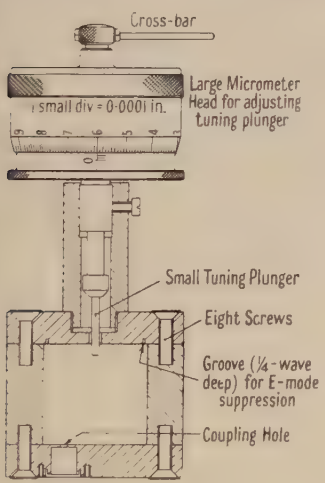

Figure 2.

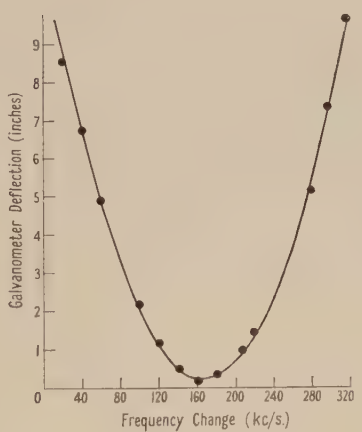

Figure 3. Resonance curve.

top wall to shift the frequency of the E_{117} mode, which, in a perfect cylinder coincides with the H_{017} mode, outside the working range of the instrument. A cavity of fixed dimensions could theoretically be used, the setting to resonance being made by adjustment of the oscillator frequency, but there are a number of practical advantages in making the cavity tunable over a small frequency range. If the setting is made by varying the oscillator frequency there is always

a danger that the power and phase of the oscillations will also be changed, thereby reducing the accuracy of setting. Moreover, in a cavity of this size, there are many possible modes of resonance and it is useful to be able to vary the resonant frequency through a small range to make sure that none of these other modes falls within the frequency range used in the experiments. As will be seen in the next section, the tuning facility also simplified the measurement of frequency change on evacuation. An additional advantage, which is not used in this work but which would be valuable in some experimental arrangements, is that if the tuning range is greater than the change on evacuation, this change can be compensated by retuning the cavity and the measurements can be made at a fixed frequency. The value of $f_v - f_g$ is then read from the calibration curve of the instrument. If this procedure is used, no particular care need be taken to ensure that the components of the circuit in which the cavity is connected are frequency insensitive and satisfactory operation would, for example, be obtained in the arrangement used by Crain (1948).

An axial plunger was therefore fitted as shown in Figure 2. The cross bar at the top of the micrometer is gripped by a spring clamp attached to a rotating sealed joint when the cavity is mounted in its vacuum chamber and thus enables the adjustment to be made from the outside.

The two cavities used, designated by the letters A and B, have the dimensions given in Table 1.

Table 1. Details of Cavities

Cavity	Mode	Diameter (cm.)	Length (cm.)	Diameter of plunger hole (cm.)	Diameter of plunger (cm.)	Plating material	Range for plunger movement of $\lambda/2$
A	H_{017}	6·660	4·491	1·25	1·09	silver	18 Mc/s.
B	H_{016}	4·125	4·030	0·63	0·31	copper	9 Mc/s.

It was found that with both cavities the setting to a minimum could be made with a precision of a few kilocycles per second as may be judged by the bottom portion of a typical resonance curve reproduced in Figure 3. The micrometer readings for the resonant condition were taken at intervals of 50 kc/s. and the complete calibration curve for cavity A is reproduced in Figure 4. This curve corresponds to a plunger movement of nearly one-half wavelength in the cavity and would have continued in a similar manner for a further penetration of the plunger. However, the nearly straight part of the curve gave the required range and sensitivity for measurements on air. The calibration was made with the cavity filled with air, evacuated, and with different settings of the tuning stub in the waveguide bridge; and it was found that although the absolute frequency of resonance was, of course, modified, the law of frequency change against plunger position was the same in each case within 1 kc/s. for the complete range of 18 Mc/s.

The method of attaching the cavity to the vacuum system and of sealing cavity A is shown in Figure 5. It will be noticed that any bending of the base plate of the containing chamber upon evacuation will not be communicated to the base of the cavity. Cavity B had a mica window 0·003 in. thick in place of the distrene plug. Tests showed that the window was pushed in at the centre by 0·0015 in. on evacuation and, although the effect of this appeared from rough

calculations to be negligible, it was decided that the solid plug one wavelength thick was to be preferred. Most of the measurements were therefore made with cavity A, which was also the more convenient because it happened to be an almost perfect match to the waveguide. Consequently, the matching stub was nearly fully withdrawn. It was, however, thought to be worth while checking

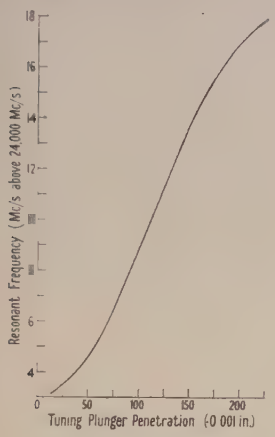

Figure 4. Cavity tuning plunger calibration.

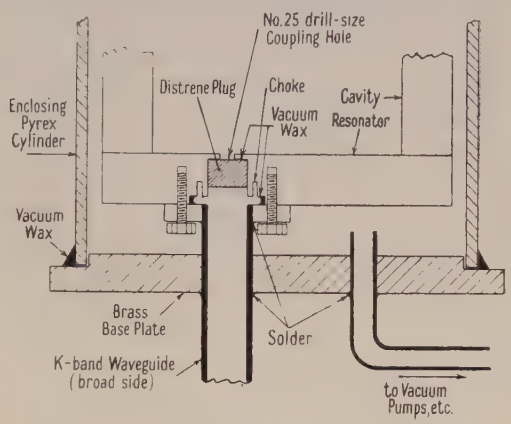

Figure 5. Coupling to cavity through vacuum enclosure.

the results with cavity B, which differed in size, surface finish, and calibration. Very close agreement was obtained between the results thus helping to establish that some of the possible sources of error, discussed in more detail in § 5, had a negligible effect.

§ 4. PROCEDURE OF OPERATION

The method used was essentially the measurement of the frequency change produced on evacuating the cavity, but the following procedure was found to be most convenient in practice. The frequency of the oscillator was set approximately to the resonant frequency of the full cavity and was then adjusted slightly so that the beat frequency in the receiver coincided with the nearest harmonic of the 100 kc/s. calibration oscillator incorporated in it. (This 100 kc/s. oscillator was itself set to give a zero beat with the N.P.L. standard.) The cavity was then adjusted to resonance by a small movement of the tuning plunger. The gas was removed and the process repeated. The frequency change was thus obtained to the nearest 100 kc/s. from the calibration of the receiver dial, the residual change being obtained from the difference in the plunger settings, and the calibration curve. In each case, the mean of six settings of the tuning plunger was taken and experience showed that the repetition accuracy of setting was then 1 kc/s. or 1 part in 24×10^6. Since only a small plunger movement was required it was possible to work on a strictly linear part of the calibration, and thus avoid the need of referring to the actual curve.

The cavity temperature was measured by a thermometer reading to $\pm 0{\cdot}01^\circ$ c., and for the gases other than water vapour the pressures were obtained from a barometer reading to 0·02 mm. Hg. Both of these instruments were calibrated shortly before and after the experiments against standards maintained at the National Physical Laboratory. The water vapour was admitted to the evacuated cavity from a vessel containing distilled water at a temperature at least 4° c.

below that of the cavity. Its pressure was measured directly on a mercury manometer made from glass tubing having an internal diameter of 1·75 cm., the height of the mercury meniscus being read to 0·005 mm. on a travelling microscope. The gases were dried by being passed through tubes containing glass wool impregnated with phosphorus pentoxide. In preliminary experiments

Table 2. Summary of Measurements on Dry Gases at 0° c., 760 mm. Hg

Gas	$(n-1)\,10^6$	$(\epsilon-1)\,10^6$	Frequency of measurement	Author	Date
Air					
	287·8 ± 0·1	575·7 ± 0·2	*	Barrell‡	1951
		576	0·5 Mc/s.	Watson	1934
		567·0 ± 1·0	1·0 Mc/s.	Hector & Woernley	1946
		572	9000 Mc/s.	Crain	1948
		577·0 ± 1·0	9000 Mc/s.	Lyons, Birnbaum & Kryder	1948
		608	3000 Mc/s.	Philips	1950
		575·4 ± 1·4	9000 Mc/s.	Birnbaum, Kryder & Lyons	1951
	288·15 ± 0·10	576·0 ± 0·2	24000 Mc/s.	Essen & Froome	1951
Nitrogen					
	290·6	581·3	*	Scheel†	1907
		587	0·5 Mc/s.	Watson	1934
		579·6 ± 1·0	1·0 Mc/s.	Hector & Woernley	1946
		587 ± 2·0	9000 Mc/s.	Lyons, Birnbaum & Kryder	1948
		586·9 ± 2·9		Birnbaum, Kryder & Lyons	1951
	294·1 ± 0·1	588·3 ± 0·2	24000 Mc/s.	Essen & Froome	1951
Oxygen					
	266·3	532·7	*	Rentschler†	1907
		531	0·5 Mc/s.	Watson	1934
		523·3 ± 1·0	1·0 Mc/s.	Hector & Woernley	1946
		532·5 ± 1·3	1·0 Mc/s.	Jelatis	1948
		532 ± 2·0	9000 Mc/s.	Lyons, Birnbaum & Kryder	1948
		530·0 ± 1·9		Birnbaum, Kryder & Lyons	1951
	266·4 ± 0·2	531·0 ± 0·4	24000 Mc/s.	Essen & Froome	1951
Argon					
	279·2	558·5	*	Burton†	1907
	277·3	554·7		Cuthbertson & Cuthbertson	1932
		550	0·5 Mc/s.	Watson	1934
		545·1 ± 0·5	1·0 Mc/s.	Hector & Woernley	1946
		554·2 ± 0·9	1·0 Mc/s.	Jelatis	1948
	277·8 ± 0·2	555·7 ± 0·4	24000 Mc/s.	Essen & Froome	1951
Carbon Dioxide					
		989	0·5 Mc/s.	Watson	1934
		987·5 ± 2·0	1·0 Mc/s.	Hector & Woernley	1946
		988 ± 2·0	9000 Mc/s.	Lyons, Birnbaum & Kryder	1948
		985·5 ± 3·0		Birnbaum, Kryder & Lyons	1951
	494 ± 1·0	988 ± 2·0	24000 Mc/s.	Essen & Froome	1951

* Optical determination, extrapolated to infinite wavelength.
† Quoted by Kaye and Laby (1948).
‡ From a revision of the most accurate determinations.

Note. Our values of $(\epsilon-1)$ are obtained from equation (1) on the assumption that the values of $(\mu-1)10^6$ are 0·4 for air, 1·9 for oxygen and zero for the other gases and for water vapour. The results of other workers are given as published by them although in the microwave determinations the quantity actually measured will have been refractive index and not dielectric constant. The permeability has been allowed for in the values given by Birnbaum, Kryder and Lyons (1951) but possibly not by the other workers.

silica gel was used to remove most of the moisture, thus lengthening the life of the phosphorus pentoxide, but there was some evidence that the gel first absorbed and later emitted other gases, especially CO_2, and thus affected the purity of the gas under test. It was also feared that such absorption might be differential for the constituents of dry air; and although there was no direct evidence of this it is perhaps significant that the standard deviation of the results was reduced by one-half after the gel had been removed from the system. At first higher values of refractive index were obtained when the cavity was filled slowly than when it was filled quickly. This was found to be due to moisture given off from the walls of the Pyrex glass cylinder surrounding the cavity or from the glass tubing in the system. When a tray of pentoxide was placed inside the Pyrex container and near the cavity the same value was obtained from measurements made with rapid and slow filling and from measurements made a few minutes and twelve hours after filling. Carbon dioxide was removed from the gases by passing them through a tube containing soda lime.

§ 5. RESULTS AND ACCURACY

The results of the measurements which have been briefly announced (Essen and Froome 1951) are given in Tables 2 and 3, together with those of a number of other workers, which will be discussed in § 7.

Table 3. Values of n for Unsaturated Water Vapour at 20° c., 10 mm. Hg

$(n-1)\,10^6$	Dipole moment $\times 10^{18}$ e.s.u.	Frequency	Author	Date
2·94		*	Barrell & Sears	1939
62·7	$1{\cdot}842 \pm 0{\cdot}008$	1 Mc/s.	Sanger	1930
$61{\cdot}3 \pm 0{\cdot}4$	$1{\cdot}831 \pm 0{\cdot}006$	0·5 Mc/s.	Stranathan	1935
61·3	1·84	9000 Mc/s.	Crain	1948
62·4	—	3000 Mc/s.	Philips	1950
$60{\cdot}7 \pm 0{\cdot}1$	$1{\cdot}839 \pm 0{\cdot}002$	24000 Mc/s.	Essen & Froome	1951

* Optical determination, extrapolated to infinite wavelength.

The air, nitrogen, oxygen and argon were free from carbon dioxide and the refractive indices are given for 0° c. and 760 mm. Hg, the pressure being measured in millimetres of mercury at 0° c. and standard gravity (760 mm. Hg = 1,013,250 dyne/cm^2). The measurements were made at a mean temperature of 20° c. and a mean pressure of 760 mm. Hg, and the results have been reduced to the standard condition by the extrapolation formula (2), given later in the paper. The measurements on water vapour were made at temperatures between 15° c. and 25° c., and with pressures between 6 mm. Hg and 14 mm. Hg, the result given being obtained from formula (8) which is based on the mean of the experimental values. The standard conditions have in this case been taken as those normally pertaining in a room because water vapour is a polar gas and its extrapolation formula cannot be given with the same confidence as that of the other gases.

A correction of $+3{\cdot}0 \times 10^{-7}$ has been added to all the measured values except that for water vapour to allow for the slight increase in the dimensions of the cavity when the container is evacuated, due to the hydrostatic expansion of the invar walls and end plates.

For the gases other than air and water vapour, 'tank' gases were used. It was found essential to flush the equipment at least eight times when changing

from one gas to another, before taking measurements; and spectroscopically pure gases are not available in large enough containers for this procedure.

The limits of error given in the tables are derived as follows:

(*a*) Air.

Random error: standard deviation of experimental results when reduced to N.T.P.	$\pm 4\times10^{-8}$
Estimated maximum systematic errors: thermometer calibration $\pm 2\times10^{-8}$; barometer calibration	$\pm 4\times10^{-8}$
Possible phase shift errors inherent in circuit	$\pm 4\times10^{-8}$
Invar expansion correction error	$\pm 3\times10^{-8}$
Statistical total =	$\pm 8\times10^{-8}$

Consequently we have adopted an error of $\pm 1\times10^{-7}$, and this should be regarded as being equivalent to a standard deviation.

(*b*) Nitrogen was stated by the suppliers to have less than 1×10^{-6} impurity and the result for this gas is therefore as accurate as that for dry air.

(*c*) Oxygen was stated to have 0·5% nitrogen as an impurity and wider limits have therefore been given to allow for an error of about 100% in the estimation of this impurity.

(*d*) Argon was stated to have 0·2% air as an impurity, so wider limits are again given.

(*e*) Carbon dioxide was stated to have 0·5% air as an impurity and for this gas the standard deviation was also higher than for the other gases, being about $\pm 2\times10^{-7}$. Wider limits are therefore given.

(*f*) For water vapour there is no thermometer error, or invar correction to take into account. Neither is there a systematic pressure error since variations in the setting on the manometer meniscus are included in the experimental spread of the results. The error given is therefore completely represented by the standard deviation. Possible effects due to adsorbed layers of moisture on the walls of the cavity are considered in §7 and it is concluded that they had no appreciable effect on our results.

No mention has yet been made of possible errors due to imperfections in the hybrid junction and to spurious reflections from the waveguide arms and joints constituting the cavity bridge. It has been tacitly assumed that this system is perfect and that the crystal detector current (Figure 1) is simply the vector sum of the wave reflected from the cavity and that from the equally spaced matching stub in the compensating arm of the bridge. In addition to these two components, however, there may be others due to the direct coupling from the input to the detector arm of the junction and to various mismatches along the cavity arm, and along the compensating arm of the bridge. Thus it is seen that the minimum galvanometer deflection corresponding to the resonant setting of the gas measuring cavity is obtained when the vector sum of these five components is zero. The spurious components will not cause any error so long as they remain constant; but since they arise from reflections which are at different distances from the detector they are likely to alter in phase, relative to the wave from the cavity, when the frequency is changed. The minimum galvanometer deflection will then be obtained at a setting of the cavity which is slightly different from the true resonant condition.

The magnitude of this effect was checked for cavity A, which was so well matched at resonance that the compensating stub could be fully withdrawn.

In this case, therefore, there were only four components in the detector arm—the wanted one from the cavity and three unwanted ones. The phase of the reflection from the cavity relative to the others was altered either by inserting near the cavity a short spacer or by leaving there a small air gap. It was estimated that the phase shift produced by these means corresponded to that which would be produced by a frequency change of 200 Mc/s. but there was only a 10–20 kc/s. change in the resonant setting of the cavity. Since in practice the frequency changes were only about 7 Mc/s., it was safe to assume that errors arising from this cause were almost entirely negligible. The allowance included in the estimation of errors is certainly more than adequate.

§6. EXTRAPOLATION FORMULA

In practice the value of the refractive index of air is required at the prevailing conditions of temperature, pressure and humidity, and the results are therefore most usefully expressed in the form of an extrapolation formula. It is sufficient for most purposes to assume that the refractive index varies proportionally with density, that dry air obeys the ideal gas laws and water vapour a simple Debye equation. But if the values obtained are to be accurate to within 1×10^{-7} over a wide range of conditions, more accurate formulae must be used to allow for observed deviations from these simple laws. Dry air, carbon dioxide and water vapour will first be treated separately.

6.1. *Dry Air*

The equation used for reducing our results at a pressure p mm. Hg and temperature $t°$ c. to standard conditions was

$$(n_{t,p}-1)=\frac{(n_{0,760}-1)p}{760{\cdot}606(1+0{\cdot}003661t)}[1+(1{\cdot}049-0{\cdot}0157t)\times10^{-6}p] \quad \ldots\ldots(2)$$

It was found by Barrell and Sears (1939) from optical refractivity measurements on dry air, and it holds good to a very high degree of accuracy over a wide range of temperature and pressure. It is expected to hold with almost equal accuracy for nitrogen, oxygen and argon.

6.2. *Carbon Dioxide*

Carbon dioxide may be assumed to obey the ideal gas laws to the accuracy of our results for this gas, and the equation is simply

$$(n_{t,p}-1)=(n_{0,760}-1)\frac{p}{760}\frac{273}{T} \quad \ldots\ldots(3)$$

where T is the absolute temperature. Absolute zero is assumed to be $-273°$ c.

6.3. *Water Vapour*

Water vapour is a polar gas with an electric dipole moment and therefore obeys Debye's (1929) equation of the form

$$\epsilon-1=p'\left(\frac{A}{T}+\frac{B}{T^2}\right) \quad \ldots\ldots(4)$$

where p' is the pressure that the vapour exerts assuming the 'ideal gas' laws to be obeyed at any fixed temperature. The A term represents the contribution to the dielectric constant of the atomic and electronic polarization, and the B term the contribution of the dipole moment. Our measurements were made over only a small temperature range and do not therefore enable the two constants to be accurately determined. Other measurements made at radio frequencies

are scarcely accurate enough to give a reliable value for A because this term is only about one-twentieth of the B term at these frequencies. It was therefore decided to use the values of A obtained by extrapolation of the optical dispersion formula to infinite wavelengths.

For $p=10$ mm. Hg and $T=293°$ K., Barrell and Sears (1939) give $n-1$ for water vapour as $2{\cdot}944\times10^{-6}$ or

$$\epsilon-1=5{\cdot}888\times10^{-6}=p'A/293. \qquad \ldots\ldots(5)$$

It is also shown in their paper that

$$p'=p(1+2{\cdot}4\times10^{-5}p). \qquad \ldots\ldots(6)$$

This formula is an averaged one; but it is accurate over the range of conditions we stipulate later; thus from (6) and (5) we obtain

$$A=1{\cdot}725\times10^{-4}. \qquad \ldots\ldots(7)$$

This value is believed to be accurate to 0·005. Using it in (4) for each of our measured values of $\epsilon-1$, values of B are calculated. The average value of B was 0·9913. Putting these values of A and B in (4), we obtain from (4) and (6), after some simplification, the working formula:

$$(n-1)\,10^6=\frac{86{\cdot}24p}{T}\left(1+\frac{5748}{T}\right)(1+2{\cdot}4\times10^{-5}p). \qquad \ldots\ldots(8)$$

The mean measured result given in Table 2 is obtained by putting $T=293$ and $p=10$ in this equation. It may be noted that any error in the value assumed for A is largely compensated by the different value of B that is obtained as a result. Thus A could be in error by 40% which is inconceivable, without affecting the validity of the equation within the required accuracy for temperatures up to 60° C. and unsaturated vapour pressures up to 100 mm. Hg. The main interest in using the most accurate obtainable value of A is that, from the value of B, it is possible to calculate the dipole moment of the water molecule.

6.4. *The Dipole Moment of the Water Molecule*

Using Debye's theoretical expression for the B term in (4) and the ideal gas laws, we obtain, converting the pressure p to dynes per cm^2,

$$B=\frac{4\pi\mu^2}{3\boldsymbol{k}^2}\frac{1{\cdot}01325\times10^6}{760} \qquad \ldots\ldots(9)$$

where $\boldsymbol{k}$ is Boltzmann's constant ($1{\cdot}3805\pm0{\cdot}0003\times10^{-16}$ erg deg^{-1}) and μ is the dipole moment.

With $B=0{\cdot}9913$ we obtain

$$\mu=(1{\cdot}839\pm0{\cdot}002)10^{-18}\ \text{E.S.U.} \qquad \ldots\ldots(10)$$

To change this value by 0·002 would need an error of 4% in the A term of Debye's equation compared with the estimated uncertainty of 0·3%.

6.5. *The Extrapolation Equation for Moist Air*

Combining equations (2) and (3) and (8), and inserting the values from Tables 2 and 3, the refractive index of air at a temperature $t°$ C. and atmospheric pressure p becomes

$$(n_{t,\,p}-1)10^6=\frac{0{\cdot}37884p_1}{1+0{\cdot}003661t}[1+(1{\cdot}049-0{\cdot}0157t)10^{-6}p_1]+\frac{1{\cdot}774p_2}{273+t}$$
$$+\frac{86{\cdot}24p_3}{273+t}\left(1+\frac{5748}{273+t}\right)(1+2{\cdot}4\times10^{-5}p_3) \qquad \ldots\ldots(11)$$

where p_1 is the partial pressure of dry, CO_2-free air, p_2 is the partial pressure of CO_2, p_3 is the partial pressure of water vapour and $p = p_1 + p_2 + p_3$. All pressures are expressed in millimetres of mercury at 0° c. at standard gravity.

Equation (11) can be used for all atmospheric conditions with temperatures between −20° c. and +60° c. and unsaturated water vapour pressures less than about 100 mm. Hg, without introducing additional errors in n as great as that of the actual experimental results. It may also be expected to hold for all radio wavelengths above 7 mm. where the strong oxygen absorption line at 5 mm. may begin to have an effect. Water vapour has a weak absorption at 1·35 cm. but it appears from Van Vleck's (1942) theoretical work that this should have an entirely negligible effect upon refractive index. The equation (8) for water vapour should in fact hold for wavelengths down to 3 mm. when the strong absorption in the region of 1 mm. becomes effective. The absorption in this region is over 1,000 times stronger than that at 1·35 cm.

For most practical work, such as radar applications, where the very highest precision is not required, equation (11) can be simplified by assuming that dry air behaves as an ideal gas and that water vapour behaves as ideal at any one temperature. Adjusting the constants to give the correct measured values, equation (11) becomes

$$(n_{t,p}-1)10^6 = \frac{103{\cdot}49p_1}{T} + \frac{177{\cdot}4p_2}{T} + \frac{86{\cdot}26}{T}\left(1+\frac{5748}{T}\right)p_3 \quad \ldots\ldots(12)$$

where $T = 273 + t$.

This equation is still fully accurate at the temperature and pressure of the measurements but introduces an error in n amounting to about 5×10^{-7} at the extremes of the specified range of temperatures and with normal water vapour pressures. For most purposes the effect of the presence of CO_2 can be neglected, since the percentage present in open air is only 0·03 by volume, but 'indoors' it may be several times this amount. Putting $p_2 = 0$, we obtain the familiar form of equation. The values are about 4×10^{-6} lower than those obtained from the equation given by Smith-Rose and Stickland (1943), for normal atmospheric conditions, and 15×10^{-6} lower than those obtained from another commonly used formula.*

The use of these extrapolation formulae involves the measurement of the water vapour pressure of the atmosphere. Some tests were made to check the accuracy with which this could be done by using the ordinary electrically operated 'wet and dry bulb' hygrometer. In these tests it was necessary to avoid the rapid absorption of moisture by the glass walls of the equipment, and rubber tubing was therefore connected directly to holes in the cavity resonator and a continuous slow-moving stream of air taken from the vicinity of the hygrometer was drawn through it until a few seconds before the measurements were made. It was estimated that the accuracy of measuring the vapour pressure was 0·05 mm. Hg, giving, in a total pressure of 10 mm., an uncertainty of 0·5% in the water vapour contribution to refractive index. This corresponds to 3×10^{-7} in the total refractive index; and it was found that the measured values agreed with the calculated values to this accuracy. Thus if precautions are taken to prevent the absorption of the vapour by the walls of the equipment, it is rather more accurate to measure the refractive index of the actual sample than to calculate it from humidity measurements made with an Assmann hygrometer.

* See Foreword to *Meteorological Factors in Radio-Wave Propagation* (London: Physical Society)

§7. DISCUSSION OF THE RESULTS

There have been many previous measurements of the refractive index and dielectric constant of dry air by optical and electrical methods, and there is no need to discuss them all here. The optical values tabulated by Bender (1938) show a total spread in n of 2×10^{-6} but quite recently, since the completion of the work described in this paper, Barrell (1951) has derived a new extrapolated value based on the most recent optical measurements and this value only is given in Table 2. Hector and Woernley (1946) give a list of values of dielectric constants obtained by electrical methods, and the spread of these values is 6×10^{-5}. Many of these earlier results are clearly unreliable and only those of Watson are included in the Table. Hector and Woernley's own results seem to have a rather large systematic error.

It will be seen that Barrell's extrapolated value of n for air is about 4×10^{-7} lower than our measured value. The difference is in part due to the magnetic permeability of oxygen, the effect of which is removed in the derived values of dielectric constant. The discrepancy is then only 3×10^{-7} (equivalent to $1{\cdot}5 \times 10^{-7}$ for n) and this is within the combined experimental error. The radio-frequency value should in any case be slightly greater than the extrapolated optical value, even when allowance has been made for permeability because of the magnetic dipole resonant absorption by oxygen at wavelengths near 5 mm. Van Vleck estimates that the effect of this on the dielectric constant of oxygen is to increase it by 2×10^{-7} giving an increase of 4×10^{-8} in the value for air.

In the extrapolation formula for dry air it has been assumed that the contribution due to permeability varies with temperature in the same way as that due to dielectric constant because, although in fact there will also be a $1/T^2$ term, neglecting this will introduce an error of only 2×10^{-8} at the extremes of temperature given. The error for pure oxygen will, of course, be five times as great, but in either case the errors will be negligible near 20° c.

Van Vleck also estimates that the effect of the water vapour absorption at 1·35 mm. is 1×10^{-4} of the total polarization. The actual effect could be much greater than this before it would invalidate the use of the extrapolation formula over the stated frequency range.

In the radio-frequency range our results agree with those of Watson (1934) obtained at 0·5 Mc/s. within the accuracy of his measurements for all the gases except argon. They also agree well with those of Lyons, Birnbaum and Kryder (1948) and Birnbaum, Kryder and Lyons (1951) obtained by a cavity method at 9,000 Mc/s. and with those of Jelatis (1948) at 1 Mc/s. for oxygen and argon.

The fairly close agreement between the various values for water vapour is satisfactory in view of the extra difficulties met with in the measurement of a vapour. Stranathan (1935), who used a frequency change method at 0·5 Mc/s. discusses the difficulties due to adsorption as the vapour pressure approaches saturation. The refractive index first increases linearly with pressure but then much more rapidly, due, it is assumed, to the sudden formation of a layer of water 100 molecules thick. But Newbound (1949), working in the optical region, states that the thickness of the molecular layer is proportional to vapour pressure and is 100 molecules thick at a pressure of 10 mm. Hg and a temperature of 20° c. Newbound's result is not substantiated by the optical

work of Barrell and Sears (1939) and Cuthbertson and Cuthbertson (1932). In the cavity apparatus the effect of a layer would be much less than in the case of a condenser with a small gap between the plates such as used by Stranathan (1935). The cavity results are therefore likely to be the more reliable and the good agreement obtained suggests that the effect of adsorbed layers, if any, must be very small, and that the values given by the present investigation are accurate within the limits stated.

ACKNOWLEDGMENTS

The work described above has been carried out as part of the research programme of the National Physical Laboratory, and this paper is published by permission of the Director of the Laboratory, and of the Controller, H.M. Stationery Office.

REFERENCES

Barrell, H., 1951, *J. Opt. Soc. Amer.*, **41,** 295.
Barrell, H., and Sears, J. E., 1939, *Phil. Trans. Roy. Soc.* A, **238,** 1.
Bender, D., 1938, *Phys. Rev.*, **54,** 179.
Birnbaum, G., Kryder, S. J., and Lyons, H., 1951, *J. Appl. Phys.*, **22,** 95.
Crain, C. M., 1948, *Phys. Rev.*, **74,** 691.
Cuthbertson, C. and Cuthbertson, M., 1932, *Proc. Roy. Soc.* A, 135, 40.
Debye, P., 1929, *Polar Molecules* (New York : Chemical Catalog Co.).
Essen, L., and Froome, K. D., 1951, *Nature, Lond.*, **167,** 512.
Hector, L. G., and Woernley, D. L., 1946, *Phys. Rev.*, **69,** 101.
Jelatis, J. G., 1948, *J. Appl. Phys.*, **19,** 419.
Kaye, G. W. C., and Laby, T. H., 1948, *Tables of Physical and Chemical Constants* (London: Longmans, Green and Co.), p. 88.
Lyons, H., Birnbaum, G., and Kryder, S. J., 1948, *Phys. Rev.*, **74,** 1210 (A).
Newbound, K. B., 1949, *J. Opt. Soc. Amer.*, **39,** 835.
Philips, W. E., 1950, *Proc. Inst. Radio Engrs.*, **38,** 786.
Pound, R. V., 1947, *Proc. Inst. Radio Engrs., N.Y.*, **35,** 1405 (see also Montgomery, C. G., 1947, *Technique of Microwave Measurements*, Vol. II (New York : McGraw-Hill).
Sanger, R., 1930, *Phys. Z.*, **31,** 306 ; 1932, *Helv. phys. Acta*, **5,** 200.
Smith-Rose, R. L., and Stickland, A. C., 1943, *J. Instn. Elec. Engrs.*, Pt. III, **90,** 12.
Stranathan, J. D., 1935, *Phys. Rev.*, **48,** 538.
Van Vleck, J. H., 1942, *M. I. T. Rad. Lab. Rep.*, No. 43-2.
Watson, H. E., 1934, *Proc. Roy. Soc.* A, **143,** 558.

Alpha-Particle Assay and the Measurement of the Thorium–Uranium Ratio in Radioactive Ores

By D. H. PEIRSON
Atomic Energy Research Establishment, Harwell, Didcot, Berks.

Communicated by D. Taylor; *MS. received 6th February* 1951, *and in amended form* 21*st May* 1951

ABSTRACT. The measurement of the alpha-particle activity of a 'thick' radioactive source containing the natural radioactive series is discussed critically.

Two methods of determining the thorium–uranium ratio are considered for use in ore or mineral assays. The energy discrimination method is simple in procedure and can take account of lack of secular equilibrium between members of a series in the radioactive sample. The beta–alpha coincidence method, making use of the difference in the disintegration constants of radium C′ and thorium C′, is more complicated.

Initial experimental verification of the theory has been obtained. The estimated statistical error in determining the thorium–uranium ratio by the energy discrimination method is $\pm 5\%$ in the region of $Th/U=1$, with a 4% sample (U_3O_8 equivalent concentration) in 4 minutes counting. A similar accuracy is obtainable in the coincidence method with a counting period 10 times greater.

§ 1. INTRODUCTION

Since the range of alpha-particles in naturally occurring radioactive materials is extremely small, of the order of 30 microns, it has been customary to make measurements of activity and alpha-particle range using thin and finely powered samples. In this condition the effect of self-absorption in the sample is thereby made as small as is practically possible so that the collection of the particles by the chamber, fluorescent screen or photographic plate is dependent mainly upon the geometry of the system. Reduction of self-absorption also serves to increase the discrimination of alpha-particle range measurements.

The application of thin-source technique to the routine assay of radioactive minerals or ores raises two serious objections to the method: (i) use of very thin sources implies low count rates, which for samples of low concentration will often be less than the detector background rate; (ii) the preparation of very thin uniform samples of complex ores, usually in powdered form, is in practice very difficult.

In view of these objections the activity of the 'thick' source has been investigated. A thick source of alpha-particles is defined as one of thickness greater than the internal range of the most energetic particle emitted.

§ 2. ALPHA-PARTICLE ASSAY

The alpha-particle activity of a radioactive source has been calculated by Finney and Evans (1935). The main steps in the calculation are repeated in order to indicate restrictions imposed by the dependence upon particle energy of the stopping power of the source and, also, to extend the argument to include some cases of disequilibrium in a radioactive series. The practical effect of self-absorption and disequilibrium upon the measured activity of a source is discussed.

2.1. *Calculation of Alpha-Particle Activity*

In Figure 1, dA represents an elementary portion of collecting area at a distance d from the surface of a semi-infinite radioactive source containing a mono-energetic

alpha-particle emitter. The area dA will receive only particles emitted by that part of the source within a total distance equivalent to the range in air R_a of the alpha-particle.

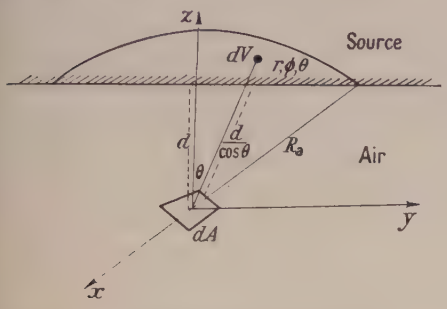

Figure 1. Collection geometry for thick source.

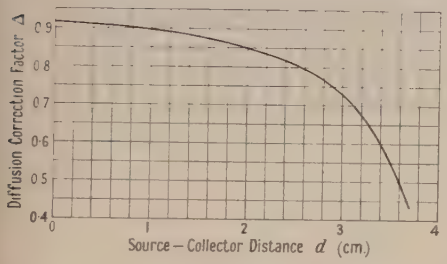

Figure 3. Diffusion correction for radon.

$$C=\frac{NA}{4S}\frac{(R_a-d)^2}{R_a}\Delta, \quad (D=0),$$

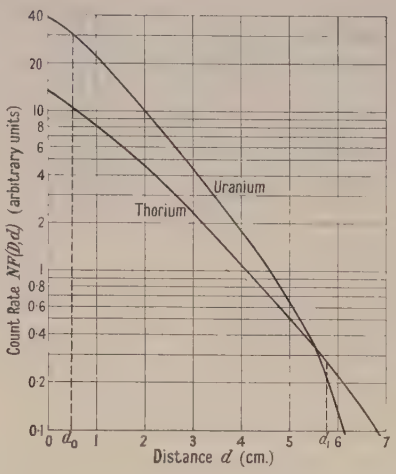

Figure 2. Counting rate plotted against collector distance for uranium (neglecting actinium) and thorium series sources.

$$C=\frac{A}{4S}NF(D, d),$$

$$F(D, d)=\Sigma_1{}^n(R_{an}-D-d)^2/R_{an}-D$$
$$=\Sigma_1{}^n(R_{an}-d)^2/R_{an} \quad (D=0).$$

Then the number of particles per second incident upon dA from an elementary volume dV at (r, ϕ, θ) is given by $(\cos\theta/4\pi r^2)\,dA\,\rho_s\,N\,dV$, where N is the intrinsic activity of source in particles/gm. sec. and ρ_s is the density of the source.

The number of particles per second (count rate) incident upon dA from the whole source is given by

$$dc=\frac{\rho_s N\,dA}{4\pi}\int_V \frac{\cos\theta}{r^2}\,dV. \qquad \ldots\ldots(1)$$

It can be shown after integration that the total count rate over the whole collecting area A is given by

$$c=(NAR_s\rho_s/4R_a)\,(R_a-D-d)^2/(R_a-D), \quad (d \gtrsim R_a-D),$$

where R_s is the range of alpha-particles in the source and D the range in air corresponding to the minimum energy detectable by the collector and associated apparatus.

Extension of the calculation to the case of an ore containing members of a radioactive series emitting particles of air range $R_{a1}, R_{a2} \ldots R_{an}$, gives for the rate of collection of particles from the nth member

$$c_n=\frac{N_nA}{4S}\frac{(R_{an}-D-d)^2}{R_{an}-D},$$

where $S=R_a/R_s\rho_s$ is defined as the mass stopping power of the source.

For the whole series

$$\sum_1^n c_n = \frac{A}{4S} \sum_1^n N_n \frac{(R_{an} - D - d)^2}{R_{an} - D}.$$

Removal of the factor S from within the summation sign is strictly justified only if S is independent of alpha-particle energy. Also, in the integration of (1), the upper limit for r involves the ratio $R_s/R_a (= 1/\rho_s S)$ which is assumed to be independent of the residual energy of the alpha-particle as it emerges from the surface of the source. Beharrel (1949) has found that calculation of S by the Bragg–Kleeman (1905) rule, which takes no account of energy dependence, gives results that are 10% too low for the common rock-forming minerals.

If the series is in equilibrium

$$N_1 = N_2 = \ldots = N_n = N \qquad \ldots\ldots(2)$$

and

$$C = \sum_1^n c_n = \frac{NA}{4S} \sum_1^n \frac{(R_{an} - D - d)^2}{R_{an} - D} = \frac{NA}{4S} F(D, d). \qquad \ldots\ldots(3)$$

The latter general form (3) can apply to source-collector geometries other than the specific case considered above.

In general, a radioactive ore will contain members of both the uranium and thorium series in intimate admixture. The rate of particle collection from such a source is given by the sum of two expressions derived from (3). Provided that the uranium and thorium are closely associated or that the respective particles are otherwise subjected to the same stopping power, then

$$C = C_U + C_{Th} = \frac{N_U UA}{4S} F_U(D, d) + \frac{N_{Th} ThA}{4S} F_{Th}(D, d)$$

$$= \frac{A}{4S} [N_U F_U(D, d) U + N_{Th} F_{Th}(D, d) Th], \qquad \ldots\ldots(4)$$

where N_U, N_{Th} are the specific activities per gramme per second of uranium and thorium and U, Th are the concentrations in gm. per gm. of uranium and thorium in the source.

Theoretical values of $NF(D, d)$ for each series are plotted in Figure 2 as a function of d for the idealized case $D = 0$. A family of curves may be so constructed for varying D.

2.2. *Practical Considerations*

2.2.1. *Self-absorption.* It is apparent from equation (4) that a straightforward alpha-particle assay of a complex radioactive source is dependent not only upon the relative concentrations of uranium and thorium but also upon the particle collection geometry and mass stopping power, i.e. self-absorption. Knowledge of the variation of the last factor with density, atomic weight and grain size is incomplete. A direct method of alpha-particle assay, even for ores containing the uranium or thorium series only, therefore proves unreliable except as an activity comparison method for range of ore samples of similar constitution. Attempts have been made by Finney and Evans (1935) and Nogami and Hurley (1948) to assess the mass stopping power for various types of radioactive ore. These are based upon the absorption rule of Bragg and Kleeman (1905) which states that the product of mass stopping power and the square root of the atomic weight is constant. Application of this rule implies a knowledge of the constituents, in their relative proportions, of the ore sample and would be impracticable in the routine assay of ore samples.

It is desirable that the accuracy of radioactivity assay should be independent of the variation of such absorption factors.

2.2.2. *Diffusion.* The alpha particle activity of a complex source as calculated in §2.1 may be modified by lack of radioactive equilibrium. Owing to the loss by diffusion of the gaseous members (radon, actinon and thoron) of the three radioactive series a different state of equilibrium is reached when the net rate of formation of each is balanced by the loss by diffusion through the surface. A severe physical disturbance such as occurs in grinding will upset equilibrium, creating a transient condition that develops into a state of practical equilibrium after several radioactive half-lives of the diffusing gas. It is estimated that the loss of radon and its products in this manner may cause an error of 10% in the calculated activity of uranium source, although knowledge of the coefficient of diffusion of radon is uncertain. Diffusion of actinon and thoron produced little effect, owing to their much shorter half-lives.

It is possible to demonstrate quantitatively the effect of diffusion upon the count rate–distance relation. In Figure 1 the depth of the elementary volume below the surface of the source is $(r\cos\theta - d)$. It can be shown that the relative deficiency of gas at this depth is given by $\exp\{-(\lambda/f)^{1/2}(r\cos\theta - d)\}$ under the new equilibrium condition, λ being the radioactive disintegration constant and f the coefficient of diffusion (per unit concentration gradient per unit area). The integral (1) is thus modified to give for the diffusing member

$$dc = \frac{\rho_a N\, dA}{4\pi} \int_V \frac{\cos\theta}{r^2} [1 - \exp\{-(\lambda/f)^{1/2}(r\cos\theta - d)\}]\, dV.$$

This may be integrated as before: a correction factor is derived for application to the calculated count rate of the diffusing gas. Factors for the descendents of the diffusing member may be obtained by substituting the appropriate values for R_a. Thus for a uranium ore the loss of activity of the radon descendents will be governed by the radon disintegration constant but dependent upon individual alpha-ranges. The activity calculated for the whole ore is made up of the unmodified contributions of members preceding radon in the series plus the radon and succeeding activities corrected for diffusion. The magnitude of the diffusion effect, for radon only, is illustrated in Figure 3 by plotting the correction factor against source–collector distance.

2.2.3. *Other disturbances of equilibrium.* Chemical or physical changes in past geological time may have upset the natural equilibrium conditions of radioactive ores. For example, the leeching and dissolution of primary uranium minerals by circulating ground waters and the deposition of secondary compounds after transportation in solution may result in considerable disturbances in secular equilibrium. In the case of a secondary deposit with excess radium, provided sufficient time has elapsed to establish a modified state of equilibrium, the condition (2) is changed to

$$\left.\begin{aligned} N_1 = N_2 = \ldots\ldots = N_{r-1} = N, \\ N_r = N_{r+1} = \ldots\ldots = N_n = N \pm N', \end{aligned}\right\}$$

where N_r represents the activity due to the transported member, and provided that the time elapsed is much longer than the half-life governing build-up from the rth to nth members in the series.

Then (3) corrected for disequilibrium becomes

$$C = \frac{A}{4S}[NF(D,d) \pm N'F_r(D,d)], \qquad \ldots\ldots(5)$$

where $$F_r(D,d) = \sum_r^n \frac{(R_{an} - D - d)^2}{R_{an} - D}.$$

§ 3. ENERGY DISCRIMINATION METHOD OF MEASURING THORIUM–URANIUM RATIO (Th/U)

3.1. *Theory*

The influence upon the measured activities of the mass stopping power restricts the use of an alpha-particle assay as a measure of the total active content of an ore or mineral sample (cf. § 2.2.1). For an estimation of the thorium–uranium ratio this difficulty may be removed. For convenience equation (4) may be written $C = (A/4S)[XU + YTh]$ where $X = N_U F_U(D,d)$, $Y = N_{Th} F_{Th}(D,d)$. By the choice of two values of either of the two parameters D or d

$$C_0 = \frac{A}{4S}[X_0 U + Y_0 Th], \quad C_1 = \frac{A}{4S}[X_1 U + Y_1 Th], \quad (C_1 < C_0)$$

and hence $$\frac{C_1}{C_0} = \frac{X_1 U + Y_1 Th}{X_0 U + Y_0 Th}. \qquad \ldots\ldots(6)$$

Since for a source containing the uranium ($Th = 0$) or thorium ($U = 0$) series only, $(C_1/C_0)_U = X_1/X_0$ and $(C_1/C_0)_{Th} = Y_1/Y_0$ respectively, then equation (6) becomes, after substitution,

$$\left.\begin{aligned} &\frac{C_1/C_0}{(C_1/C_0)_{Th} - C_1/C_0} = \frac{X_1 Y_0}{X_0 Y_1 - X_1 Y_0} + \frac{Y_1 Y_0}{X_0 Y_1 - X_1 Y_0}\frac{Th}{U} \\ \text{or} \quad &\frac{C_1/C_0}{C_1/C_0 - (C_1/C_0)_U} = \frac{X_0 Y_1}{X_0 Y_1 - X_1 Y_0} + \frac{X_0 X_1}{X_0 Y_1 - X_1 Y_0}\frac{U}{Th} \\ \text{or} \quad &\frac{C_1/C_0 - (C_1/C_0)_U}{(C_1/C_0)_{Th} - C_1/C_0} = \frac{Y_0}{X_0}\frac{Th}{U}. \end{aligned}\right\} \qquad \ldots\ldots(7)$$

The equations (7), which are similar to that obtained by Finney and Evans (1935), represent alternative forms of the same relation, each is linear in Th/U (or U/Th) and use of a particular form depends upon the availability of thorium or uranium standards or both.

Methods of measuring Th/U may be based upon this relation, thereby discriminating between the alpha-particle range or energy characteristics of the thorium and uranium series. For very weak activities Finney and Evans (1935) used an ionization chamber as detector with absorbers of various thickness: Curie (1946) used a photographic plate and discrimination by individual estimation of path length for this purpose. In the present work, which is primarily directed towards devising a method suitable for routine ore analysis, the scintillation counter is used as the detector. Discrimination is introduced by varying the minimum output pulse amplitude accepted by the counting circuit, i.e. discrimination effectively in terms of the parameter D, the minimum detectable alpha-particle range. In practice this is achieved by simple adjustment of a pulse-amplitude discriminator control and represents a considerable gain in speed and convenience compared with the previous methods.

It should be noted that a determination of Th/U by the method outlined may only be attempted when the unknown sample is known to be in equilibrium. Alternatively, it is possible in a range of samples to measure disequilibrium of a given type provided Th/U is constant. Proceeding as before in the simple case of an uranium series sample with no thorium present ($Th=0$) the disequilibrium equation (5) gives three alternative equations similar to (7) of the form

$$\frac{C_1/C_0-(C_1/C_0)_U}{(C_1/C_0)_M-C_1/C_0}=K\frac{M}{U} \text{ etc.,} \qquad \ldots\ldots(8)$$

where M is the concentration gm. per gm. of radium (say) excess or deficit compared with the natural equilibrium amount, $(C_1/C_0)_M$ is the count ratio for a sample containing radium and its descendents only and K is a constant. Equations (7) and (8) may be interpreted qualitatively for uranium ore samples that are either out of equilibrium or contain thorium but not both. Thus, if the count ratio C_1/C_0 is greater than that of a standard sample containing the uranium series known to be in equilibrium, then the unknown sample contains thorium or an excess of radium. If C_1/C_0 is smaller than for the standard then the unknown has a radium deficit.

In the general case of course, the unknown sample will be out of equilibrium and also contain thorium. It is possible that by taking a third value of either of the parameters D or d, the ratios Th/U and M/U might be determined uniquely in the general case. In the present work, however, measurements of disequilibrium and Th/U are considered separately and simultaneous determinations of the two ratios in a single ore have not been attempted.

3.2. *Apparatus and Procedure*

The apparatus used in making Th/U measurements by this method comprises a scintillation counter, linear amplifier, pulse-amplitude discriminator and scaling unit.

The scintillation counter consists of a silver-activated zinc sulphide (Levy and West G 86) screen and an RCA type 931A photo-multiplier operated at a final anode voltage of 1,000. This is followed by a linear amplifier (AERE type 1008) operated between the gain ranges 160 to 1,600, having a gain stability of about 0·5%; the pulse-amplitude discriminator (AERE type 1028) is set in conjunction with the amplifier gain control. The scaling unit used was a modified Cinema-Television type UC2A.

The discriminator is employed as a means of effectively varying the minimum detectable alpha-particle range D. Direct conversion of discriminator readings in terms of D and the computation of the constants of (7) are undesirable and unnecessary. Such computation, as carried out by Finney and Evans (1935), involves the evaluation of the function $F(D, d)$ for each value used of D and d and demands a precise knowledge of the geometry of the alpha-particle counter. The constants of (7) are best determined by calibration with sources of known Th/U.

With collecting and source areas of 20 cm² and a source-collector distance of 2 mm. the overall sensitivity of the apparatus is such that 1% uranium source will give about 1,500 counts per minute: under these conditions the photo-multiplier 'noise' count is about 100 per minute. Alternatively by reducing the amplifier gain so that the noise count becomes negligible the sensitivity is reduced to 500 counts per minute for a 1% uranium source.

3.3. *Experimental Results and Discussion*

A series of ore samples was prepared from pitchblende (70% U_3O_8) and thorium oxide in varying proportions. These samples, diluted with powdered quartz to assay roughly 4% U_3O_8 equivalent concentration provided a range of Th/U values at a uniform density. The count ratio functions are plotted against Th/U in Figure 4, for two settings of the pulse-amplitude discriminator, and demonstrate initial verification of equation (7).

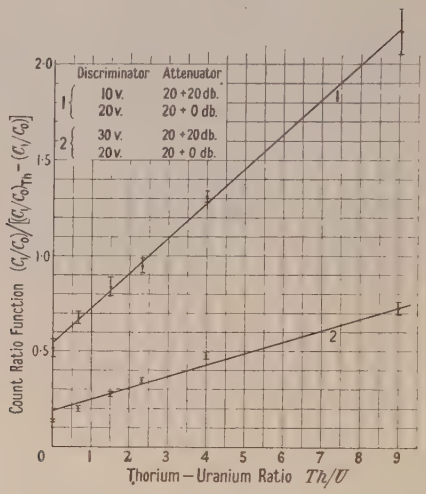

Figure 4. Count ratio function plotted against thorium–uranium ratio.

Another series of ore samples was prepared from separate pitchblende and monazite (9% ThO_2, 0·35% U_3O_8) sources diluted with varying proportions of powdered lead and magnesium oxides to give a range of density variation at values of Th/U of 0 and approximately 25. According to equation (6) the count ratio C_1/C_0 should be independent of density. With the ore samples used C_1/C_0 was found to increase with decrease of bulk density at both Th/U values. In particular this was due to decrease in C_0, as predicted by equation (3), but a disproportionately smaller decrease in C_1.

Closer inspection of these samples showed a range of grain size in the inactive materials of from 4 to 80 microns. The layers in and near the surface, as in the bulk of the sample, consist of mixed active and inactive grains. Since the internal range of the most energetic alpha-particle is about 50 microns, particles from submerged active grains will be wholly or in some cases partly absorbed by adjacent inactive grains. The partial absorption is determined by the average stopping power of the two types of inactive grain. Because of the range of grain sizes this absorption may act selectively such that the particles of longer range as measured by C_1 possibly suffer proportionately less absorption than those of shorter range which are included in the measurement of C_0. The decrease of bulk density is achieved by increasing the proportion of magnesium oxide, thereby increasing the average mass stopping power of the inactive dilutant grains. It is conceivable that the increase in mass stopping power will account for the observed variation of C_1/C_0 with density.

This explanation has not yet been tested experimentally, but if valid, it follows that the minimum grain size in a heterogeneous ore sample should be greater

than 50 microns, i.e. each grain, active and inactive, should represent a thick source with respect to the alpha-particles emitted within the sample.

As a further check of a possible density effect a careful comparison was made of pitchblende (70% U_3O_8) and davidite (9% U_3O_8) samples known to contain negligible amounts of thorium. The intrinsic specific gravities of these minerals are respectively 8 and 4·5. The count ratios C_1/C_0 of the two samples were identical over the practical range of pulse-amplitude discriminator setting, and hence independent of the markedly different densities and concentrations of the two samples.

The count ratio C_1/C_0 was next shown to be independent, for all practical pulse-amplitude discriminator settings, of the grain size in samples of davidite and torbernite (*c.* 60% U_3O_8, zero ThO_2). Ranges of grain sizes used were: below 76 microns, 76–104 microns, 104–152 microns, extending, in the case of davidite, up to 850 microns.

Count ratio measurements upon a variety of minerals are presented in Table 1. Values of the ratio C_1/C_0 were obtained with a statistical accuracy of $\pm 1{\cdot}5\%$. Taking the pitchblende sample as standard the results are given as a simple difference of count ratios. As the thorium–uranium ratio had not been determined for these ores by chemical or independent radiometric methods quantitative comparison is impossible. The negative count ratio difference for uraninite and torbernite indicates an apparent deficiency of radium.

Table 1. Count Ratio Measurements upon Natural Mineral Samples

Sample No.	Mineral	$\frac{C_1}{C_0}$	$\frac{C_1}{C_0} - \left(\frac{C_1}{C_0}\right)_U$	Remarks
265	Pitchblende	0·0647	0	Uranium
266	Uraninite	0·0625	−0·0022	Uranium
267	Thorite	0·1130	0·0483	Thorium, possible traces of uranium
252	Torbernite	0·0582	−0·0065	Uranium, probable radium deficiency
249	Uranothorite	0·0679	0·0032	Thorium, some uranium
238	Uranothorianite	0·0799	0·0152	Uranium and thorium in similar quantities

Grain size of each sample 104 to 152 microns.

As an estimate of the statistical accuracy of the energy discrimination method, the thorium–uranium ratio of a sample of activity equivalent to 4% U_3O_8 may be measured with error of less than $\pm 5\%$ in a counting time of 4 minutes. This excludes time devoted to counting any standard samples, and applies in the region of $Th/U = 1$.

§ 4. THE BETA-ALPHA COINCIDENCE METHOD OF MEASURING Th/U

4.1. *Theory of Method*

An inspection of the various and widely spaced half-lives (1 μsec. to 10^{10} years) of the uranium and thorium series suggests a means of discriminating between the two series. For practical reasons the shorter half-lives are most amenable to treatment by electronic circuits: the disintegrations considered here will be those

of radium C′ (140 μsec.) and thorium C′ (0·3 μsec.). By virtue of the Geiger-Nuttall relation this discrimination by half-life may be considered complementary to the method of discrimination by energy or range.

Each of the above disintegrations produces an alpha-particle and is preceded by a beta-disintegration, from radium C and thorium C respectively. Assuming the source to be presented simultaneously to alpha- and beta-particle counters, it is therefore necessary to design two gate circuits to be initiated by the beta-particle pulses and to accept alpha-particle pulses whilst in the open condition. The open periods or gate widths are fixed to enable mainly radium C′ alpha-particles to be counted through the 'wide' gate and mainly thorium C′ alpha-particles through the 'narrow' gate and in magnitude will be similar to the respective half-lives. Thus each gate admits both types of related coincidences together with unrelated or accidental coincidences, the latter being calculated from the total alpha- and beta-particle counts.

The related coincidence counts may be calculated by considering the probabilities of ThC′ and RaC′ disintegrations occurring within a time $d\tau$. These are respectively $\lambda_{\mathrm{Th}} \exp(-\lambda_{\mathrm{Th}}\tau)\, d\tau$ and $\lambda_{\mathrm{U}} \exp(-\lambda_{\mathrm{U}}\tau)\, d\tau$ where λ_{Th} and λ_{U} are the respective disintegration constants. The number of ThC′ alpha-particle counts in a counting period t, each occurring within τ of a related beta-particle count is

$$mThtk_{\mathrm{Th}} \int_0^{\tau} \lambda_{\mathrm{Th}} \exp(-\lambda_{\mathrm{Th}}\tau)\, d\tau = mThtk_{\mathrm{Th}}\{1 - \exp(-\lambda_{\mathrm{Th}}\tau)\}, \quad \ldots\ldots(9)$$

where m is the mass of the source (gm.) and k_{Th} is an instrumental constant dependent upon the beta-particle activity of the ThC and the counting efficiency for ThC beta- and ThC′ alpha-particles. It is assumed that the ThC present is in equilibrium with a mass mTh of thorium. Similarly the number of RaC′ alpha-particle disintegrations in a counting period t each occurring within τ of a related beta-particle disintegration is

$$mUtk_{\mathrm{U}}\{1 - \exp(-\lambda_{\mathrm{U}}\tau)\}, \quad \ldots\ldots(10)$$

where k_{U} corresponding to k_{Th} is an instrumental constant for the uranium series disintegrations.

Each coincidence gate admits related coincidences arising from both ThC′ and RaC′ disintegrations plus unrelated or accidental coincidences. If P is the total alpha-particle count and Q the total beta-particle count the number of accidental coincidences admitted by the two gates during a counting period t are respectively

$$PQ\tau_1/t \quad \text{and} \quad PQ\tau_2/t, \quad \ldots\ldots(11)$$

where τ_1 is the narrow gate width and τ_2 the wide gate width. By combination of (9), (10) and (11) the total narrow coincidence count V and wide coincidence count W are given by

$$\left.\begin{aligned} V &= mUtk_{\mathrm{U}}\{1 - \exp(-\lambda_{\mathrm{U}}\tau_1)\} + mThtk_{\mathrm{Th}}\{1 - \exp(-\lambda_{\mathrm{Th}}\tau_1)\} + PQ\tau_1/t, \\ W &= mUtk_{\mathrm{U}}\{1 - \exp(-\lambda_{\mathrm{U}}\tau_2)\} + mThtk_{\mathrm{Th}}\{1 - \exp(-\lambda_{\mathrm{Th}}\tau_2)\} + PQ\tau_2/t. \end{aligned}\right\} \ldots(12)$$

The ratio of total coincidence counts, each corrected for accidentals, is given by

$$\frac{V'}{W'} = \frac{V - PQ\tau_1/t}{W - PQ\tau_2/t} = \frac{k_{\mathrm{U}}\{1 - \exp(-\lambda_{\mathrm{U}}\tau_1)\}U + k_{\mathrm{Th}}\{1 - \exp(-\lambda_{\mathrm{Th}}\tau_1)\}Th}{k_{\mathrm{U}}\{1 - \exp(-\lambda_{\mathrm{U}}\tau_2)\}U + k_{\mathrm{Th}}\{1 - \exp(-\lambda_{\mathrm{Th}}\tau_2)\}Th}.$$

As in equation (6), this may be written in the form

$$\frac{V'}{W'} = \frac{x_1 U + y_1 Th}{x_2 U + y_2 Th},$$

where $x = k_U\{1 - \exp(-\lambda_U \tau)\}$ and $y = k_{Th}\{1 - \exp(-\lambda_{Th}\tau)\}$ with appropriate suffixes.

Continuing as in § 3.1,

$$\frac{V'/W'}{(V'/W')_{Th} - V'/W'} = \frac{x_1 y_2}{x_2 y_1 - x_1 y_2} + \frac{y_1 y_2}{x_2 y_1 - x_1 y_2}\frac{Th}{U} \text{ etc.} \quad \ldots\ldots(13)$$

The coincidence count ratio function is thus linearly related to Th/U.

To minimize counting errors, optimum gate widths may be calculated to give the smallest standard deviations in V' and W'. The optimum values of τ_1 and τ_2 may be expressed in terms of the ratios of related to accidental coincidences $V't\,PQ\tau_1$, $W't/PQ\tau_2$. The magnitude of these ratios will depend upon experimental conditions, in particular upon the source–counter geometry.

4.2 *Apparatus and Procedure*

The alpha-particle counter consists of a rectangular screen (area 32 cm²) coated with a layer of activated zinc sulphide and backed by three 931A photomultiplier tubes connected in parallel. The ore samples, evenly spread on shallow copper trays are inserted immediately beneath the screen. The beta-particles are counted through the 0·005 in. base of the tray by two Twentieth-Century type B6 counter tubes situated underneath the tray. The combined counter is mounted in a light-tight box.

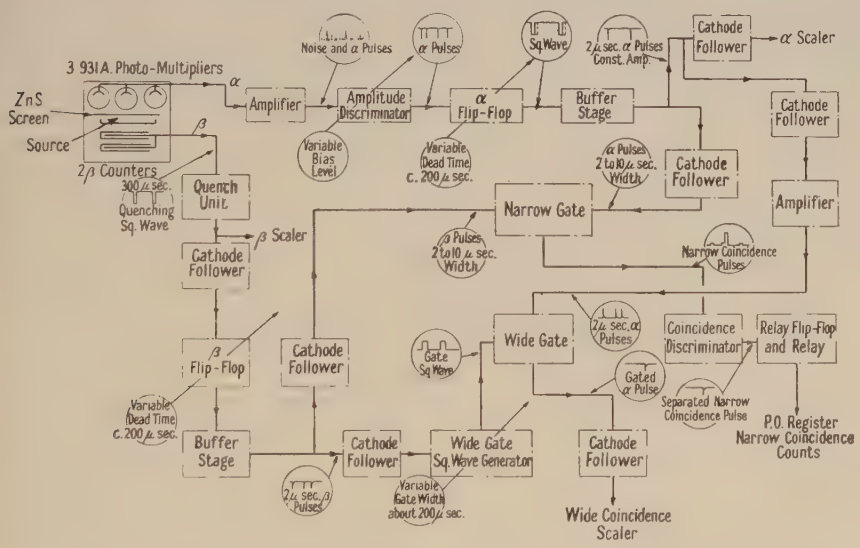

Figure 5. Schematic diagram of beta–alpha coincidence counting equipment.

As illustrated in Figure 5, the resultant alpha-particle pulses pass through a linear amplifier (type 1008) and pulse-amplitude discriminator (type 1028) and thence to the two gate circuits and the alpha-particle scaling unit. The beta-particle pulses pass via a quenching circuit (type 1014) to the beta-particle scaler and to the gate circuits. The narrow gate consists of a coincidence pair, width

being determined by a delay line, and is followed by an amplitude discriminator and Post Office register. Since this type of circuit may be initiated by pulses from both alpha- and beta-particles, the resolving time for accidental coincidences is twice the gate width. Equation (12) should be interpreted accordingly. The wide gate circuit consists of a square wave generator initiated by beta-particle pulses controlling a gating valve which admits alpha-particle pulses to a scaling unit during open periods. The particular experimental conditions gave optimum values of 0·43 and 115 μsec. for the narrow and wide gate widths respectively. The narrow gate width was increased to 1 or 2 μsec. to lessen the effect of variable rise time in the alpha-scintillation counter pulses, the amplitudes of which are dependent upon the energy of the incident alpha-particles. The gate widths could be approximately calibrated by an oscilloscope or more accurately by the conventional method using separate sources of alpha- and beta-particles. A time-lag between the passage of an initiating beta-particle and the operation of a beta-counter tube may modify the practical definition of the gate widths. This modification corresponds to lower limits, in the integrals leading to (9) and (10), equal to the average time-lag. The effect of counter tube time-lags in coincidence counting has been discussed by Rotblat (1941): in the case of the B6 counter tubes the lag may be about 0·1 μsec. and is accounted for by calibrating the apparatus with known standard ore samples.

The equations (12) indicate that the errors in coincidence counting may be decreased by reducing the ratio of accidental to related coincidences. Ideally this ratio approaches a minimum when the source thickness becomes indefinitely small. In practice this degree of thinness is not attainable and the ore samples are spread as finely as possible on the trays.

Except for very active samples the coincidence count rates are low: as long counting times are required for reasonable statistical accuracy, it is imperative to maintain stable conditions throughout the coincidence counting equipment. Most trouble was experienced in the alpha channel owing to a drifting count rate and was traced to variations in the type CV188 neon tube used for stabilization in the amplitude discriminator. The tube was replaced by a Mullard type 85A1, drift in alpha-particle counting rate being reduced to 1% per day. As an additional precaution the alpha-particle counting rate was continuously monitored by a stable counting ratemeter and pen recorder.

4.3. *Experimental Results and Discussion*

Equation (13) was tested with a range of ore samples containing pitchblende and thorium oxide in varying proportions. The experimental results obtained are illustrated by the graph of Figure 6, in which the coincidence count ratio function is plotted against the uranium–thorium ratio. The detailed coincidence counts are listed in Table 2. The range of samples was similar to but richer (to provide higher counting rates) than those used in the energy discrimination measurement of §3.3. In consequence there is an appreciable and progressive bulk density variation from 1·8 to 2·2 gm/cm^3 over the range of samples.

In addition to possible variable density effects in alpha-particle assay, similar to those encountered in the energy discrimination method, the variation of beta-particle self-absorption may present similar difficulties on account of the different maximum energies of the related beta-particles from RaC (3·15 Mev.) and ThC (2·2 Mev.). Fortunately, sample thicknesses are necessarily small

compared with the beta-particle ranges and this effect may introduce no serious errors in beta-particle counting.

With the present experimental arrangement the statistical counting accuracy is such that the thorium–uranium ratio may be measured to within $\pm 5\%$ for a sample of equivalent uranium concentration of 4% after 50 minutes counting (these figures apply in the region of $Th/U = 1$). An earlier, more sensitive, counter arrangement (consisting of six 931A photo-multiplier tubes in an outer ring

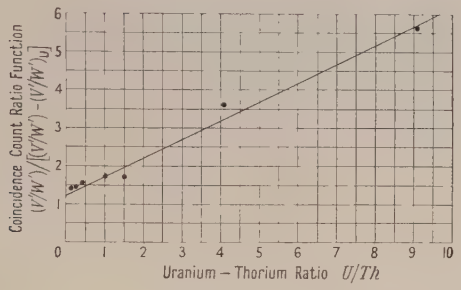

Figure 6. Coincidence count ratio function plotted against uranium–thorium ratio.

concentric with a cylindrical scintillation screen which surrounded the sample deposited upon tracing cloth fitted over a single inner cylindrical beta-particle counter tube) was rejected as too inconvenient and too liable to contamination for routine use. A more practicable system inverts the present counter arrangement; the beta-particle counter tubes are placed above the open tray which has a transparent Perspex base and contains sample and scintillation screen, both being considered expendable. The E.M.I. photo-multiplier with the larger cathode area registers the alpha-particle scintillations through the base of the tray.

Table 2. Coincidence Count Ratio Functions

Sample No.	$\frac{U}{Th}$	V	W	V'	W'	$\frac{V'}{W'}$	Φ
—	∞	—	—	—	—	0·0900*	—
5	9·1	359	9377	199	1814	0·1094	5·63
6	4·0	429	10048	260	2083	0·1250	3·56
8	1·5	823	12604	616	2848	0·2163	1·71
9	1·0	807	12491	602	2821	0·2134	1·73
11	0·43	1246	15953	990	3873	0·2557	1·54
14	0·25	1741	16511	1499	5081	0·2949	1·43
15	0·11	2599	17427	2383	7237	0·3292	1·38

* By extrapolation.

Counting time $t = 50$ minutes; gate widths : $2\tau_1 = 2{\cdot}39 \pm 0{\cdot}06 \times 10^{-6}$ seconds;
$\tau_2 = 115{\cdot}0 \pm 0{\cdot}4 \times 10^{-6}$ seconds; $\Phi = (V'/W')/[V'/W' - (V'/W')_U]$.

It is estimated that such an arrangement should measure 1% samples to the same accuracy and within the same time as above. A further improvement in statistical accuracy is possible by delaying the operation of the wide gate by a few microseconds so that no related coincidences from ThC′ disintegrations are admitted.

Despite the initial satisfactory results reported above further development of the beta–alpha coincidence method has been discontinued as it was felt the method and apparatus are too complicated for the purposes of routine geological assay. Any future work would include consideration of a possible density effect, extension of the measurements to natural mineral samples and simplification and compression of the circuit and counting arrangements.

§ 5. CONCLUSION

Two methods of thorium–uranium ratio measurement in radioactive minerals and ores have been developed and tested experimentally. Both methods provide satisfactory counting accuracies using less than 1 gm. of sample, comparing favourably in this respect with beta- and gamma-methods. Comparing the two, the energy discrimination method is much simpler and more straightforward than the beta–alpha coincidence method, which involves greater complication of circuits and apparatus to an extent that probably precludes use in routine assay.

Systematic errors may arise due to variations in sample density, to diffusion and to equilibrium disturbance. The effect of density variations is likely to be most marked in the case of heterogeneous ores. Investigation of this effect is incomplete but for the moment errors in estimating the thorium–uranium ratio in this type of ore are reduced by calibrating with standard samples of similar density. Diffusion errors are minimized by similar treatment of unknown and standard samples during grinding and preparation. The effect of other disturbances of equilibrium on the energy discrimination method has been indicated and in certain cases it is possible to measure the amount of the disturbance.

Estimated statistical errors in the determinations of Th/U are: energy discrimination method: $\pm 5\%$ in a 4% (U_3O_8 equivalent concentration) sample in 4 minutes counting; beta–alpha coincidence method: $\pm 5\%$ in a 4% (U_3O_8 equivalent concentration) sample in 50 minutes counting. These figures apply in the region of $Th/U = 1$.

ACKNOWLEDGMENTS

The work contained in this paper was carried out as part of the programme of the Electronics Division, Atomic Energy Research Establishment, Harwell. Acknowledgments are due to Dr. E. Franklin for many valuable discussions, to Mr. C. Sharpe for contributions to the design and construction of the coincidence circuits and to Miss J. Martin who carried out most of the counting. Mr. S. H. U. Bowie of the Geological Survey prepared the mineral samples and advised on the geology of the problem.

This paper is published with the permission of the Director of the Atomic Energy Research Establishment and of the Controller, H.M. Stationery Office.

REFERENCES

Beharrel, J., 1949, *Trans. Amer. Geophys. Un.*, **30**, 333.
Bragg, W. H., and Kleeman, R., 1905, *Phil. Mag.*, **10**, 318.
Curie, I., 1946, *J. Phys. Radium*, **7**, 313.
Finney, G. D., and Evans, R. D., 1935, *Phys. Rev.*, **48**, 503.
Nogami, H. H., and Hurley, P. M., 1948, *Trans. Amer. Geophys. Un.*, **29**, 335.
Rotblat, J., 1941, *Proc. Roy. Soc.* A, **177**, 260.

The Trajectories of Heavy, Solid Particles in a Two-Dimensional Jet of Ideal Fluid Impinging Normally upon a Plate

By C. N. DAVIES and MARY AYLWARD
London School of Hygiene and Tropical Medicine, Keppel Street, London W.C.1

MS. received 1*st March* 1951

ABSTRACT. An expression is derived for the flow field in a two-dimensional jet of ideal fluid impinging normally upon a plate situated at an arbitrary distance from a parallel sided orifice. Numerical data are given when the orifice is at an infinite distance and in three other cases. In each example the trajectories of solid particles carried by the fluid are calculated by a stepwise method, and the conditions determining whether a particle will strike the plate or not are found.

§1. INTRODUCTION

The problem discussed in this paper arose in connection with the study of dust-sampling instruments in which particles are deposited from dusty air, on account of their mass, when an air jet is directed on to a plate. An experimental investigation has been made using different kinds of particles, from $\frac{1}{2}$ to 10 microns in diameter, and jets ranging from low-velocity slits, several millimetres wide, down to small orifices in which the air approached the speed of sound.

The experiments enabled practical information to be collected about the design of the jet, the adhesion of dust to the precipitation plate and the break-up of particles on impact, as well as other factors. To assist in interpreting the experimental results it was considered worth while to explore, theoretically, the performance of an idealized impingement system; this would make clear and definite the purely dynamical factors involved and would set up a criterion of efficiency for the collection of particles against which real apparatus could be compared.

The equations of motion of a massive particle moving in a fluid have been solved by G. I. Taylor (1940) for conditions near a stagnation point where the streamlines of fluid flow approximate to rectangular hyperbolae. He followed the idea of Albrecht (1931) in considering the fluid ideal, that is, non-viscous, as far as the flow field was concerned, but taking it as viscous relative to the particles so that the drag upon them could be calculated by Stokes' law. The particles were assumed to be massive points, creating negligible disturbance, whose size only came into the expression for their drag.

In the dust-sampling instrument, however, the air jet has finite width, while the distance of the jet orifice from the plate is variable and exerts an important influence upon performance.

The two-dimensional flow field for an ideal fluid emerging from a parallel-sided opening at an arbitrary distance from a plate can be calculated by a conformal representation method. Since the jets in dust-sampling instruments are frequently slit-shaped, it seemed that this method would give as close an approach to real conditions as could be expected, while preserving a rigid dynamic definition. The complexity of the expressions derived in this way for the flow field made it clear that no direct solution of the particle equations would be possible on the lines of Taylor's attack on the simpler problem.

Accordingly, the particle trajectories were calculated step by step after the flow fields had been fully computed from theoretical formulae.

Discrepancies between the computed and the real flows must arise on account of the viscosity and compressibility of air, the contour of the jet intake and its spread due to turbulence. In the theoretical work the air stream is supposed to be laminar and to flow with uniform velocity U_0 between parallel planes which terminate at the slit orifice at distance d from the plate (Figure 1); the stream then spreads out symmetrically against the plate and rises to velocity V_0 at right angles to the original flow.

In practice, the velocity at the walls of the jet and on the surface of the impingement plate is zero. A velocity gradient therefore exists adjacent to the solid boundaries, and the velocities at infinity are not constant and equal to U_0 and V_0 across the incident and deflected streams as assumed.

The Reynolds' numbers of the jets in dust-sampling instruments are usually high, and in most cases the stream approaches the orifice between converging walls. These circumstances favour the existence of a fairly flat velocity contour across the jet section together with a thin boundary layer. It is considered that ideal fluid theory should provide a reasonable approximation in this respect. The existence of a boundary layer along the plate is probably of little significance.

Converging airflow also tends to inhibit turbulence in the stream approaching the orifice. When the jet emerges, the boundary layer forms a region of discontinuity between the rapidly flowing jet and the stagnant air outside. Ultimately, therefore, it will roll up into vortices and give rise to an increasing zone of turbulence in the outer parts of the jet. This behaviour was observed in one type of instrument, but seemed to have little effect on the dynamics of particle impingement.

Other possible causes of difference between theory and experiment, which are related to fluid mechanics, are the compressibility of air and the existence of a contracted vein outside the orifice. In general, however, it was found that the most striking deviations of the experimental results were due to particles shattering on impact with the plate or else failing to adhere.

The assumption of Stokes' law of resistance in calculating the particle trajectories is a close approximation unless the relative motion of particle and stream becomes too great. A correction can be introduced by using the known relationship between Reynolds' number and drag coefficient for spheres; since the velocity difference is not constant the drag will, in fact, not be given accurately, but for spheres representing dust particles error on this account should be small. Diffusion of particles is quite negligible when they exceed diameters of about 0·2 micron in systems like those considered, and no account need be taken of it.

In the theoretical work the particle was assumed to start with the stream some distance upstream of the orifice. Actually, heavy particles lag behind the stream owing to the acceleration of the air approaching the jet, but discussion of such points is beyond the scope of the present paper.

§ 2. THE FLOW FIELD IN A TWO-DIMENSIONAL JET OF IDEAL FLUID IMPINGING NORMALLY UPON A PLATE

Let $z = x' + iy'$. Then the boundaries of the parallel-sided jet AB, A'B' and the plate DED' are shown on the z plane in Figure 1 with the origin at E and the x' axis along EF, which is also an axis of symmetry. The width of the jet is $AA' = BB' = h$, and the distance of the orifice from the plate is d.

The jet emerges and spreads sideways over the plate, being bounded by the free streamlines BC, B′C′ along which the pressure, and therefore the velocity, is constant. AFA′, CD and C′D′ are at infinity.

At AA′ the stream velocity is $-U_0$, at CD it is V_0 and at C′D′ it is $-V_0$. Let $V_0/U_0=\alpha$. From continuity, $CD=C'D'=h/2\alpha$.

If the pressure at AA′ exceeds that outside the free streamline by an amount P, then equation of the potential energy at AA′ to the total energy at CD, C′D′ gives $PhU_0=\frac{1}{2}\rho(V_0{}^3h\,\alpha-U_0{}^3h)$, where ρ is the density of the fluid, so that $P=\frac{1}{2}\rho U_0{}^2(\alpha^2-1)$. Since $P\geqslant 0$, $\alpha\geqslant 1$. When d is infinite, $\alpha=1$ and BB′ coincides with AA′; otherwise, for a finite value of d, $\alpha>1$.

If U' and V' are the resolutes of the velocity q parallel to x' and y', then $U'=q\cos\theta$, $V'=q\sin\theta$. If ϕ is the velocity potential and ψ the stream function, then $U'=-\partial\phi/\partial x'$, $V'=-\partial\phi/\partial y'$, and $U'=-\partial\psi/\partial y'$, $V'=\partial\psi/\partial x'$. The assignment of ideal properties to the fluid, implying volume continuity and zero vorticity, leads to $\nabla^2\phi=\nabla^2\psi=0$. Thus ϕ and ψ are conjugate functions obeying the Cauchy–Riemann conditions, so that we can put $w=\phi+i\psi=f(x'+iy')$.

We now transform the boundaries in the z plane to the w plane. Let $\phi=0$ at E, then ϕ tends to ∞ at AA′ and to $-\infty$ at CD, C′D′. Let $\psi=0$ along FED, FED′, then $\psi=U_0h/2$ along ABC and $-U_0h/2$ along A′B′C′. The w plane is shown in Figure 2.

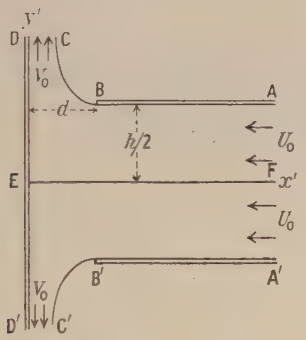

Figure 1. z plane.

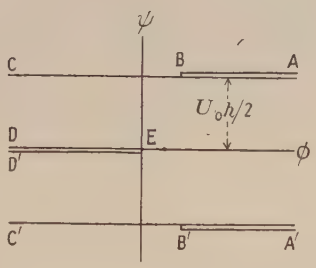

Figure 2. w plane.

Since the boundaries of flow are now straight lines they constitute a polygon with vertices ABCDED′C′B′A′. The interior of this polygon can be mapped on the positive half of a ζ plane, so that the vertices lie at corresponding points along the real axis of ζ, by applying the Schwarz–Christoffel theorem. Proceeding, let E fall at $\zeta=0$, C′D′ at $\zeta=1$, CD at $\zeta=-1$, etc., as shown in Figure 3. Then $dw/d\zeta=K(\zeta+1)^{-1}\zeta(\zeta-1)^{-1}$, which, from a consideration of Figures 2 and 3, integrates to

$$\zeta^2=1-\exp(aw), \qquad \ldots\ldots(1)$$

where $a=2\pi/U_0h$.

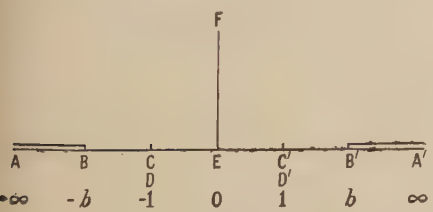

Figure 3. ζ plane.

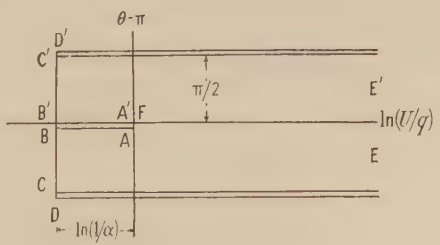

Figure 4. Ω plane.

By means of the Kirchhoff transformation a relation can be obtained between dw/dz and ζ.

Let $$\Omega = \ln (U_0 dz/dw). \qquad \ldots\ldots (2)$$

Now it can be shown that $-dw/dz = U' - iV' = \overline{Q} = qe^{-i\theta}$, where $Q = U' + iV'$; so that $\Omega = \ln (U_0/q) + i(\theta - \pi)$. This relationship enables the boundaries to be plotted on the Ω plane (Figure 4), where they again appear as straight lines since q is constant along BC, B′C′. A further application of the Schwarz–Christoffel theorem then maps the interior of the polygon in the Ω plane on to the ζ plane with the vertices as before. Hence

$$d\Omega/d\zeta = K(\zeta + b)^{-1/2}(\zeta + 1)^{-1/2}\zeta^{-1}(\zeta - 1)^{-1/2}(\zeta - b)^{-1/2},$$

from which, by integration, $\Omega = \ln \{(\zeta^2 - b^2)^{1/2} + b(\zeta^2 - 1)^{1/2}\} - \ln \{\alpha\zeta(b^2 - 1)^{1/2}\}$, where $b = (\alpha^2 + 1)/(\alpha^2 - 1)$, for the field A′B′C′D′E, where $\zeta > 0$; since $1 < b < \alpha$, $\alpha > 1$.

Eliminating Ω between this expression and (2) we find

$$Udz/dw = (\alpha^2 - 1)\{(\zeta^2 - b^2)^{1/2} + b(\zeta^2 - 1)^{1/2}\}/2\alpha^2\zeta. \qquad \ldots\ldots (3)$$

Also, from (1), $dw/d\zeta = 2\zeta/a(\zeta^2 - 1)$. Eliminating dw,

$$U_0 z = \{(\alpha^2 - 1)/a\alpha^2\}\{\int b d\zeta/(\zeta^2 - 1)^{1/2} + \int (\zeta^2 - b)^{1/2} d\zeta/(\zeta^2 - 1)\}$$

or
$$\frac{U_0 a\alpha^2 z}{\alpha^2 + 1} = \ln\left\{\frac{\zeta + (\zeta^2 - 1)^{1/2}}{i}\right\} + \frac{\alpha^2 - 1}{2(\alpha^2 + 1)} \ln\left\{\frac{(\zeta^2 - b^2)^{1/2} + \zeta}{(\zeta^2 - b^2)^{1/2} - \zeta}\right\}$$
$$+ \frac{\alpha}{i(\alpha^2 + 1)} \ln\left\{\frac{i(\zeta^2 - b^2)^{1/2} - 2\alpha\zeta/(\alpha^2 - 1)}{i(\zeta^2 - b^2)^{1/2} + 2\alpha\zeta/(\alpha^2 - 1)}\right\}. \qquad \ldots\ldots (4)$$

At B′, $x' = d$, $y' = h/2$ and $\zeta = b$, so that, from equation (4), d can be expressed as a function of α,

$$d = \frac{h}{2}\left\{\frac{(\alpha^2 + 1)\ln(\alpha + 1)/(\alpha - 1)}{\pi\alpha^2} + \frac{1}{\alpha}\right\}. \qquad \ldots\ldots (5)$$

Since $-dw/dz = U' - iV' = \overline{Q}$, equation (3) gives

$$U_0/\overline{Q} = (1 - \alpha^2)\{(1 - b^2/\zeta^2)^{1/2} + b(1 - 1/\zeta^2)\}/2\alpha^2. \qquad \ldots\ldots (6)$$

Elimination of ζ between equations (4) and (6) will therefore lead to a relationship between z and Q. This elimination is carried out by substituting $t = (1 - b^2/\zeta^2)^{1/2}$ into equations (4) and (6) so that the latter reduces to $t = (\alpha^2 U_0/\overline{Q} - \overline{Q}/U_0)/(1 - \alpha^2)$. Putting this value of t into equation (4) and separating real and imaginary parts we have

$$\left.\begin{aligned} x = \frac{2x'}{h} &= \frac{\alpha^2 + 1}{4\pi\alpha^2} \ln \frac{(\alpha^2 + 1)^4 - 2(\alpha^2 + 1)^2(4\alpha^2 + A^2\cos 2\tau) + \sigma^4}{[(\alpha^2 + 1)^2 - (\alpha^2 + 1)^2\{2(\sigma^2 + 4\alpha^2 + A^2\cos 2\tau)\}^{1/2} + \sigma^2]^2} \\ &+ \frac{\alpha^2 - 1}{4\pi\alpha^2} \ln \frac{A^4 - 2(\alpha^2 - 1)^2 A^2 \cos 2\tau + (\alpha^2 - 1)^4}{\{A^2 - 2(\alpha^2 - 1)A\cos\tau + (\alpha^2 - 1)^2\}^2} + \frac{1}{\pi\alpha} \tan^{-1} \frac{4\alpha A \cos\tau}{A^2 - 4\alpha^2}, \\ y = \frac{2y'}{h} &= \frac{\alpha^2 + 1}{2\pi\alpha^2} \tan^{-1} \frac{(\alpha^2 + 1)\{2(\sigma^2 - 4\alpha^2 - A^2\cos 2\tau)\}^{1/2}}{(\alpha^2 + 1)^2 - \sigma^2} \\ &+ \frac{\alpha^2 - 1}{2\pi\alpha^2} \tan^{-1} \frac{2(\alpha^2 - 1)A\sin\tau}{(\alpha^2 - 1)^2 - A^2} + \frac{1}{2\pi\alpha} \ln\left\{\frac{\sigma^4}{(A^2 + 4\alpha A\sin\tau + 4\alpha^2)^2}\right\}, \end{aligned}\right\} \ldots (7)$$

where $A\cos\tau = -\cos\theta(\alpha^2 U_0/q - q/U_0)$, $A\sin\tau = -\sin\theta(\alpha^2 U_0/q + q/U_0)$, $\sigma^4 = 16\alpha^4 + 8\alpha^2 A^2\cos 2\tau + A^4$. If $\alpha = 1$, these expressions reduce to

$$\left.\begin{aligned} x = \frac{2x'}{h} &= \frac{2}{\pi}\left(\tfrac{1}{2}\ln\frac{U_0/q + q/U_0 + 2\cos\theta}{U_0/q + q/U_0 - 2\cos\theta} + \tan^{-1}\frac{-2q\cos\theta/U_0}{1 - q^2/U_0^2}\right), \\ y = \frac{2y'}{h} &= \frac{2}{\pi}\left(\tan^{-1}\frac{-2q\sin\theta/U_0}{1 - q^2/U_0^2} + \tfrac{1}{2}\ln\frac{U_0/q + q/U_0 + 2\sin\theta}{U_0/q + q/U_0 - 2\sin\theta}\right), \end{aligned}\right\} \quad \ldots\ldots(8)$$

which represent the flow field when the jet is at an infinite distance from the plate. In this case symmetry exists about lines through the origin making angles $\pi/4$ with the axes.

Along the free streamline B′C′, q is equal to V_0 and $\tau = \pi/2$. Equations (7) then reduce to the equations of the free streamline as follows:

$$\left.\begin{aligned} x &= \frac{\alpha^2+1}{2\pi\alpha^2}\ln\frac{\alpha^2+1-2\alpha\cos\theta}{\alpha^2+1+2\alpha\cos\theta} + \frac{1}{\alpha}, \\ y &= -\frac{\alpha^2+1}{2\pi\alpha^2} - \frac{\alpha^2-1}{\pi\alpha^2}\tan^{-1}\frac{1-\alpha^2}{2\alpha\sin\theta} - \frac{1}{\pi\alpha}\ln\frac{1-\sin\theta}{1+\sin\theta}. \end{aligned}\right\} \quad \ldots\ldots(9)$$

Along A′B′ the velocity rises from $-U_0$ to $-V_0$ and we have

$$\left.\begin{aligned} x &= \frac{\alpha^2+1}{2\pi\alpha^2}\ln\frac{\alpha^2+1+(4\alpha^2+A^2)^{1/2}}{\alpha^2+1-(4\alpha^2+A^2)^{1/2}} + \frac{\alpha^2-1}{2\pi\alpha^2}\ln\frac{\alpha^2-1+A}{\alpha^2-1-A} + \frac{2}{\pi\alpha}\tan^{-1}\frac{2\alpha}{A} \\ y &= -1; \end{aligned}\right\} \quad \ldots(10)$$

while from F to E the velocity falls from $-U_0$ to zero and

$$\left.\begin{aligned} x &= \frac{\alpha^2+1}{2\pi\alpha^2}\ln\frac{\alpha^2+1+(4\alpha^2+A^2)^{1/2}}{-\alpha^2-1+(4\alpha^2+A^2)^{1/2}} + \frac{\alpha^2-1}{2\pi\alpha^2}\ln\frac{\alpha^2-1+A}{-\alpha^2+1+A} + \frac{1}{\pi\alpha}\tan^{-1}\frac{4\alpha A}{A^2-4\alpha^2} \\ y &= 0. \end{aligned}\right\} \quad \ldots\ldots(11)$$

Finally, from E to D′ the velocity rises from 0 to $-V_0$ and

$$\left.\begin{aligned} x &= 0 \\ -y &= \frac{\alpha^2+1}{\pi\alpha^2}\tan^{-1}\frac{\alpha^2+1}{(A^2-4\alpha^2)^{1/2}} + \frac{\alpha^2-1}{\pi\alpha^2}\tan^{-1}\frac{\alpha^2-1}{A} + \frac{1}{\pi^2}\ln\frac{A+2\alpha}{A-2\alpha}. \end{aligned}\right\} \quad \ldots\ldots(12)$$

The same order of the terms has been preserved in all these expressions.

§ 3. COMPUTATION OF FLOW FIELDS

The formulae derived above relate to the field A′B′C′D′EF. Alternative quadrants can be represented by a suitable selection of signs at an early stage of the argument. Table 1 gives values of the velocity and its direction at important points on the flow boundaries.

Table 1. Values of U', V', q and θ at Salient Points on the Boundaries of the Flow Field

Point	A′	B′	C′	D′	E	F
U'	$-U_0$	$-V_0$	0	0	0	$-U_0$
V'	0	0	$-V_0$	$-V_0$	0	0
q	U_0	V_0	V_0	V_0	0	U_0
θ	π	π	$3\pi/2$	$3\pi/2$	$3\pi/2$	π

For $\alpha = 1$ equations (8) were computed directly for a range of values of $\tan\theta$ and q/U_0, and the results are exhibited in Table 2 (*a*)–(*d*). By reflecting

Table 2 (*a*). Values of x for $\alpha = 1$ and given values of $\tan\theta$

q/U_0 \ $\tan\theta$	1	0·8	0·6	0·5	0·4	0·3	0·2	0·1	0·08	0·06	0·04	0·02	0·01	0
0·1	0·181	0·199	0·219	0·228	0·237	0·245	0·250	0·253	0·253	0·255	0·255	0·255	0·255	0·255
0·2	0·362	0·397	0·437	0·456	0·472	0·488	0·499	0·507	0·508	0·508	0·509	0·512	0·512	0·512
0·3	0·540	0·596	0·654	0·682	0·709	0·733	0·751	0·761	0·763	0·764	0·764	0·765	0·765	0·766
0·4	0·719	0·791	0·869	0·907	0·943	0·975	1·003	1·018	1·021	1·021	1·023	1·024	1·024	1·024
0·5	0·891	0·981	1·080	1·130	1·176	1·222	1·258	1·281	1·285	1·287	1·288	1·290	1·290	1·293
0·6	1·058	1·157	1·276	1·337	1·403	1·467	1·520	1·557	1·561	1·566	1·568	1·570	1·570	1·570
0·7	1·210	1·319	1·455	1·532	1·615	1·706	1·791	1·856	1·867	1·871	1·878	1·882	1·882	1·882
0·8	1·345	1·459	1·608	1·697	1·805	1·932	2·074	2·198	2·220	2·234	2·242	2·258	2·258	2·260
0·85	1·400	1·520	1·673	1·767	1·884	2·030	2·207	2·394	2·427	2·450	2·463	2·490	2·490	2·500
0·9	1·465	1·574	1·728	1·827	1·951	2·113	2·332	2·602	2·678	2·700	2·749	2·808	2·808	2·810
0·95	1·500	1·623	1·777	1·878	2·004	2·177	2·422	2·800	2·891	2·972	3·079	3·242	3·242	3·250
0·99	—	1·660	1·812	1·911	2·039	2·217	2·470	2·897	3·060	3·189	3·410	3·77	4·12	4·37

Table 2 (*b*). Values of y for $\alpha = 1$ and given values of $\tan\theta$

q/U_0 \ $\tan\theta$	1	0·8	0·6	0·5	0·4	0·3	0·2	0·1	0·08	0·06	0·04	0·02	0·01	0
0·1	0·181	0·159	0·132	0·115	0·095	0·074	0·050	0·025	0·020	0·015	0·010	0·005	0·003	0
0·2	0·362	0·318	0·262	0·228	0·190	0·146	0·100	0·052	0·041	0·031	0·021	0·010	0·005	0
0·3	0·540	0·476	0·393	0·343	0·285	0·222	0·152	0·077	0·062	0·046	0·031	0·015	0·008	0
0·4	0·719	0·635	0·526	0·460	0·385	0·298	0·204	0·104	0·083	0·063	0·042	0·021	0·011	0
0·5	0·891	0·793	0·661	0·581	0·488	0·383	0·263	0·135	0·109	0·082	0·054	0·028	0·013	0
0·6	1·058	0·945	0·800	0·712	0·604	0·481	0·335	0·174	0·140	0·106	0·070	0·035	0·018	0
0·7	1·21	1·093	0·943	0·852	0·738	0·603	0·432	0·230	0·185	0·124	0·094	0·047	0·024	0
0·8	1·345	1·231	1·089	1·003	0·896	0·762	0·581	0·328	0·267	0·204	0·137	0·069	0·034	0
0·85	1·40	1·302	1·160	1·080	0·982	0·858	0·683	0·413	0·341	0·263	0·179	0·090	0·045	0
0·9	1·465	1·357	1·230	1·157	1·071	0·964	0·812	0·546	0·464	0·367	0·256	0·132	0·067	0
0·95	1·50	1·414	1·299	1·234	1·162	1·076	0·964	0·764	0·690	0·589	0·445	0·251	0·130	0
0·99	—	1·457	1·350	1·292	1·232	1·166	1·094	0·999	0·971	0·933	0·868	0·717	0·506	0

Table 2 (*c*). Values of $U = U'/U_0$ for $\alpha = 1$ and given values of $\tan\theta$

q/U_0 \ $\tan\theta$	1	0·8	0·6	0·5	0·4	0·3	0·2	0·1	0·08	0·06	0·04	0·02	0·01	0
0·1	0·071	0·078	0·086	0·090	0·093	0·096	0·098	0·100	0·100	0·100	0·100	0·100	0·100	0·100
0·2	0·141	0·156	0·172	0·179	0·186	0·192	0·196	0·199	0·200	0·200	0·200	0·200	0·200	0·200
0·3	0·212	0·235	0·258	0·268	0·279	0·288	0·295	0·299	0·299	0·300	0·300	0·300	0·300	0·300
0·4	0·283	0·313	0·343	0·358	0·371	0·383	0·393	0·398	0·399	0·399	0·400	0·400	0·400	0·400
0·5	0·354	0·391	0·429	0·447	0·464	0·479	0·491	0·498	0·499	0·499	0·500	0·500	0·500	0·500
0·6	0·425	0·469	0·515	0·536	0·557	0·575	0·589	0·597	0·598	0·599	0·600	0·600	0·600	0·600
0·7	0·496	0·547	0·601	0·626	0·650	0·671	0·687	0·697	0·698	0·699	0·700	0·700	0·700	0·700
0·8	0·576	0·625	0·687	0·715	0·743	0·767	0·785	0·796	0·798	0·799	0·799	0·800	0·800	0·800
0·85	0·602	0·664	0·730	0·760	0·789	0·815	0·834	0·846	0·848	0·849	0·849	0·850	0·850	0·850
0·9	0·636	0·703	0·772	0·805	0·835	0·862	0·883	0·896	0·898	0·898	0·899	0·900	0·900	0·900
0·95	0·672	0·742	0·815	0·850	0·882	0·910	0·932	0·946	0·947	0·948	0·949	0·950	0·950	0·950
0·99	—	0·773	0·850	0·885	0·919	0·949	0·971	0·985	0·987	0·988	0·989	0·990	0·990	0·990

Table 2 (*d*). Values of $V = V'/U_0$ for $\alpha = 1$ and given values of $\tan\theta$

q/U_0 \ $\tan\theta$	1	0·8	0·6	0·5	0·4	0·3	0·2	0·1	0·08	0·06	0·04	0·02	0·01	0
0·1	0·071	0·063	0·052	0·045	0·037	0·029	0·020	0·010	0·008	0·006	0·004	0·002	0·001	0
0·2	0·141	0·125	0·103	0·090	0·075	0·058	0·039	0·020	0·016	0·012	0·008	0·004	0·002	0
0·3	0·212	0·188	0·154	0·135	0·112	0·087	0·059	0·030	0·024	0·018	0·012	0·006	0·003	0
0·4	0·283	0·250	0·206	0·179	0·149	0·115	0·079	0·040	0·032	0·024	0·016	0·008	0·004	0
0·5	0·354	0·313	0·257	0·224	0·186	0·144	0·098	0·050	0·040	0·030	0·020	0·010	0·005	0
0·6	0·425	0·375	0·309	0·269	0·223	0·173	0·118	0·060	0·048	0·036	0·024	0·012	0·006	0
0·7	0·496	0·438	0·360	0·314	0·261	0·202	0·137	0·070	0·056	0·037	0·028	0·014	0·007	0
0·8	0·576	0·500	0·411	0·359	0·298	0·231	0·157	0·080	0·064	0·048	0·032	0·016	0·008	0
0·85	0·602	0·532	0·437	0·381	0·316	0·245	0·167	0·085	0·068	0·051	0·034	0·017	0·009	0
0·9	0·636	0·563	0·463	0·403	0·335	0·259	0·177	0·090	0·072	0·054	0·036	0·018	0·009	0
0·95	0·672	0·594	0·489	0·426	0·354	0·274	0·186	0·095	0·076	0·056	0·038	0·019	0·010	0
0·99	—	0·619	0·509	·444	0·369	0·285	0·194	0·090	0·079	0·060	0·040	0·020	0·010	0

this table about the bisector of the angle between the coordinate axes the remainder of the flow field can be obtained. Table 3 contains the coordinates of points along the free streamline.

Table 3. Free Streamline. $\alpha = 1$

$\lvert x \rvert$	1·001	1·013	1·019	1·026	1·038	1·051	1·064	1·076
$\lvert y \rvert$	5·398	3·932	3·674	3·491	3·233	3·050	2·908	2·792
$\lvert x \rvert$	1·102	1·127	1·191	1·255	1·382	1·509	1·561	
$\lvert y \rvert$	2·609	2·468	2·212	2·033	1·785	1·616	1·561	

Since $\ln U_0/q$ and $\theta - \pi$ are conjugate functions of x and y an orthogonal network is plotted on joining up the points given in Table 2 to make lines of constant q and constant θ. This facilitates the interpolation which is required later when drawing particle trajectories.

Using equation (5), the distance d of the orifice from the plate was calculated as a function of α, the ratio of the velocities of the deflected and incident streams. This is plotted in Figure 5.

Equations (10), (11) and (12) were then used to calculate the velocities round the boundaries of the flow fields taking α as 1·0, 1·6, 2·5, 5·0 and 10·0. These curves are plotted on Figures 6, 7 and 8. Figure 9 shows the free streamlines for the same values of α.

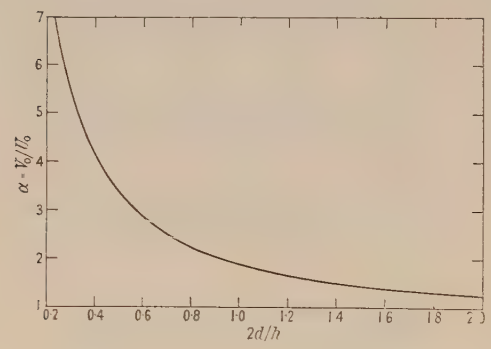

Figure 5. Ratio of velocities of deflected and incident streams as a function of the distance between orifice and plate.

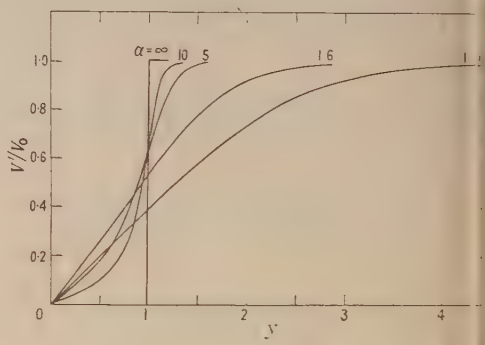

Figure 7. Velocity along the plate.

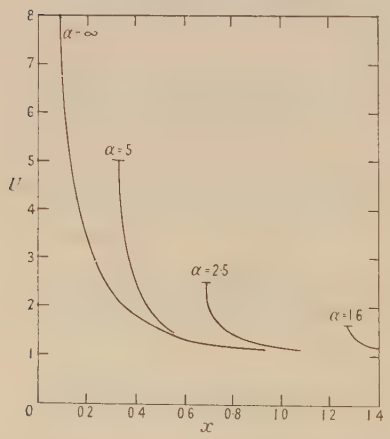

Figure 6. Velocity along wall of jet.

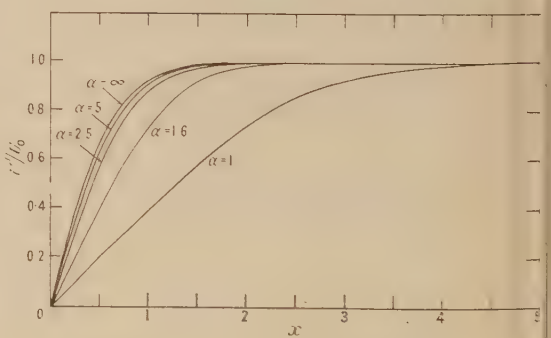

Figure 8. Velocity along the x axis.

Guided by the values of U and V round the boundaries, the flow fields for α equal to 1·6 and 2·5 were calculated by the method of relaxation. This part of the work was performed by Scientific Computing Services Ltd. Their results are shown in Table 4 (*a*) and (*b*), U and V, and Table 5, free streamline. Corresponding figures for $\alpha = 2{\cdot}5$ appear in Tables 6 (*a*), (*b*) and 7. This system of computation gives a rectangular grid of points.

For $\alpha = 5$ the theoretical formulae were again employed; the flow field is given in Table 8 and the free streamline in Table 9. Orthogonal curves are once more obtained for q and θ and have been drawn in Figure 10.

This completed the establishment of the flow fields and made it possible to proceed to study the trajectories of particles carried along by the fluid leaving the jet orifice.

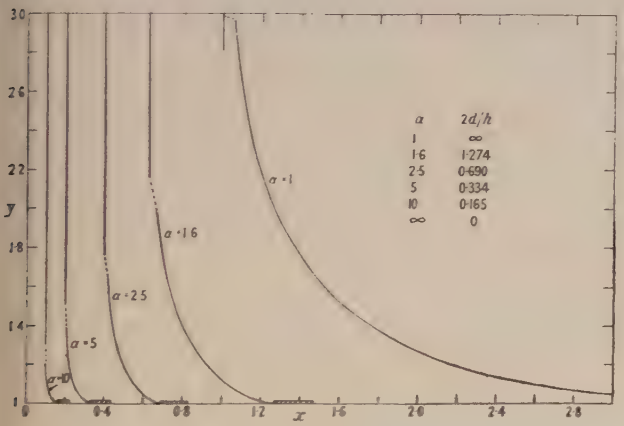

Figure 9. Free streamlines.

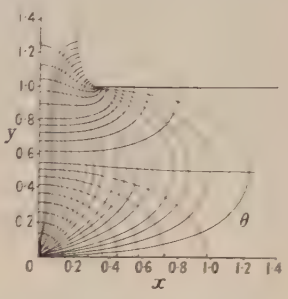

Figure 10. Orthogonal curves of q and θ for $\alpha = 5$.

§ 4. THE EQUATIONS OF MOTION OF THE PARTICLES

Let u', v' be the resolutes of particle velocity and U', V' as hitherto the resolutes of stream velocity. Assuming Stokes' law of resistance, the equations of motion of a particle are

$$\frac{m}{6\pi r\eta}\frac{du'}{dt'} = U' - u' \qquad \text{and} \qquad \frac{m}{6\pi r\eta}\frac{dv'}{dt'} = V' - v',$$

where r is the radius of the particle, m its mass and η the viscosity of the fluid. The equations can be rendered dimensionless by measuring the velocities in units of U_0, the distances in units of $\frac{1}{2}h$, the half width of the jet and the times in units of $h\,2U_0$. Hence $u = u'\,U_0$, $x = x\,\frac{1}{2}h$, $t = t'\,U_0\,\frac{1}{2}h$, etc. The equations transform to

$$P\frac{du}{dt} = U - u, \qquad P\frac{dv}{dt} = V - v, \qquad \ldots\ldots(13)$$

where $P = 2mU_0\,6\pi r\eta h$ is the dimensionless particle parameter. It is actually equal to the distance (measured in units of $\frac{1}{2}h$) that a particle will travel through fluid at rest when its initial velocity is U_0.

§ 5. COMPUTATION OF PARTICLE TRAJECTORIES

The step-by-step method of computing particle trajectories can be followed by referring to Table 10 in which the complete derivation of a trajectory for $P = 0{\cdot}046$ and $\alpha = 5$ is set out. The particle is started at a given value of y with

Table 4 (*a*). Flow Field for $\alpha = 1{\cdot}6$ calculated by Relaxation (values of 1,000 U)

y \ x	0·1	0·2	0·3	0·4	0·5	0·6	0·7	0·8	0·9	1·0	1·1	1·2	1·3	1·4	1·5	1·6	1·7
0	81	162	242	321	398	471	542	609	671	728	778	822	860	891	916	936	951
0·1	81	162	242	322	399	473	544	612	674	731	781	825	863	894	919	938	953
0·2	82	163	244	324	402	478	550	619	683	740	792	836	872	902	926	945	959
0·3	83	165	248	329	409	487	561	632	698	757	809	853	889	917	939	956	969
0·4	85	168	252	335	417	497	575	649	717	780	834	878	914	939	958	971	980
0·5	86	171	256	342	426	510	592	671	744	811	868	913	946	968	982	990	994
0·6	87	174	261	349	436	525	613	698	779	852	914	960	990	1006	1011	1012	1011
0·7	88	176	265	355	447	541	635	729	820	904	975	1024	1047	1051	1045	1036	1027
0·8	88	177	268	360	456	555	658	763	869	970	1057	1114	1124	1105	1081	1060	1044
0·9	88	178	269	363	462	566	678	797	922	1050	1169	1252	1230	1163	1113	1079	1055
1·0	88	176	267	361	462	571	690	823	972	1139	1319	1494	1600				
1·1	85	171	261	354	455	565	689	832	1004	1215	1289						
1·2	82	165	250	340	438	545	667	812	995	1045							
1·3	77	155	235	319	410	509	622	755	835								
1·4	71	143	216	292	373	460	555	661									
1·5	64	129	194	261	330	402	476	520									
1·6	56	113	170	227	284	340	393	407									
1·7	49	98	146	193	238	280	316	318									
1·8	42	83	123	162	197	227	248										
1·9	35	70	103	134	161	182	193										
2·0	29	58	85	109	130	145	156										
2·1	24	47	69	88	104	114	117										
2·2	20	38	56	71	83	90	91										
2·3	16	31	45	57	65	70	71										
2·4	13	25	36	45	51	55	55										
2·5	10	20	28	35	40	43	43										
2·6	8	16	22	28	31	33	33										
2·7	6	12	18	22	25	26	26										
2·8	5	10	14	17	19	20	20										
2·9	4	8	11	13	15	16	16										
3·0	3	6	8	10	11	12	12										

Table 4 (*b*). Flow Field for $\alpha = 1{\cdot}6$ calculated by Relaxation (values of 1,000 V)

y / x	0	0·1	0·2	0·3	0·4	0·5	0·6	0·7	0·8	0·9	1·0	1·1	1·2	1·3	1·4	1·5	1·6
0·1	81	81	81	80	78	76	73	69	65	60	54	47	41	34	28	22	17
0·2	163	163	162	160	156	152	146	139	130	120	108	94	81	68	55	44	34
0·3	245	245	244	241	236	230	222	211	197	181	163	143	121	101	81	64	50
0·4	329	328	326	323	318	310	299	285	268	246	220	191	161	132	104	81	63
0·5	414	413	411	407	401	393	380	363	341	314	280	241	200	160	124	94	71
0·6	500	499	497	494	487	479	466	447	421	388	345	294	238	184	137	101	74
0·7	587	587	585	582	577	569	557	537	509	470	418	351	274	199	140	98	68
0·8	675	674	674	673	670	664	654	637	609	566	504	417	309	198	126	82	55
0·9	763	763	765	765	765	764	758	746	723	682	613	505	348	157	83	49	31
1·0	851	852	854	858	862	866	869	867	855	825	762	643	421	0	0	0	0
1·1	938	939	943	950	959	971	984	996	1004	1000	968	948					
1·2	1020	1022	1029	1039	1054	1074	1099	1129	1165	1203	1211						
1·3	1100	1103	1111	1124	1144	1172	1209	1258	1324	1365							
1·4	1174	1177	1186	1202	1226	1260	1307	1371	1457								
1·5	1241	1244	1254	1272	1299	1337	1389	1460	1513								
1·6	1300	1304	1315	1333	1361	1400	1453	1523	1547								
1·7	1353	1357	1368	1386	1413	1450	1500	1564	1568								
1·8	1398	1402	1412	1430	1455	1489	1533	1580									
1·9	1438	1441	1450	1466	1488	1518	1555	1588									
2·0	1470	1473	1481	1495	1514	1539	1570	1593									
2·1	1496	1499	1506	1518	1534	1555	1580	1596									
2·2	1517	1520	1526	1536	1549	1566	1586	1597									
2·3	1535	1537	1542	1550	1561	1575	1591	1598									
2·4	1549	1550	1554	1561	1570	1582	1594	1599									
2·5	1560	1561	1564	1570	1577	1586	1596	1599									
2·6	1569	1570	1573	1577	1582	1589	1597	1600									
2·7	1576	1577	1579	1582	1586	1591	1598	1600									
2·8	1581	1582	1584	1586	1589	1593	1598	1600									
2·9	1585	1586	1588	1590	1592	1595	1599	1600									
3·0	1589	1590	1591	1592	1594	1596	1599	1600									

$x \to \infty$. This is interrupted as the value for x for which the stream velocity is about 0·99. The particle of Table 10, was launched at $x_1 = 1{\cdot}4$, $y_1 = 0{\cdot}1$; the suffix n refers to the number of the step and is given in column 1 of the Table. Opposite the row n are entered the particle velocities u_n, v_n, in columns 2 and 3, and coordinates x_n, y_n, in columns 10 and 11. The length of the step resolute δx is then decided and entered in column 8. Estimates are now made of the velocity changes $\delta_1 u$, $\delta_1 v$ during the step (columns 4 and 5); the suffix denotes that these are approximations.

Table 5. Free Streamline for $\alpha = 1{\cdot}6$

x	y	1,000 U	1,000 V	x	y	1,000 U	1,000 V
1·2741	1·0	1600	0	0·6476	2·2	90·8	1597·4
1·25	1·0026	1580	249	0·6426	2·3	70·7	1598·4
1·2	1·0141	1533	457	0·6387	2·4	55·0	1599·1
1·15	1·0320	1476	617	0·6356	2·5	42·7	1599·4
1·1113	1·05	1424	730	0·6333	2·6	33·3	1599·7
1·1	1·0559	1407	761	0·6314	2·7	25·9	1599·8
1·05	1·0865	1325	897	0·6300	2·8	20·1	1599·9
1·0306	1·1	1289	948	0·6289	2·9	15·6	1599·9
1·0	1·1240	1227	1026	0·6280	3·0	12·2	1600·0
0·9708	1·15	1163	1099	0·6274	3·1	9·5	1600·0
0·9230	1·2	1045	1211	0·6268	3·2	7·4	1600·0
0·9	1·2281	983	1263	0·6264	3·3	5·7	1600·0
0·8504	1·3	835	1365	0·6261	3·4	4·4	1600·0
0·8	1·3948	669	1453	0·6259	3·5	3·5	1600·0
0·7976	1·4	661	1457	0·6257	3·6	2·7	1600·0
0·7581	1·5	520	1513	0·6255	3·7	2·1	1600·0
0·7280	1·6	406·8	1547·4	0·6254	3·8	1·6	1600·0
0·7048	1·7	317·6	1568·2	0·6253	3·9	1·3	1600·0
0·7	1·7247	299	1572	0·6252	4·0	1·0	1600·0
0·6870	1·8	247·6	1580·7	0·6252	4·1	0·8	1600·0
0·6732	1·9	192·9	1588·3	0·6251	4·2	0·6	1600·0
0·6624	2·0	150·2	1592·9	0·6251	4·3	0·5	1600·0
0·6541	2·1	116·8	1595·7	0·6251	4·4	0·4	1600·0

Suppose δt is the time taken by the particle to cover the first step. Then $\delta t \simeq \delta x/(u_n + \frac{1}{2}\delta_1 u) \simeq \delta y/(v_n + \frac{1}{2}\delta_1 v)$. The value of δy, corresponding to the resolute δx, is calculated from

$$\delta y = \delta x(v_n + \tfrac{1}{2}\delta_1 v)/(u_n + \tfrac{1}{2}\delta_1 u), \qquad \ldots\ldots(14)$$

using columns 6 and 7, and is entered in column 9. With δx and δy known, the diagram of the flow field can be consulted to interpolate U_n, U_{n+1}, and V_n, V_{n+1}, the fluid velocity resolutes at the beginning and end of the step (columns 12 and 18). Then, from equation (13), we can calculate a more accurate value of δu as follows:

$$\delta u = \frac{\delta t}{P}\{\tfrac{1}{2}(U_n + U_{n+1}) - (u_n + \tfrac{1}{2}\delta_1 u)\} = \frac{\delta x}{P}\left\{\frac{\frac{1}{2}(U_n + U_{n+1})}{u_n + \frac{1}{2}\delta_1 u} - 1\right\}. \qquad \ldots\ldots(15)$$

This is entered in column 17 while columns 13–16 facilitate the arithmetic. Similarly,

$$\delta v = \frac{\delta y}{P}\left\{\frac{\frac{1}{2}(V_n + V_{n+1})}{v_n + \frac{1}{2}\delta_1 v} - 1\right\} \qquad \ldots\ldots(16)$$

Table 6 (*a*). Flow Field for $\alpha = 2{\cdot}5$ calculated by Relaxation (values for 1,000 *V*)

y \ x	0	0·1	0·2	0·3	0·4	0·5	0·6	0·7	0·8	0·9	1·0	1·1	1·2	1·3	1·4	1·5
0	0	117	230	340	444	539	624	699	763	816	860	894	920	940	957	969
0·1	0	118	233	343	448	544	630	705	769	821	864	897	923	943	959	970
0·2	0	121	240	354	461	559	646	723	785	836	877	908	932	950	963	974
0·3	0	126	251	370	482	585	675	751	813	862	899	926	946	961	971	979
0·4	0	134	266	394	514	623	718	794	854	898	929	951	966	976	983	988
0·5	0	144	287	425	556	676	777	856	912	948	970	983	991	995	997	998
0·6	0	156	312	465	612	746	859	941	989	1012	1020	1021	1018	1015	1012	1009
0·7	0	170	339	510	678	837	971	1062	1093	1092	1078	1062	1047	1035	1026	1019
0·8	0	182	366	557	754	956	1133	1235	1232	1186	1139	1103	1074	1053	1038	1028
0·9	0	190	386	598	830	1095	1375	1540	1408	1276	1190	1132	1093	1066	1047	1034
1·0	0	191	393	616	879	1213	1688	2406	1539	1320	1209	1145	1102	1071	1051	1036
1·1	0	184	377	593	855	1010	1200	1437								
1·2	0	166	338	526	742	867	1004									
1·3	0	140	284	432	584											
1·4	0	113	225	333	430											
1·5	0	88	171	246	303											
1·6	0	65	125	176	208											
1·7	0	46	89	123	142											
1·8	0	32	62	85	98											

Table 6 (*b*). Flow Field for $\alpha = 2{\cdot}5$ calculated by Relaxation (values of 1,000 *V*)

y \ x	0	0·1	0·2	0·3	0·4	0·5	0·6	0·7	0·8	0·9	1·0	1·1	1·2	1·3	1·4	1·5
0	0	0	0	0	0	0	0	0	0	0	0	0	0	0	0	0
0·1	117	116	112	107	100	91	80	69	58	48	38	30	23	18	14	11
0·2	236	234	227	216	201	182	161	138	115	94	75	59	45	34	26	19
0·3	360	357	347	330	306	277	243	207	171	138	109	84	64	48	36	27
0·4	491	487	473	450	417	376	328	276	225	178	138	105	79	59	44	33
0·5	630	625	608	579	537	482	416	344	274	211	159	119	88	65	48	35
0·6	780	774	755	721	669	598	509	409	314	233	170	123	89	65	47	34
0·7	943	937	917	883	823	734	613	473	341	237	164	115	81	58	42	30
0·8	1118	1113	1095	1064	1004	901	740	529	336	211	137	91	63	44	32	23
0·9	1303	1300	1290	1272	1227	1129	927	563	258	135	82	53	35	24	17	12
1·0	1493	1494	1498	1503	1499	1461	1305	535	0	0	0	0	0	0	0	0
1·1	1680	1686	1705	1741	1798	1886										
1·2	1854	1864	1898	1961	2070	2260										
1·3	2007	2020	2061	2137	2264											
1·4	2134	2147	2189	2264	2381											
1·5	2234	2246	2283	2348	2443											
1·6	2311	2321	2351	2403	2474											
1·7	2367	2375	2399	2438	2488											
1·8	2408	2414	2432	2460	2496											
1·9	2437	2441	2454	2474	2498											
2·0	2458	2461	2470	2483	2499											
2·1	2473	2475	2481	2489	2500											

is evaluated from equation (14) (column 9) with the aid of columns 19–22. δv is entered in column 23.

If the values of δu and δv in columns 17 and 23 are not in fair agreement with the estimates $\delta_1 u$, $\delta_1 v$ the step is repeated using intermediate values. Steps 10 and 13 in Table 10 had to be repeated for this reason.

As the particle approaches the plate the size chosen for δx is decreased because the path turns round and tends to run parallel with the y axis. In the example illustrated the particle actually struck the plate with a residual velocity component u equal to 0·029. This was for $P=0{\cdot}046$; when the process was repeated

Table 7. Free Streamline. $\alpha=2{\cdot}5$

x	y	U	V	x	y	U	V
0·713	1·0	2·5	0	0·7	1·002	2·432	0·578
0·614	1·05	1·893	1·633	0·65	1·024	2·137	1·297
0·567	1·1	1·535	1·973	0·6	1·063	1·792	1·744
0·533	1·15	1·255	2·162	0·55	1·123	1·397	2·074
0·508	1·2	1·029	2·279	0·5	1·218	0·958	2·309
0·488	1·25	0·845	2·353	0·45	1·389	0·488	2·452
0·471	1·3	0·693	2·402	0·4	∞	0	2·500
0·448	1·4	0·468	2·456				
0·432	1·5	0·316	2·480				
0·422	1·6	0·213	2·491				
0·415	1·7	0·144	2·496				
0·410	1·8						
0·407	1·9						
0·405	2·0						

for $P=0{\cdot}025$, u_n became equal to zero before the plate was encountered and a negative value was obtained on subtracting δu from the last value of u_n. By constructing a graph of P against u_n (positive or negative) at $x=0$ it was possible to interpolate and find accurately the value of P, for which the particle just met the plate with zero velocity component u. This is the critical value P_c and the corresponding trajectory is the critical trajectory. P_c depends on the starting point of the particle y_1, and a number of trajectories were calculated for different values of y_1.

The interpolation of P_c was linear except in one case for which a quadratic was required. When $P=P_c$ impact with the plate takes place at $y=\infty$.

If P_c was assessed accurately in the first instance, it became difficult to tell if the particle would just hit or just miss as it was swept along close to and nearly parallel with the plate. The uncertainty was resolved as follows: Suppose at the end of the ith step at (y_i, x_i) the particle velocity was (u_i, v_i), whereas the stream velocity was practically $(0, V_0)$. The equations of motion of the particle then reduce to

$$P\,du/dt=u \quad \text{or} \quad u-u_i=(x_i-x)/P$$

and

$$y-y_i\simeq \frac{V_0 t}{U_0}=\frac{PV_0}{U_0}\ln\left(1+\frac{x_i-x}{Pu_i}\right). \qquad \ldots\ldots(17)$$

The first expression gives $u>0$ when $x=0$ for a hit and $u<0$ for a miss, remembering that the particle velocity is always negative. The criterion for a critical value of P is $u=0$. The second equation shows that $y=\infty$ at $x=0$ for $P=P_c$.

§ 6. DISCUSSION OF PARTICLE TRAJECTORIES

The critical trajectories of particles starting at a number of different positions in the incident air stream ($0<y_1<1$) are plotted in Figures 11 to 14. All the curves meet the plate $x=0$ at $y\to\infty$. When $P>P_c$ a curve lying below the critical path is obtained which meets the plate at a finite value of y. For $P<P_c$ the particles fail to strike the plate and travel parallel to it with the emergent fluid stream at a finite value of x.

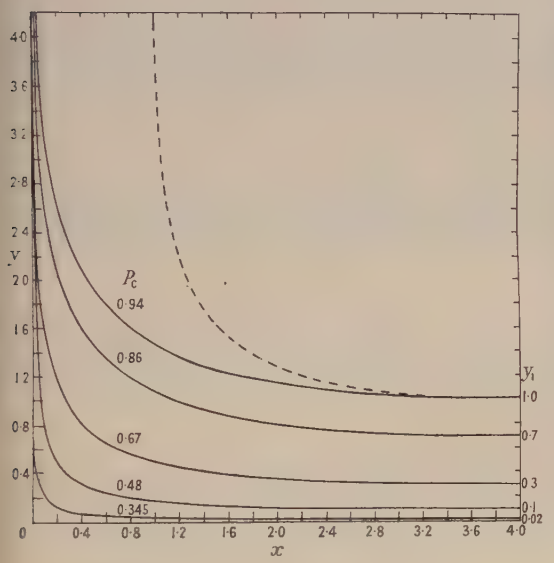

Figure 11. Critical trajectories. $\alpha=1$.

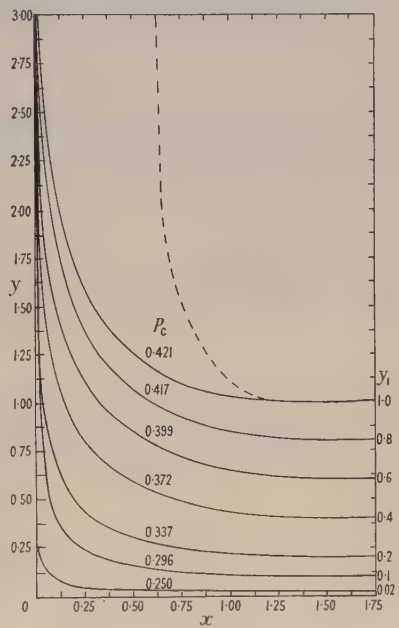

Figure 12. Critical trajectories. $\alpha=1{\cdot}6$.

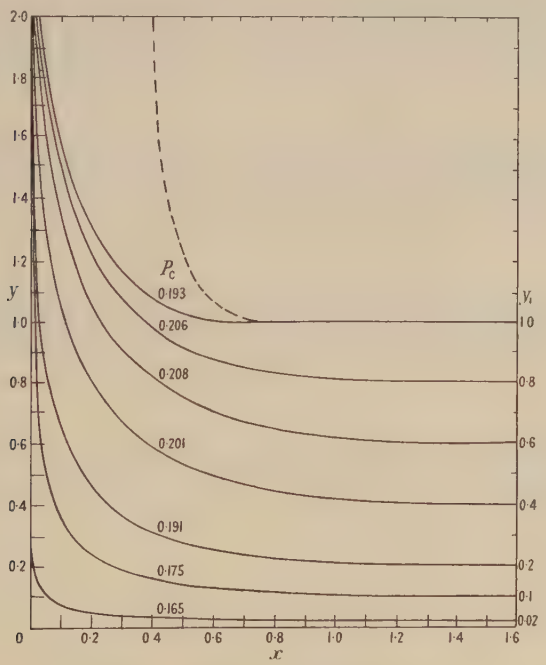

Figure 13. Critical trajectories. $\alpha=2{\cdot}5$.

Table 8 (*a*). Values of x for $\alpha = 5$ and given values of $\tan\theta$

q/U_0 \ $\tan\theta$	0·05	0·1	0·15	0·2	0·3	0·4	0·5	0·6	0·8	1·0
0·1	0·06899	0·06774	0·06742	0·06768	0·06601	0·06399	0·06154	0·05892	0·05372	0·04857
0·2	0·13926	0·13875	0·13785	0·13643	0·13312	0·12855	0·12268	0·11798	0·10636	0·09485
0·3	0·21231	0·21120	0·20972	0·20756	0·20161	0·19456	0·18562	0·17677	0·15839	0·14025
0·4	0·29022	0·28858	0·28591	0·28275	0·27292	0·26108	0·24798	0·23747	0·20811	0·18428
0·5	0·37491	0·37199	0·36802	0·36184	0·34701	0·32834	0·30891	0·28976	0·25351	0·22251
0·6	0·46306	0·45873	0·45351	0·44259	0·42424	0·39317	0·36628	0·34001	0·29329	0·25570
0·7	0·58550	0·57630	0·56223	0·54447	0·50472	0·46081	0·42189	0·38616	0·32680	0·27088
0·8	0·73304	0·71109	0·68081	0·64571	0·57833	0·51728	0·46497	0·41100	0·35057	0·29951
0·9	0·95127	0·88083	0·80687	0·74196	0·63821	0·55606	0·49408	0·44300	0·36658	0·31102
1·0	1·22901	1·00344	0·87624	0·78650	0·66012	0·57211	0·50586	0·45312	0·37434	0·31781
1·2	0·81226	0·78132	0·74183	0·69899	0·61778	0·54973	0·49317	0·44597	0·37248	0·31812
1·4	0·63743	0·62713	0·61138	0·59182	0·54767	0·50205	0·45653	0·41264	0·35312	0·30978
1·6	0·54541	0·53988	0·53087	0·51967	0·48935	0·45834	0·42709	0·39710	0·34340	0·30136
1·8	0·48720	0·48367	0·47762	0·46957	0·44887	0·42484	0·39935	0·37649	0·32852	0·28966
2·0	0·44775	0·44488	0·44026	0·43417	0·41870	0·40073	0·37707	0·35648	0·31622	0·28121
2·5	0·38972	0·38794	0·38503	0·38028	0·37056	0·35736	0·34299	0·32705	0·30028	0·26816
3·0	0·36039	0·35953	0·35737	0·35445	0·34656	0·33680	0·32511	0·31254	0·28785	0·26406
3·5	0·34591	0·34488	0·34317	0·34090	0·33463	0·32657	0·31784	0·30737	0·28533	0·26678
4·0	0·33816	0·33742	0·33606	0·33420	0·32912	0·32264	0·31573	0·30700	0·28918	0·27374
4·5	0·33489	0·33421	0·33313	0·33161	0·32745	0·32215	0·31603	0·30943	0·29578	0·28426

	1·2	1·5	2	2·5	3	4	5	6	8	10
0·1	0·04384	0·03798	0·02976	0·02540	0·02157	0·01655	0·01342	0·01133	0·00847	0·00665
0·2	0·08347	0·07406	0·05994	0·04965	0·04124	0·03228	0·02607	0·02188	0·01601	0·01312
0·3	0·12253	0·11141	0·08696	0·07185	0·06093	0·04655	0·03753	0·03147	0·02372	0·01897
0·4	0·16446	0·14069	0·11097	0·09137	0·07735	0·05897	0·04641	0·03995	0·03006	0·02442
0·5	0·19669	0·16624	0·13183	0·10721	0·09065	0·06909	0·05560	0·04642	0·03495	0·02801
0·6	0·22295	0·18901	0·14817	0·12119	0·10222	0·07752	0·06229	0·05230	0·03937	0·03151
0·7	0·24507	0·20447	0·15916	0·12980	0·10751	0·08290	0·06673	0·05678	0·04142	0·03364
0·8	0·26004	0·21621	0·16789	0·13654	0·11489	0·08708	0·07000	0·05854	0·04401	0·03548
0·9	0·26993	0·22404	0·17355	0·14120	0·11879	0·09006	0·07234	0·06043	0·04541	0·03639
1·0	0·27527	0·22847	0·17708	0·14410	0·12120	0·09179	0·07380	0·06169	0·04640	0·03716
1·2	0·27687	0·23060	0·17938	0·14600	0·12311	0·09338	0·07908	0·06278	0·04724	0·03526
1·4	0·26869	0·22775	0·17807	0·14564	0·12069	0·09329	0·07516	0·06556	0·04698	0·03790
1·6	0·26656	0·22565	0·17535	0·14438	0·12173	0·09150	0·07449	0·06256	0·04706	0·03928
1·8	0·25714	0·21645	0·17860	0·14251	0·12080	0·09216	0·07430	0·06222	0·04689	0·03761
2·0	0·25058	0·21795	0·17165	0·14169	0·12014	0·09184	0·07424	0·06222	0·04761	0·03760
2·5	0·24235	0·21003	0·16756	0·14538	0·13032	0·09411	0·07632	0·06456	0·05012	0·03897
3·0	0·24242	0·21435	0·17162	0·15080	0·13026	0·10277	0·08514	0·07253	0·05339	0·04244
3·5	0·24750	0·22384	0·19092	0·16541	0·14694	0·11629	0·09643	0·08147	0·06277	0·05049
4·0	0·25415	0·23820	0·21044	0·18832	0·17024	0·14210	0·12153	0·10634	0·08357	0·06823
4·5	0·27049	0·25456	0·23324	0·21673	0·20271	0·18070	0·16397	0·15143	0·12538	0·10684

Table 8 (*b*). Values of y for $\alpha = 5$ and given values of $\tan\theta$

q/U_0 \ $\tan\theta$	0·05	0·1	0·15	0·2	0·3	0·4	0·5	0·6	0·8	1·0
0·1	0·00330	0·00700	0·01020	0·01345	0·01994	0·02578	0·03102	0·03563	0·04323	0·04882
0·2	0·00713	0·01290	0·02118	0·02796	0·04095	0·05270	0·06330	0·07260	0·08753	0·09553
0·3	0·01079	0·02242	0·03339	0·04398	0·06417	0·08225	0·09835	0·11217	0·13525	0·14992
0·4	0·01613	0·03213	0·04776	0·06280	0·09061	0·11167	0·13743	0·15569	0·18371	0·20323
0·5	0·02247	0·04450	0·06569	0·08647	0·12453	0·15594	0·18270	0·20470	0·23723	0·25903
0·6	0·03017	0·05960	0·08789	0·11437	0·16154	0·20069	0·23079	0·25534	0·29022	0·31229
0·7	0·05471	0·08847	0·12861	0·16317	0·22312	0·26525	0·29868	0·32258	0·35463	0·37427
0·8	0·07144	0·13660	0·19173	0·23617	0·30013	0·34178	0·36999	0·38992	0·41429	0·43154
0·9	0·14268	0·24484	0·30440	0·35152	0·40080	0·42863	0·44663	0·45908	0·48453	0·48432
1·0	0·50255	0·50495	0·50780	0·51051	0·51433	0·51881	0·52443	0·52602	0·53187	0·53630
1·2	0·91859	0·84789	0·78795	0·75101	0·69516	0·66845	0·65066	0·64015	0·62889	0·62405
1·4	0·95991	0·91674	0·88012	0·84804	0·79779	0·76296	0·73921	0·72266	0·70354	0·69399
1·6	0·97125	0·94074	0·91708	0·89403	0·85257	0·81832	0·79817	0·78137	0·76074	0·74876
1·8	0·97874	0·95777	0·93782	0·91633	0·88664	0·86012	0·83980	0·82429	0·80414	0·79264
2·0	0·98341	0·96698	0·95100	0·93783	0·90967	0·88776	0·87037	0·85692	0·83889	0·82889
2·5	0·99015	0·98036	0·97080	0·95187	0·94548	0·93174	0·92065	0·91201	0·89668	0·89328
3·0	0·99380	0·98778	0·98203	0·97641	0·96636	0·95823	0·95165	0·94678	0·94149	0·94201
3·5	0·99626	0·99260	0·98905	0·98574	0·97967	0·97534	0·97163	0·97029	0·97122	0·97223
4·0	0·99835	0·99556	0·99407	0·99243	0·98724	0·98763	0·98689	0·98681	0·99036	0·99606
4·5	0·99886	0·99839	0·99788	0·99697	0·99625	0·99635	0·99733	0·99916	1·00498	1·01301

	1·2	1·5	2	2·5	3	4	5	6	8	10
0·1	0·05299	0·05733	0·06196	0·06385	0·06565	0·06667	0·06734	0·06775	0·06812	0·06836
0·2	0·10658	0·11467	0·12283	0·12718	0·12967	0·13229	0·13361	0·13439	0·13513	0·13543
0·3	0·16024	0·17236	0·18366	0·18942	0·19265	0·19634	0·19792	0·19892	0·19995	0·20021
0·4	0·21699	0·22998	0·24328	0·24960	0·25364	0·25758	0·25952	0·26062	0·26165	0·26227
0·5	0·27380	0·28807	0·30111	0·30796	0·31175	0·31576	0·31773	0·31879	0·31934	0·32044
0·6	0·32790	0·34226	0·35539	0·36191	0·36582	0·36981	0·37162	0·37271	0·37375	0·37422
0·7	0·38601	0·39828	0·40959	0·41496	0·41779	0·42119	0·42299	0·42360	0·42440	0·42482
0·8	0·44012	0·45043	0·45846	0·46297	0·46545	0·46809	0·46922	0·46994	0·47062	0·47091
0·9	0·49217	0·49863	0·50451	0·50753	0·50932	0·51111	0·51214	0·51259	0·51306	0·51330
1·0	0·53967	0·54315	0·54708	0·54851	0·54962	0·55065	0·55143	0·55181	0·55194	0·55230
1·2	0·62127	0·62075	0·62048	0·62048	0·62067	0·62099	0·62111	0·62110	0·62125	0·62126
1·4	0·68833	0·68458	0·68196	0·68109	0·68055	0·68037	0·68005	0·68173	0·68164	0·68170
1·6	0·74211	0·73681	0·73325	0·73196	0·73129	0·73074	0·73051	0·73049	0·73090	0·73119
1·8	0·78635	0·78097	0·77766	0·77671	0·77552	0·77528	0·77496	0·77494	0·77503	0·77503
2·0	0·82284	0·81826	0·81759	0·81482	0·81812	0·81435	0·81446	0·81483	0·81464	0·81456
2·5	0·89199	0·89105	0·89243	0·89356	0·89497	0·89675	0·89782	0·89867	0·89805	0·89944
3·0	0·94264	0·94427	0·95162	0·95784	0·96190	0·96739	0·96920	0·97150	0·97135	0·97473
3·5	0·97670	0·98260	0·99698	1·00887	1·01533	1·02605	1·03233	1·03534	1·03949	1 04195
4·0	1·00310	1·01459	1·03309	1·04890	1·06177	1·08069	1·09760	1·10050	1·11156	1·11656
4·5	1·02181	1·03610	1·05878	1·07932	1·09682	1·12515	1·14690	1·16300	1·18579	1·19995

Table 9. Free Streamline. $\alpha = 5$

$\tan\theta$	x	y	$\tan\theta$	x	y	$\tan\theta$	x	y
0·1	0·334	1·0	0·6	0·313	1·009	2·5	0·248	1·097
0·15	0·333	1·0	0·8	0·303	1·015	3·0	0·240	1·116
0·2	0·332	1·0	1·0	0·292	1·024	4·0	0·231	1·149
0·3	0·328	1·002	1·2	0·283	1·034	5·0	0·225	1·177
0·4	0·324	1·004	1·5	0·272	1·050	7·0	0·218	1·217
0·5	0·319	1·005	2·0	0·258	1·075	10·0	0·213	1·267

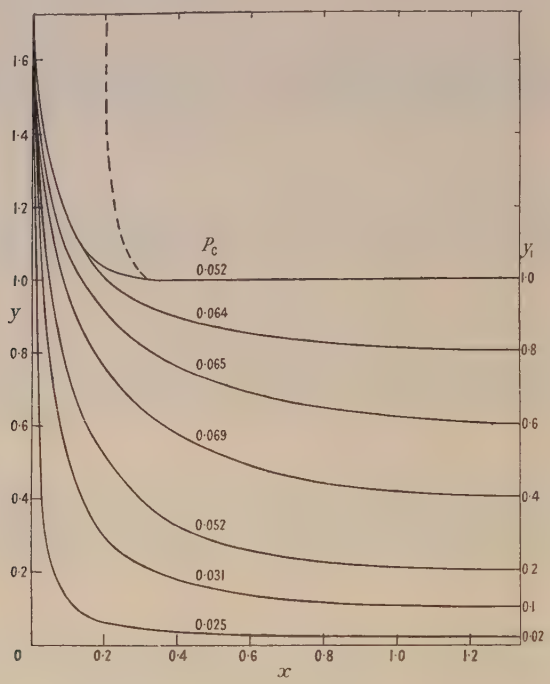

Figure 14. Critical trajectories. $\alpha = 5$.

In Figure 15, for the same set of values of α, P_c is shown as a function of y_1, the starting coordinate. The smallest value of P_c resulting in impingement is achieved in the case of particles launched near the axis. Conditions on the axis require further consideration and will be studied later.

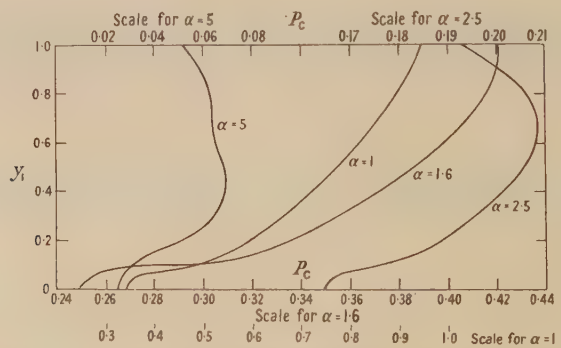

Figure 15. Variation of the critical particle size parameter P_c with the starting coordinate y_1.

1	2	3	4	5	6	7	8	9	10	11	12
n	u_n	v_n	$\delta_1 u$	$\delta_1 v$	$u_n+\frac{1}{2}\delta_1 u$	$v_n+\frac{1}{2}\delta_1 v$	δx	δy	x_n	y_n	U_n
1	1	0	0·054	0·020	0·973	0·010	0·2	0·0020	1·4	0·1	0·9716
2	0·948	0·020	0·026	0·004	0·935	0·022	0·2	0·0046	1·2	0·1020	0·950
3	0·922	0·025	0·070	0·022	0·887	0·036	0·2	0·0082	1·0	0·1066	0·908
4	0·848	0·045	0·044	0·016	0·826	0·053	0·1	0·0064	0·8	0·1148	0·836
5	0·805	0·069	0·062	0·020	0·774	0·079	0·1	0·0102	0·7	0·1212	0·784
6	0·746	0·086	0·080	0·034	0·706	0·103	0·1	0·0146	0·6	0·1314	0·722
7	0·672	0·117	0·096	0·050	0·624	0·142	0·1	0·0227	0·5	0·1460	0·642
8	0·572	0·165	0·096	0·074	0·524	0·202	0·1	0·0385	0·4	0·1687	0·551
9	0·476	0·240	0·118	0·128	0·411	0·304	0·1	0·0740	0·3	0·2072	0·451
10	0·358	0·369	0·136	0·210	0·290	0·474	0·1	0·1642	0·2	0·2812	0·337
										0·4454	0·208
10	0·358	0·369	0·128	0·332	0·294	0·535	0·1	0·1820	0·2	0·2812	0·337
11	0·232	0·705	0·020	0·250	0·222	0·830	0·025	0·0935	0·1	0·4636	0·217
12	0·215	0·949	0·016	0·360	0·207	1·129	0·025	0·1375	0·075	0·5571	0·213
13	0·198	1·319	0·036	0·480	0·180	1·559	0·025	0·2073	0·055	0·6946	0·189
									0·025	0·9019	0·147
13	0·198	1·319	0·036	0·928	0·180	1·783	0·025	0·2475	0·05	0·6946	0·189
14	0·157	2·237	0·126		0·094				0·025	0·9386	0·143
15	0·029										0

13	14	15	16	17	18	19	20	21	22	23
$\frac{U_n+U_{n+1}}{2}$	$\frac{U_n+U_{n+1}}{2(u+\frac{1}{2}\delta u)}$	1−col. 14	$\frac{\delta x}{P}$	δu	V_n	$\frac{V_n+V_{n+1}}{2}$	$\frac{V_n+V_{n+1}}{2(v+\frac{1}{2}\delta v)}$	col. 20−1	$\frac{\delta y}{P}$	δv
0·9608	0·988	0·012	4·348	0·052	0·011	0·0145	1·45	0·45	0·0434	0·020
0·929	0·996	0·006	4·348	0·026	0·018	0·023	1·045	0·045	0·100	0·005
0·872	0·983	0·017	4·348	0·074	0·028	0·040	1·112	0·112	0·1782	0·020
0·810	0·980	0·020	2·174	0·043	0·052	0·062	1·170	0·170	0·1391	0·024
0·753	0·973	0·027	2·174	0·059	0·072	0·085	1·075	0·075	0·2220	0·017
0·682	0·966	0·034	2·174	0·074	0·098	0·113	1·096	0·096	0·3180	0·031
0·5965	0·954	0 046	2·174	0·100	0·128	0·156	1·098	0·098	0·494	0·048
0·501	0·956	0·044	2·174	0·096	0·184	0·220	1·090	0·090	0·838	0·075
0·394	0·946	0·054	2·174	0·118	0·256	0·328	1·080	0·080	1·610	0·129
0·2725	0·939	0·061	2·174	0·133	0·400	0·565	1·194	0·194	3·57	0·692
					0·730					
0·277	0·942	0·058	2·174	0·126	0·400	0·581	1·085	0·085	3·96	0·336
0·215	0·968	0·032	0·5435	0·017	0·762	0·930	1·120	0·120	2·031	0·244
0·201	0·970	0·030	0·5435	0·017	1·098	1·269	1·124	0·124	2·99	0·370
0·168	0·942	0·068	0·5435	0·037	1·440	1·974	1·266	0·266	4·51	1·200
					2·508					
0·166	0·924	0·076	0·5435	0·041	1·440	2·085	1·170	0·170	5·38	0·918
0·0715	0·761	0·239	0·5435	0·129	2·730					

For the two greatest values of α there is a value of y_1 giving minimum efficiency of impingement since P_c rises to maximal values at $y_1 \simeq 0{\cdot}65$ ($\alpha = 2{\cdot}5$) and $y_1 \simeq 0{\cdot}45$ ($\alpha = 5$).

If particles of the same size and density are uniformly distributed in the approaching air stream the proportion striking the plate depends on the relationship between P_c and y_1. For $\alpha = 1{\cdot}0$ and $1{\cdot}6$, where P_c increases steadily with y_1, the graph of the efficiency of impingement, or the fraction of the incident cloud of particles which hits the plate, is the same as the (y_1, P_c) curve; 100% efficiency corresponds to $y_1 = 1$, and so on. With $\alpha = 2{\cdot}5$ or 5, owing to the maximum of P_c, particles from a certain region of y_1 may miss the plate, while those starting at smaller and greater values strike it. The efficiency curve in this event is constructed by making due allowance for this above a certain value of P_c.

Graphs of efficiency of impingement as a function of P are plotted in Figure 16 for different values of α. These curves can be interpreted as expressing the performance of an ideal dust-sampling instrument on the assumption that all particles striking the plate actually adhere to it, whatever the angle of impact. Collisions between airborne particle have been neglected.

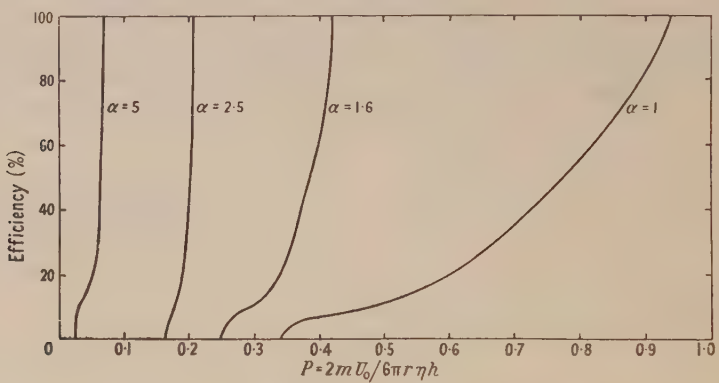

Figure 16. Efficiency of impingement of particles.

It is clear that the impingement of small particles is facilitated by diminishing d, the distance of the orifice from the plate; this also improves the selectivity of the system since the range of values of P over which impingement changes from zero to 100% narrows considerably. Figure 17 illustrates the last point. When α is less than 2·5 the range of P spreads out, while a sharp cut-off is obtained for $\alpha = 3$. There would seem to be no advantage in increasing α above 3 since the accompanying reduction in particle size can also be obtained by increasing the velocity U_0 or decreasing the width h of slit.

Calculation of P for different particle radii (microns) and different values of the ratio U_0/h (sec^{-1}) is rapid with the help of Figure 18.

§ 7. PARTICLES MOVING ALONG THE X AXIS

The velocities of particles moving along the x axis were computed by the step method and also by approximating the flow field to a simple form allowing integration of the equation of motion of the particle. Inspection of Figure 8 shows that the stream velocity along the x axis tends linearly to zero with x. Only some distance away from the plate is the deceleration more gradual; it

was thus thought that a reasonable approximation to the motion of the particles could be made by assuming $U=cx$; $U=U_0$, $x=x_0$ at $t=0$. The solution of the equation of motion then becomes

$$x=x_0\left\{\cos pt+\frac{1}{2Pp}(1-2P_c)\sin pt\right\}e^{-t/2P} \qquad \ldots\ldots(18)$$

for $P>1/4c$, and

$$x=\frac{x_0}{2q}\left\{\left(\frac{1}{P}+q-2c\right)e^{qt/2}-\left(\frac{1}{P}-q-2c\right)e^{-qt/2}\right\}e^{-t/2P} \qquad \ldots\ldots(19)$$

for $P<1/4c$, where $p=(4cP-1)^{1/2}/2P$ and $q=(1-4cP)^{1/2}/P$.

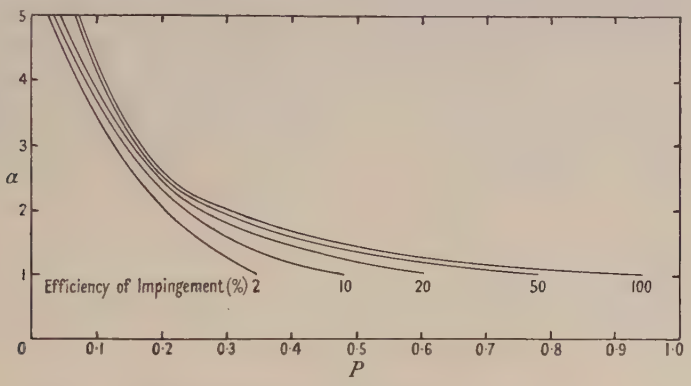

Figure 17. Illustrating how the sharpness of cut-off depends on α.

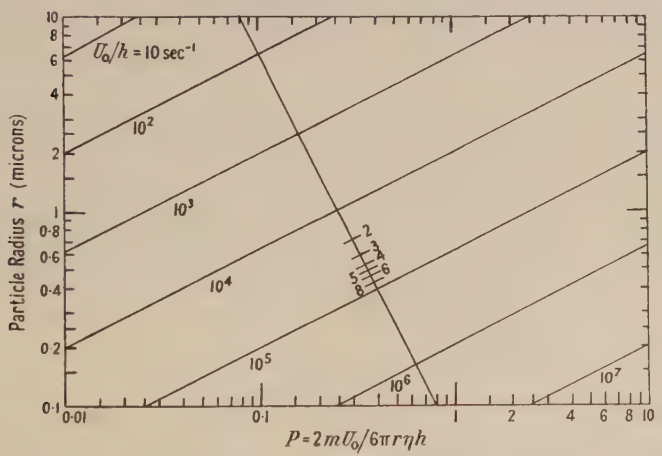

Figure 18. Diagram for calculating P in air at 20° c. and 760 mm. Hg. The parallel, diagonal lines give the relationship between r and P for different values of U_0/h.

In the first case the particle strikes the plate with a finite velocity, and in the second with zero velocity. However, it is not travelling with the stream unless P tends to 0. The critical case is $P_c=1/4c$ when $x=(x_0+U_0t)\exp(-t/2P_c)$.

This method of calculation was quite reliable near the plate but made P_c rather larger than the stepwise method, which was used finally for all values of α.

In Table 11 values of P_c calculated by both methods are given for particles on the x axis.

Table 11. Critical Values of the Particle Parameter P_c on and near the Axis

α	Stepwise method		$P_c=1/4c$
	$y_1=0$	$y_1=0{\cdot}02$	
1	0·60	0·345	0·64
1·6	0·31	0·25	0·325
2·5	0·195	0·16	0·225
5·0	0·140	0·025	0·1875
∞	—	—	0·1625

Figure 19 illustrates the velocity of impact as a function of P for $\alpha=1$, 1·6, 2·5 and 5, while Figure 20, with $\alpha=5$, shows the velocity as a function of x.

P_c has not the same significance for particles on the axis as it had for those starting with non-zero values of y_1 since, clearly, all particles on the axis must strike the plate. Examination of Figures 11 to 14 will show that the curve of y_1 plotted

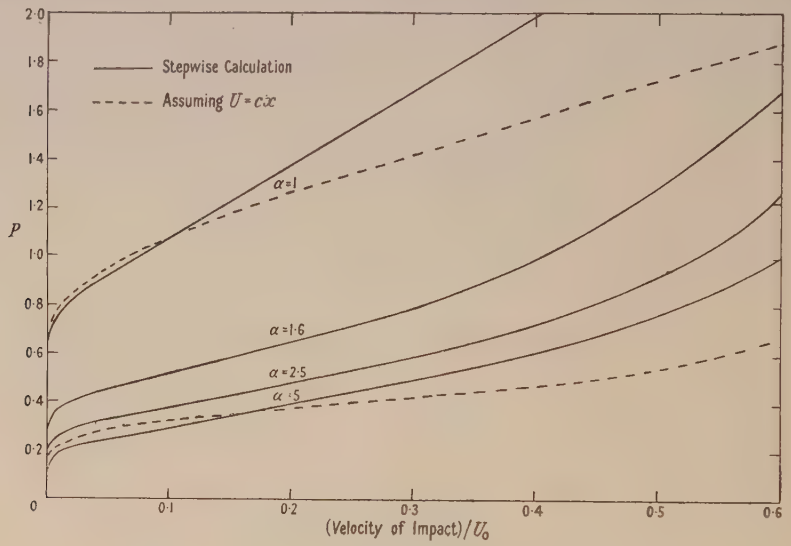

Figure 19. Impact velocities of particles on the x axis.

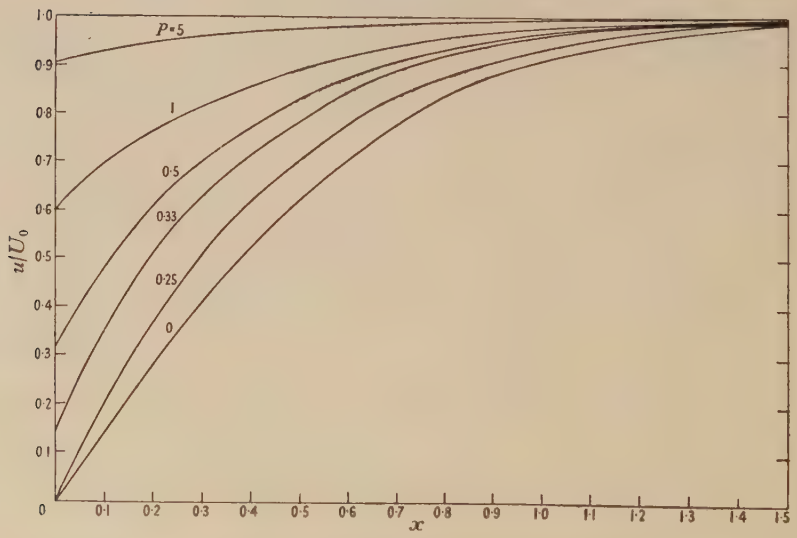

Figure 20. Velocities of particles travelling along the x axis for $\alpha=5$.

against P_c seems to meet the axis $y_1 = 0$ at a value of P_c which is substantially less than that found for a particle on the axis. The smallest finite value of y_1 for which trajectories were computed was 0·02, and what happens to the curve between here and zero is conjectural. It seems likely that there is a discontinuity, so that, in effect, a definite value of P exists below which no impingement takes place. Probably the cut-off occurs close to the values of P_c for $y_1 = 0{\cdot}02$, and these are shown in Table 11 for comparison with the figures for the axis.

ACKNOWLEDGMENTS

The authors of this paper are members of the staff of the Medical Research Council. They are grateful to Mr. A. C. Stevenson for his interest in this work.

REFERENCES

Albrecht, F., 1931, *Phys. Z.*, **32**, 48.
Davies, C. N., Aylward, M., and Leacey, D., 1951, *Archives of Industrial Hygiene and Occupational Medicine*, in the press.
Taylor, G. I., 1940, *Aeronautical Research Committee*, 4350, D.W.T. 3.

Fluctuations in the Energy-Loss of Fast Electrons in a Proportional Counter

By P. Rothwell
Atomic Energy Research Establishment, Harwell, Didcot, Berks.

Communicated by W. J. Whitehouse; *MS. received* 17*th April* 1951

ABSTRACT. The fluctuations in the energy lost by fast electrons over a fixed small fraction of their range have been studied by measuring the pulses the electrons produce in passing through a proportional counter. The energy loss distribution calculated theoretically by Landau is approximately gaussian with a high-energy tail. The experimental distribution is in agreement with the theoretical on the high-energy side of the peak, but is wider than Landau predicts on the low-energy side; this discrepancy is greater in krypton than in argon. The experimental values of the most probable energy loss agree with the theoretical values.

§ 1. Introduction

When a fast particle passes through a layer of matter, it loses energy chiefly by ionizing collisions. The amount of energy lost by an individual particle over a fixed small fraction of its range is not constant, but varies considerably. There are fluctuations in the amount of energy lost at each collision, fluctuations in the number of collisions, and a fairly high chance, which increases as the number of collisions increases, that a very high energy loss, due to a close collision, may occur.

Landau (1944) has calculated theoretically the probability function $W(\Delta, x)$ of a single charged particle such as an electron or meson losing an amount of energy Δ in a small distance x. Curve *a* of Figure 2 shows Landau's distribution, which is approximately gaussian with a high-energy tail. It is given, for convenience,

in terms of a parameter $(\Delta - \Delta_0)/\xi$, and the probability function $W(\Delta, x)$ may be obtained from this universal curve at once. Δ_0 is the most probable energy loss in the particular layer of matter considered, and

$$\xi = x \frac{2\pi \boldsymbol{N} e^4 \rho}{mv^2} \frac{\Sigma Z}{\Sigma A},$$

is proportional to the number of electrons in the layer of matter. ($\boldsymbol{N}$ is Avogadro's number, Z, A, the atomic number and atomic weight of the material, and ρ its density; m, v are the mass and velocity of the ionizing particle, and $\boldsymbol{e}$ is the electronic charge in E.S.U.)

$$\Delta_0 = \xi \left(\log \frac{\xi}{\epsilon'} + 0{\cdot}37 \right) \quad \text{where} \quad \epsilon' = \frac{I^2}{2mv^2} \left(1 - \frac{v^2}{\boldsymbol{c}^2} \right) \exp (v^2/\boldsymbol{c}^2).$$

I is an average ionization potential of the atom which Landau takes as $I_0 Z$, where $I_0 = 13{\cdot}5$ ev.

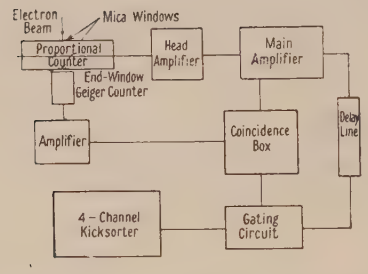

Figure 1. Block diagram of apparatus.

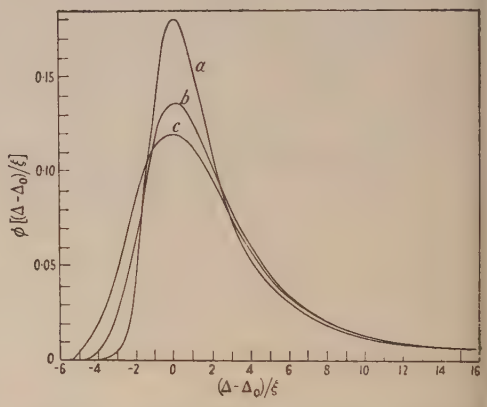

Figure 2. Energy-loss distributions for minimum ionizing electrons: curve *a*, theoretical distribution according to Landau; curve *b*, average experimental distribution in argon; curve *c*, average experimental distribution in krypton.

Two assumptions are made in his calculation: (i) the most probable energy loss is small compared with the energy of the primary particle; (ii) the observed energy losses are large compared with the average atomic binding energy.

These large fluctuations are of interest in proportional counter work, since they set a limit to the precision with which the momenta or energy of fast particles may be measured.

Two interesting points arise from the theoretical calculations when the Landau distribution is plotted in terms of energies: for any given material, the relative width of the energy loss distribution does not become much narrower as the most probable energy loss is increased, and for a given thickness of the layer of matter, the distribution is narrower in materials of lower Z (even though the most probable energy loss is lower) than in materials of higher Z.

These points are illustrated numerically in Table 1, in which are given the theoretical values of the most probable energy loss, and of the widths of the energy distributions for 1·5 MEV. electrons.

Table 1

Gas	x (cm. at N.T.P.)	ξ (kev.)	Δ_0 (kev.)	% width at half height
Argon	1·0	0·116	1·14	42·6
	5·0	0·58	6·65	36·6
	10·0	1·16	14·4	34·6
	100·0	11·6	62·5	29·9
Hydrogen	10·0	0·143	0·232	25·9
Helium	10·0	0·143	0·212	28·3
Neon	10·0	0·715	9·4	32·0
Argon	10·0	1·16	14·1	34·6
Krypton	10·0	2·32	26·6	36·0
Xenon	10·0	3·90	44·3	37·4

§ 2. EXPERIMENTAL

The shape of the energy-loss distribution was investigated experimentally by firing a narrow beam of mono-energetic electrons from a beta-spectrometer through a proportional counter. It is assumed that the ionization produced by the primary particle and the secondary electrons in the counter gives a measure of the energy lost by the primary particle. A block diagram of the apparatus used is given in Figure 1.

The proportional counter used was a Maze type (Maze 1946) glass counter, 5·5 cm. in diameter, with two thin mica windows, one on either end of a diameter. The counter was placed with one window as close as possible to the slit of a beta-spectrometer, and an end-window Geiger counter was placed directly in front of the other window. The two counters were connected in coincidence, and the coincidence pulse opened a gate which allowed the delayed proportional counter pulse into the four-channel kicksorter. In this way only those electrons which passed right through the counter were recorded. Thus errors due to scattering of electrons in the counter were minimized, and background from cosmic rays and other sources was practically eliminated.

The counter was calibrated with K-capture x-rays from radioactive sources (Rothwell and West 1950); the calibration lines used were Zn (8·1 kev.), Se (10·5 kev.) and Pd (20·2 kev.). The pulse size distribution from these x-ray lines is gaussian in shape. The spread is caused by fluctuations in the number of collisions made by the conversion electrons, and fluctuations in the multiplication process. This spread becomes very much wider if there are slight impurities in the counter; the half-widths at half height of the distributions from the x-ray lines were therefore measured at each calibration to test whether the counter had deteriorated in any way.

Two points arise in connection with the mica windows:

(i) To test the shape of the distribution fairly the energies of the electrons used must be greater than 1 MEV. This is because the beam of electrons actually entering the counter is not quite mono-energetic, owing to fluctuations in the amount of energy lost in the mica window (the average energy lost is of the order of 100 kev.). For particles of energies greater than 1 MEV., the specific ionization is practically constant, and for fluctuations in energy of the order of those produced in the window, all electrons have the same ionizing power. For energies less than 1 MEV., the specific ionization increases sharply as the energy of the ionizing electron decreases, and so the electron beam contains electrons with a considerable range in ionizing power.

(ii) The additional ionization caused by secondary electrons, formed in the first mica window, entering the counter, is assumed to be equal to the ionization lost in the walls by secondary electrons formed in the counter.

§ 3. RESULTS

The results of a series of measurements are recorded in Table 2. The experimental values of Δ_0 are slightly lower than the theoretical values, except with the 1·0 MEV. electrons. In this case the experimental values of Δ_0 are slightly higher than the theoretical. The latter effect is no doubt due to the energy loss of the particles in the mica windows, which begins to be important at about 1 MEV. (see column (7) of Table 2).

Table 2

(1)	(2)	(3)	(4)	(5)	(6)	(7)
1	$Kr+CH_4$	52·2+ 3·0=55·2	2·0	10·2	10·8	
2	$Kr+CH_4$	52·2+ 3·0=55·2	2·0	10·4	10·8	
3	$Kr+CH_4$	52·2+ 3·0=55·2	1·5	10·0	10·6	
4	$Kr+CH_4$	52·2+ 3·0=55·2	1·5	9·75	10·6	
5	$Kr+CH_4$	60·0+10·0=70·0	2·0	12·5	13·1	
6	$Kr+CH_4$	60·0+10·0=70·0	2·0	$12·5_5$	13·1	
7	$Kr+CH_4$	60·0+10·0=70·0	2·0	$12·5_5$	13·1	
8	$Kr+CH_4$	60·0+10·0=70·0	1·0	13·4	12·9	13·3
9	$Kr+CH_4$	60·0+10·0=70·0	1·0	13·3	12·9	13·3
10	$A+CO_2$	52·0+ 4·8=56·8	1·5	6·3	6·4	
11	$A+CO_2$	56·0+ 6·4=62·4	1·5	7·2	7·2	
12	$A+CH_4$	52·0	1·0	5·75	5·6	5·8
13	$A+CH_4$	52·0	1·0	5·8	5·6	5·8

(1) run; (2) gas; (3) pressure (cm. Hg); (4) energy of incident electron (MEV.); (5) Δ_0 (experimental); (6) Δ_0 (theoretical); (7) Δ_0 (theoretical, corrected for mica window).

Figures 3 and 4 show the pulse size distributions for the argon and the krypton counters respectively, plotted in terms of the parameter $(\Delta-\Delta_0)/\xi$. Each set of points is normalized so that the area under the curve is unity, as is that under Landau's. The ordinate of the resultant curve is then represented by $\phi[(\Delta-\Delta_0)/\xi]$. The averages of the argon and krypton distributions are drawn in curves *b* and *c* of Figure 2.

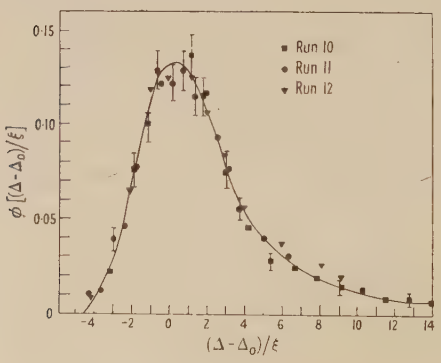

Figure 3. Energy-loss distribution for minimum ionizing electrons in argon.

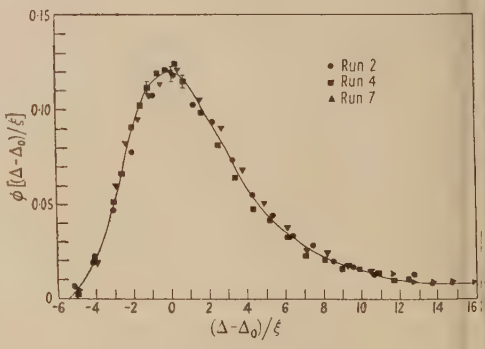

Figure 4. Energy-loss distribution for minimum ionizing electrons in krypton.

There is a considerable discrepancy between the experimental curves and the theoretical curve on the low-energy side, and the distribution in argon is narrower than the distribution in krypton. When plotted in terms of the parameter $(\Delta - \Delta_0)\ \xi$ the distributions should, in theory, both lie on the same curve.

Corrections were made for:

(*a*) Fluctuations in the multiplication process. A spread of approximately the width of the x-ray line corresponding to Δ was assigned to each point on the theoretical curve. The shape of the distribution was hardly altered.

(*b*) The average lengthening of path due to multiple scattering. This was calculated from a formula due to Rossi and Greisen (1941); it is found to be about 10% with the krypton fillings and about 5·5% with the argon fillings. (The value is probably somewhat lower in this experiment, since particles scattered through angles greater than 8° are not counted.) If several Landau distributions with slightly different values of Δ_0 are superimposed, the result is a distribution broadened on the low-energy side, but a 15% variation in Δ_0 is needed to account for the discrepancy between the theoretical and the mean experimental argon curve, and an even greater variation (of the order of 25%) for the krypton curve.

CONCLUSION

It seems possible that there may be a genuine discrepancy between the theoretical and the experimental curves which cannot be accounted for by defects in the apparatus alone. In his calculation, Landau assumes an average value for I, the ionization potential of an atomic electron, i.e. all the atomic electrons are treated as though they had the same average ionization potential and the same chances of collision; this assumption becomes farther from the truth as the atomic number increases. Maybe the energy-loss distribution in argon fits Landau's curve slightly better than in krypton because the electrons in the argon counter behave more like those in Landau's theoretical picture than the electrons in the krypton counter, as well as because the scattering is less in argon than in krypton. It follows that the distribution from a helium counter should fit Landau's curve more closely still.

ACKNOWLEDGMENTS

The author would like to thank Dr. B. Pontecorvo for his encouragement and many helpful discussions in the earlier stages of the experiment and Mr. D. West for his interest and advice. She is grateful to Dr. P. Cavanagh and Mr. W. H. Taylor for the use of the beta-spectrometer and associated electronic equipment. This work is published by permission of the Director, Atomic Energy Research Establishment, Harwell.

REFERENCES

Landau, L., 1944, *J. Phys., U.S.S.R.*, **8**, 201.
Maze, R., 1946, *J. Phys. Radium*, **6**, 164.
Rossi, B., and Greisen, K., 1941, *Rev. Mod. Phys.*, **13**, 241.
Rothwell, P., and West, D., 1950, *Proc. Phys. Soc.* A, **63**, 541.

The Mechanism of the Low-Frequency Electrodeless Discharge in Chlorine and the Influence of Irradiation

By W. L. HARRIES and A. von ENGEL
Clarendon Laboratory, Oxford

MS. received 2nd February 1951, *and in amended form 13th June* 1951

ABSTRACT. The current flowing through a 50 c/s. electrodeless discharge in a short cylindrical glass vessel with plane electrodes at the ends filled with chlorine at 5–50 mm. Hg was investigated with an oscillograph. It consists essentially of between one and fifty or more distinct pulses per half cycle, the number increasing with the voltage. At sufficiently large voltage these pulses cover the greater part of a half cycle including the instant of zero voltage. By irradiating the discharge with light from an incandescent lamp the average pulse height decreases, radiation below 4,800 A. being strongly active. By irradiating only the central portion of the vessel the pulse height does not change. Irradiating one wall reduces the height of the pulses in every second half cycle, namely those pulses whose electron avalanches start from that wall.

Once the discharge starts, electric charges collect on the inner surface of the vessel. Each current pulse consists of a series of avalanches which develop between small areas of the inner glass walls. One such area may discharge within a half cycle in several steps. The time variation of the applied field, the wall-charge field and the field in the gas are discussed and a new mechanism is developed which appears to apply to discharges between solid dielectrics.

At room temperatures, chlorine molecules form an adsorbed layer, several molecules thick, on the glass walls. Irradiation produces photo-dissociation of Cl_2, the atoms being effective in capturing electrons in this layer where slow electrons and many-body collisions are likely. This reduction of the number of secondary electrons reduces the pulse height. Adsorbed molecular gas layers also explain observations at higher temperatures. At higher voltages the interval between two successive pulses becomes so small that one pulse reduces the height of the following one. This is probably due to metastable Cl atoms and resonance radiation diffusing to the wall where they cause dissociation of molecules in the adsorbed layers, the chlorine atoms capturing electrons as before. It also explains why at high voltages the effect of irradiation becomes insignificant.

§ 1. INTRODUCTION

When a low-frequency discharge of between 50 and 500 c/s. is established in a glass vessel with external electrodes, filled with a halogen, it has been found by Joshi and others (Joshi and Deshmukh 1941, Joshi and Deo 1943, Deo 1944) that the r.m.s. value of the discharge current decreases when the vessel is irradiated with light from an incandescent lamp. The gas pressures were from 1 to 600 mm. of mercury.

We have investigated with a double-beam oscillograph the discharge current and the applied voltage in chlorine at pressures from 5 to 50 mm. Hg, in cylindrical hard glass vessels of length 1 cm. and 3 cm. and diameter 6 cm., with external electrodes fixed on the ends. The alternating electric fields were up to 6,000 volts per cm. r.m.s. at 50 c/s. parallel to the axis of the vessel. Figure 1 shows a diagram of the circuit. Distortion of the wave form and phase changes were avoided by using suitable carbon resistances.

The chlorine was prepared from concentrated hydrochloric acid and potassium permanganate. After washing with water and drying with calcium chloride, it was frozen in a side tube immersed in liquid air. This was then joined to the

apparatus, the whole evacuated and the vessel cleaned by passing a discharge through Cl_2 and re-evacuating, etc. The pressure of the chlorine was controlled by altering the temperature of the side tube by cooling it above the liquid air surface. The temperature of the tube was measured by a thermocouple and the pressure obtained from vapour pressure curves.

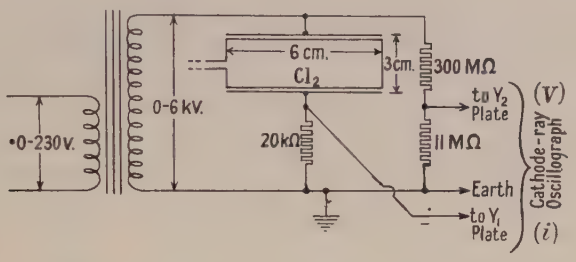

Figure 1. Circuit for measuring current and applied voltage with a cathode-ray oscillograph.

§ 2. GENERAL OBSERVATIONS

At small voltages a capacitative sine current flowed. When the field in the gas exceeded a critical value, a number of pulses or damped oscillations appeared every half cycle superimposed on the sine wave. The height of these pulses was always large compared with the amplitude of the sine wave.

As the applied voltage was increased, the number of pulses on each half cycle increased, but their average height remained practically unchanged; at the same time the pulses started at an earlier phase of the cycle and took up an ever increasing part of it. Though there were continuous fluctuations in individual pulse heights, any changes in the average pulse height could easily be observed.

Figure 2 shows oscillograms of the current for various applied voltages in complete darkness and with irradiation. When the vessel was irradiated with light from an ordinary 60 watt bulb at about half a metre distance, with the voltage just above the starting voltage of the discharge, it was found that the pulses were reduced in height (Joshi 1944). At higher voltages the reduction in pulse height became smaller and at sufficiently high voltages there was no change in pulse height, except for the first pulse in each half cycle. This first pulse was reduced in height by irradiation up to the highest voltages applied (about ten times the starting voltage).

We shall first discuss the nature of the pulses and afterwards the effect of light on the pulse height.

§ 3. NATURE OF THE DISCHARGE PULSES

(i) *Description and Origin of Pulses*

By using a small high-voltage transformer ($\simeq 100$ watts) critically damped pulses were obtained (Figure 3). Their peaks were up to about 200 μa., the time from the start to the peak of the pulse was about 2×10^{-5} sec. and the total pulse time about 2×10^{-4} sec.

In the circuit shown in Figure 1 the glass walls act as condensers which are charged by the ionization current flowing through the gas. When the field in the gas is sufficiently strong, an initial electron starting at the negative wall will cause an electron avalanche in the gas; thus electrons are driven to the positive wall and positive ions to the negative one. Positive ions, light and metastable atoms will

release further electrons from the negative wall (as in counters with insulated walls) and a series of avalanches develops. This increase in number of ions and electrons and the corresponding rise in current would only continue if the field in the gas remained unchanged. Because unlike charges collect on opposite walls a voltage drop develops across the glass walls. Since the applied potential is sensibly

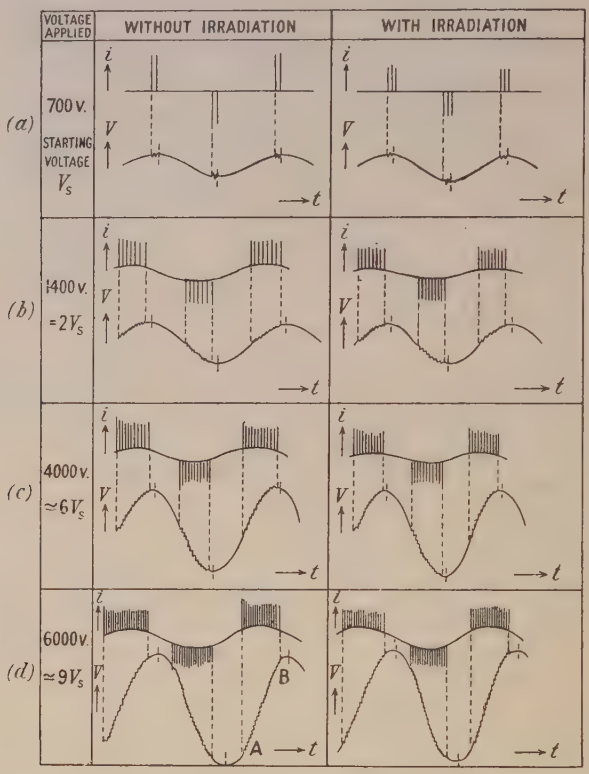

Figure 2. Oscillograms of the discharge current and the applied voltage (r.m.s. values) with and without irradiation.

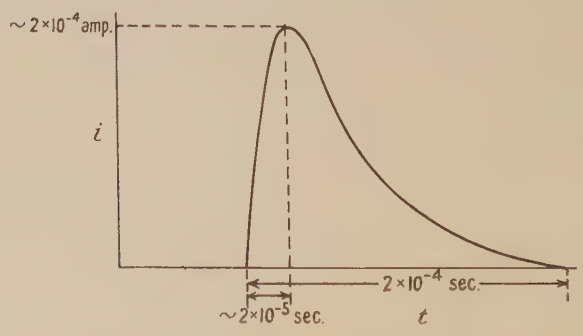

Figure 3. The current waveform of a pulse.

constant during the pulse time, the potential difference across, and the field in, the gas are thus gradually lowered. Consequently the rate of ionization and the current decrease and approach zero value. (Field distortion through space charges would tend to increase the rate of ionization here.)

There is also another cause for the decrease of the field in the gas : when the current rises a voltage drop occurs in the unavoidable inductances thereby reducing the electrode voltage. This can be seen from the voltage oscillogram (Figure 2) : each current pulse is accompanied by a kick in the voltage oscillogram.

(ii) *Effect of Wall Charges*

Pulses can occur at an instant when the voltage between the external electrodes is zero (Figure 2). Since a pulse can only be initiated when the field in the gas exceeds a critical value estimated of order 300 v/cm. at $p = 5$ mm. Hg, it can then only be due to wall charges produced during the previous half cycle if we neglect space-charge fields (cf. point corona in Cl_2, Thornton 1939).

At still higher voltages the current pulses can be seen to occur during almost the whole time interval between two successive peaks of the applied voltage (B to A of Figure 2 (*d*)). However the polarity of the current pulses remains the same although the applied voltage changes sign. This again follows from the existence of a wall-charge field ; between A and B the field in the gas which is the difference between the instantaneous values of the applied and wall-charge fields is always in the same direction (see also Figure 4 (*b*)), and so the current pulses must have the same polarity. Since similar results have been found in atmospheric air (not given here), we believe that the arguments discussed later in § 4 apply to other gases and higher pressures than those used above (cf. Gross 1950).

At high voltage the number of pulses per half cycle is large. Since the average pulse height and duration do not change appreciably with voltage, the quantity of charge passing through the discharge tube per half cycle is large, and thus intense wall-charge fields develop. Their magnitude can be seen from the fact that at the instant after the last pulse of a group (B in Figure 2 (*d*)) the maximum applied field is approximately balanced by the wall-charge field.

§ 4. POSSIBLE MECHANISMS OF THE DISCHARGE

(i) The charged inner glass surface of the vessel which lies under the electrodes is considered to be an equipotential surface at any instant. Each pulse then discharges the whole of these surfaces uniformly but not necessarily completely.

'Discharging a surface' does not necessarily mean that a quantity of the adsorbed charges from opposite walls of the vessel are released and travel through the gas to the other wall. It is rather the charges produced by electron multiplication in the gas that move to the walls, first neutralizing the charges already there and eventually building up charges of opposite polarity. Hence, during a pulse the field in the gas decreases from breakdown to nearly zero value, while the current first rises and then ceases. After that the applied field has to rise again until the field in the gas reaches breakdown value, when another pulse occurs, and so on (Figure 4).

When the peak of the field in the gas is just above breakdown value (Figure 4 (*a*)) only one pulse per half cycle can develop. This is because the field in the gas, which is equal to the sum of the external field and the wall charge field, exceeds the breakdown value (dotted lines) only once per half cycle. In the steady state the wall charge field must have the same magnitude in both half cycles and opposite sign. It must be equal to the peak applied field ; also Figure 4 shows that if it were larger the pulse would occur too soon before the peak, contrary to observations.

At applied voltages well above breakdown voltage (Figure 4 (*b*)), because of the large number of pulses, the wall-charge field at the instant before the first pulse of a group is large. Since the wall-charge field is then opposite to the applied field, the field in the gas can reach breakdown value while the external field decreases towards zero. This is why pulses can occur at decreasing parts of the applied voltage curve. The current pulses do not change direction when the applied voltage changes sign, because the polarity of a current pulse depends on the sign of the change of charge, which remains the same for each group of pulses.

When a pulse occurs, the wall-charge field is suddenly reduced by an amount which is only a fraction of the initial value (Figure 4 (*b*)). This causes the field in the gas to drop to zero at the end of a pulse. Then the applied field, and hence the field in the gas, rise again until the latter reaches breakdown value, when another pulse occurs and so on. The wall-charge field thus changes in steps, the last pulse occurring just before the peak applied voltage.

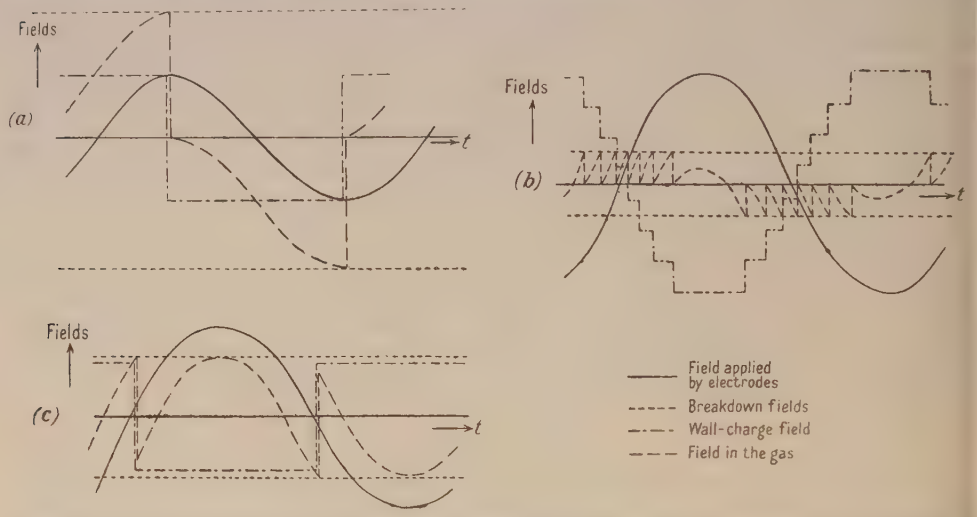

Figure 4. (*a*) Electric fields at low applied voltages. This diagram applies either for the whole of the inner glass surface being discharged once per half cycle or for one small area discharging. (*b*) Electric fields at large applied voltages. This diagram applies either for the whole of the inner glass surface being discharged several times per half cycle or for one small area discharging in steps (mechanisms (i) and (iii) respectively). (*c*) Fields for one elementary area with a pulse occurring near zero applied field (mechanism (ii)).

The following objections can be raised to this mechanism :

At low voltage, i.e. when the number of pulses per half cycle is small, the pulses occur very close together. From the above mechanism the pulses should be spaced far apart as a large time interval is required near peak voltage for the field in the gas to reach breakdown value again.

For large applied fields (Figure 4 (*b*)) the pulses should occur closer together when the applied voltage passes through zero as the interval between the pulses depends on the rate of change of the applied field. Such a clustering has not been observed.

For the largest applied fields of the order of ten times the starting field, we should expect to have approximately ten pulses per half cycle, whereas three to five times this number have always been observed.

(ii) A second view is that a pulse discharges only small areas of the charged inner glass surface under the electrodes. Thus, contrary to (i), the inner surfaces

are here in general non-equipotential. When electron avalanches develop, the discharge is confined to a narrow cylinder extending between two opposite areas. After a pulse has occurred the field in the gas in front of these areas is reduced, preventing further discharge; for other regions of the vessel the field in the gas is effectively unchanged, so other areas can still discharge. As the wall-charge density, the nature of the glass surface etc., vary over the inner surfaces, a pulse starts from another small area at a different value of the applied field, and so a group of pulses develops. Now each pulse originates from a different small area and reverses the charge on it from $+q$ to $-q$ or vice versa once in a half cycle. If, however, a pulse reduces the field in the gas over adjacent areas, then the following pulse could only occur some distance away from the first where the field has not been reduced. This was observed at low voltages, where the pulses were few; the luminous paths of the discharge appeared to originate from small areas of the glass and jump about from point to point inside the vessel.

Figures 4 (*a*) and (*c*) show the fields for a single elementary area. If the applied field is just above breakdown value (Figure 4 (*a*)) a single pulse will result near its peak. The wall-charge fields are assumed constant between pulses, implying that recombination in the gas is neglected.

At large applied fields the pulse is shifted to the left in the diagram. A pulse at an earlier phase is only reconcilable with a larger wall-charge and applied field. Figure 4 (*c*) shows this for a pulse occurring near zero applied field. These conditions are, however, incompatible; when the wall-charge reverses, the applied field available would be much too weak to build up a strong wall charge in the reverse direction. So this view cannot explain pulses which occur near zero applied field.

Other objections to this mechanism are that according to Figure 4 (*a*) and (*c*) the pulse carries charges which would increase with the applied field, contrary to observation. Also it would be difficult to understand how the two elementary areas which provide the first and last pulse of a group (Figure 2 (*d*) A and B) should have such vast differences of starting potential. Also large potential differences would develop between adjacent areas of opposite polarity and a discharge occurs along the glass surface.

A third mechanism is proposed which is based on both (i) and (ii).

(iii) Each pulse is associated with a discharge covering a small elementary area. In addition each pulse is accompanied by a change of wall charge which may be partial only, and need not necessarily result in a change of polarity.

For low applied fields where there is only one pulse per half cycle, as in Figure 4 (*a*), this single pulse originates from that elementary area which has the lowest starting potential at that time. The next pulse can come from a different area because their starting potentials may change (e.g. if adsorbed gas is removed by the pulse).

At large applied fields the pulses would only partially discharge the areas, and the wall-charge field would change in steps (Figure 4 (*b*)). This would explain why the pulses have the same sign whether they occur before or after zero applied field. It also accounts for the constancy of the average height of the pulses. Taking the starting potential and the average size of an area as being constant, the change of wall charge is proportional to the starting potential. Also for an elementary area the number of pulses per half cycle cannot exceed peak applied voltage divided by starting voltage. However, the number of pulses observed

was very much larger than this, which suggests that a number of elementary areas was being discharged.

Also the wall-charge field for an area will not remain constant between two pulses, as shown in Figure 4 (*b*), because discharges in the neighbourhood as well as surface conduction may change its value. Further discharges along the inner surface would occur if the potential difference between two adjacent sites exceeds the corresponding breakdown value.

It can be seen that the objections raised to mechanism (i) and (ii) can all be overcome by mechanism (iii). The same mechanism may be applicable to discharges in cavities (voids) in insulators (see Austen and Whitehead 1941, Mason 1951).

§ 5. FURTHER EXPERIMENTS AND THEIR DISCUSSION

(i) *Experiments with Split Electrodes*

In order to test whether a discharge takes place between small areas on opposite walls, one of the external electrodes was replaced by two semicircular plates with a narrow earthed electrode between them. The currents to the two electrodes were observed with a double-beam cathode-ray oscillograph. At voltages just above starting potential, a considerable number of the pulses to the two halves occurred at different instances. This means that discharges originate from areas each small compared with that of the electrode.

(ii) *Experiments with a Point Electrode*

One of the external electrodes was replaced by a point electrode (wire of 1 mm. radius) touching the centre of the glass wall. One pulse per half cycle appeared up to voltages corresponding to roughly twice the starting potential, and at four times the starting potential the number of pulses per half cycle varied between three and five. Thus the average number of pulses per half cycle seems to be proportional to the ratio of the peak applied voltage to the starting voltage. Also the time interval between these pulses was much greater than that between pulses with plane electrodes. The number and height of the pulses in two consecutive half cycles were always the same.

The following conclusions can be drawn from this experiment: Since the field of a point electrode is only strong within a narrow region, discharges can only develop from a small area and so a smaller number of pulses per half cycle occurred. One might have expected a larger number of pulses as the field under the point electrode is much higher than the uniform field for the same voltage. Thus, probably only one pair of small areas was involved in the discharge process; the fact that the number of pulses was roughly equal to the number of times the peak field is greater than the starting field (see above) supports this view. It also explains why the interval between the pulses here is much larger than with a uniform field: with only one small area sufficient time had to elapse until the applied field changed by an amount which corresponded to the starting potential.

It should be mentioned that at high voltages a corona discharge developed externally in air under the wire electrode producing its characteristic current pattern on the screen. The corona current flowing to the plane electrodes was negligible at all voltages.

Although a point–plane gap has a non-symmetrical field, the number and height of the pulses in two consecutive half cycles were always about the same. It would seem as if the current, the period of oscillation, and hence the charge per pulse, are

essentially controlled by the properties of the electric circuit, whereas the discharge acts as a switch triggered by the field. Apparently at low pressures and in the presence of a glass wall which evened out the field, polarity effects were not pronounced or covered by fluctuations. This is in contrast to the breakdown with dissimilar (internal) electrodes of molecular gases at atmospheric pressure.

(iii) *The Number of Electron Avalanches in a Pulse*

A pulse appears to consist of a large number of electron avalanches; this can be seen by the following arguments.

The current at the peak of a pulse has been found to be of the order of 10^{-4} amp. Assuming the pulse of Figure 3 (*b*), its total charge is approximately 10^{-8} coulomb, hence the number of electrons is of the order of 10^{11}. Assuming an average field in the gas of about 300 v/cm. (Figure 2 (*a*)) and a pressure of 5 mm. Hg, the value of $X\,p$ would be about 60. Taking the corresponding value of α for HCl as approximately 3 (unknown for Cl_2) (Townsend 1915, von Engel and Steenbeck 1932) and the length of the vessel as 3 cm., the total number of electrons in an avalanche produced by one electron would only be about 10^4. Hence a very large number of avalanches seem necessary to transfer the pulse charge assuming a small number of initial electrons at the instant of the first avalanche.

The time from the start of an individual pulse up to its peak has been found to be of the order of 10^{-5} sec. (Figure 3), its total duration of the order of 10^{-4} sec. Estimating the mobility of an electron in chlorine at 1 mm. Hg to be of the order of 10^6 cm sec. per volt/cm., then at 5 mm. Hg and 300 v/cm., the velocity of the electrons would be of the order of 10^8 cm/sec. The transit time between the glass walls is about 10^{-8} sec., which is small compared with 10^{-5} sec., and thus a large number of avalanches have occurred by the time the peak current is reached.

(iv) *Approximate Size of the Area discharged by one Pulse*

Each pulse causes a quantity of charge Δq to be carried over to the opposite wall. Assume that it forms a uniform layer over an area A. Let the capacity between this area and the electrode be C, then the change of field in the gas for a vessel of length d will be of the order

$$\Delta E \sim \Delta q/Cd. \qquad \ldots\ldots(1)$$

At the end of the pulse the field in the narrow volume considered would be zero. Hence E will be of the order of the breakdown field, i.e. 300 v/cm. at a few mm. Hg. From (1) and with the pulse of Figure 3 ($q = 10^{-8}$ coulomb, $d = 3$ cm.), C is about 10 pF. Since the glass wall is about 0·1 cm. thick and its dielectric constant about 4, A is of order 1 cm^2. Though this value represents the upper limit, as Δq was taken for one of the largest pulses, it is small compared with the area under an electrode.

(v) *The Height and Length of the Pulse*

Assume that V_s, the starting potential of the discharge, is given and that only one discharge exists at a time. If the shape and height of the pulse were controlled by the external circuit only, the maximum current flowing through the gas would be

$$i_m \sim V_s/(L/C)^{1/2}. \qquad \ldots\ldots(2)$$

With $V_s \sim 1{,}000$ volts, $L \sim 50$ henries (the leakage inductance of the transformer) and $C \sim 10^{-11}$ F., we have $i_m \sim 5 \times 10^{-4}$ amp. which agrees in order with observations (Figure 3 (*b*)); the measured values should be smaller because the voltage drop

across the discharge was neglected in (2). When a longer vessel was used, i_m was larger because V_s increases with the length of the vessel for $p = \text{const.}$

Again the length of the pulse, neglecting damping by the discharge, can be obtained from $\omega \sim 1/(LC)^{1/2} = 5 \times 10^4$ per sec.; hence the time of the quarter wave is about 3×10^{-5} sec. which agrees with the observed time up to the peak of approximately 2×10^{-5} sec. The damping influence of the discharge and the leakage capacity of the transformer would tend to lengthen the period of oscillation.

(vi) *Fluctuations in Height and Phase of the Current Pulses*

The cathode-ray oscillograph patterns showed that the peak values and the instant of occurrence of the pulses were fluctuating continuously (Joshi 1944). One major cause seems to be the variation of secondary electron emission from the glass wall, produced by positive ions. The emission coefficient γ (number of electrons per positive ion) depends, as we know, on the state of the glass surface, on the type of glass used, its preparation, and particularly on the adsorption of gases. γ varies from point to point on a wall and, in addition, it varies with time. Also the distribution of charges on the walls will not be uniform, as the pulses occur in narrow channels. These phenomena cause fluctuations in phase as well as in amplitude.

(vii) *Separation of the Pulses*

Although the pulses fluctuate in height and phase, they have always been observed to be separated, i.e. the peaks never merge into one another. The main reason seems to be that the current pulse produces a voltage drop in the leakage inductance of the transformer, and stray inductance of the circuit (neglecting the resistance), so that the applied field decreases while a pulse develops. This stops other areas from developing avalanches (see voltage curves, Figure 2). When the pulse ceases, the applied field returns to its original value and a discharge can develop from other areas.

§ 6. THE EFFECT OF IRRADIATION ON THE DISCHARGE

(i) *Photo-dissociation of Chlorine*

By irradiating the discharge vessel using incandescent lamps with various filters, we again verified (Joshi and Deshmukh 1941, Joshi and Deo 1943, Deo 1944) that light of $\lambda \leqslant 4{,}800$ A. caused the reduction in pulse heights. This wavelength corresponds to quanta of energy 2·58 ev., which is the energy of dissociation of a chlorine molecule (Bowen 1946). Thus irradiation seems to cause photo-dissociation of the chlorine molecules into two atoms (one of which is in a metastable state, 0·1 ev. above the ground state).

Chlorine atoms attach electrons readily forming Cl^- when (*a*) the electron velocity is low, (*b*) the attachment occurs in the presence of a third body (Cl_2). In this case the probability of attachment is large because the affinity energy (3·5 ev.) can be transformed either into potential energy leading to dissociation of Cl_2, or into kinetic energy of the particles. In the absence of a third body, the affinity energy has to be emitted as a quantum of radiation, which is a rare process.

The electrons so lost from the avalanches no longer produce electron multiplication and the height of the pulse drops. The negative ions formed have a negligible mobility compared with the electrons, and do not contribute to the current. The probability of electron attachment to the molecule to form Cl_2^- is very small indeed (Loeb 1939).

Electrons are also lost by first dissociating a molecule and then becoming attached to one of the atoms. However this process goes on whenever a discharge occurs, and represents a loss of electrons independent of irradiation. The next step is to show numerically the effect of photo-dissociation by an incandescent lamp.

(ii) *The Rate of Photo-dissociation*

The tungsten filament of a 40-watt bulb was considered a black body radiator at constant temperature $T=2{,}500°$ K. The number of quanta emitted per second in an elementary wavelength range is given by Planck's distribution law. At low p only few quanta are absorbed by the gas, the absorption depending on the wavelength. Multiplication of these two factors and integration over the wavelength range bounded by the band convergence limit of chlorine and by the transmission limit of the glass vessel, gives the rate of absorption of quanta, and thus the rate of photo-dissociation occurring.

If E is the energy per unit volume in a wavelength range λ to $\lambda+d\lambda$ then $\boldsymbol{c}E_\lambda$ is the radiant flow in erg cm^{-2} sec^{-1} where $\boldsymbol{c}$ is the velocity of light. The number of photons n_λ emitted per unit area of surface per second in an elementary range is

$$n_\lambda=\boldsymbol{c}_\gamma E_\lambda/\boldsymbol{h}\nu=8\pi\boldsymbol{c}/\lambda^4(e^x-1), \qquad \ldots\ldots(3)$$

where $x=\boldsymbol{hc}/\lambda\boldsymbol{k}T$, $\boldsymbol{h}=6{\cdot}55\times10^{-27}$ erg sec., $\boldsymbol{k}=1{\cdot}377\times10^{-16}$ erg deg^{-1} and $T=2{,}500°$ K.

The number n_a of quanta absorbed in passing through d cm. of gas in the wavelength range $d\lambda$, expressed as a fraction of the number n_0 entering is

$$(n_a/n_0)_\lambda=1-\exp(-\alpha_\lambda Cd)\sim\alpha_\lambda Cd \quad (\alpha_\lambda Cd\ll1), \qquad \ldots\ldots(4)$$

where C is a concentration. α_λ as a function of λ was taken from the measurements of von Halban and Siedentopf (1922). By graphic integration $n_\lambda(n_a/n_0)_\lambda$, the number of quanta absorbed per second in a square glass vessel of 6 cm. side and 3 cm. wide (the beam traversing 6 cm. of gas) at 5 mm. Hg, assuming a 40-watt bulb 50 cm. away with an emitting surface area of 0·4 cm^2 (emissivity of tungsten = 0·43) was found to be $7{\cdot}1\times10^{12}$ quanta per sec. The number of chlorine atoms formed per second is twice this in a volume of $(6\times6\times3)\times100$ cm^3, or the rate of formation is $dN/dt=1{\cdot}4\times10^{11}$ atoms/cm^3 sec.

(iii) *The Equilibrium Concentration of Atoms*

The equilibrium concentration of chlorine atoms can be found from an estimated value of the life of a chlorine atom. Bodenstein and Lütkemeyer (1924) found that about one collision in one thousand for bromine atoms results in recombination, which means as we know now that 1 collision in every thousand is a three-body collision. We assume that this figure applies approximately to chlorine. Thus the equilibrium concentration N per cm^3 of chlorine atoms is found from

$$dN/dt=N/\tau, \qquad \ldots\ldots(5)$$

where τ is the average life of a chlorine atom. At room temperature, since the collision interval is l/v, but only a fraction N/M collisions occur between Cl and Cl_2 and every thousandth collision leads to recombination, we have

$$\tau=10^3 lM/vN, \qquad \ldots\ldots(6)$$

where l is the mean free path of chlorine atoms, $4{\cdot}4\times10^{-4}$ cm., v their velocity, $3{\cdot}8\times10^4$ cm/sec., and M the number of chlorine molecules present, all at 5mm. Hg pressure, viz. $2{\cdot}7\times10^9\times5/760$. Thus we have from (6) $N\tau=2\times10^{12}$.

From this, the rate of formation given at the end of § 6 (ii), and equation (5) we have $N \sim 5 \times 10^{11}$ atoms/cm^3 and $\tau \sim 4$ sec.

This shows that chlorine atoms do not recombine appreciably in the gas phase.

Another way of obtaining N and τ is by using the equation for three-body recombination:

$$dN/dt = -KMN^2, \qquad \ldots\ldots(7)$$

where K is the coefficient of recombination, M is the concentration of 'third-bodies', and N that of Cl atoms.

Taking the value of K as $0{\cdot}8 \times 10^{-32}$ for chlorine (Noyes and Leighton 1947), we have

$$dN/dt = -1{\cdot}4 \times 10^{-15} N^2. \qquad \ldots\ldots(8)$$

Equating (8) and the above rate of formation, we obtain the equilibrium concentration $N \sim 2 \times 10^{13}$ atoms/cm^3 and $\tau \sim 8$ sec. Thus from these two results N is of order 10^{12} or 10^{13} and $\tau \sim 4$–8 sec., assuming that the atoms do not strike the walls.

If recombination occurred entirely at the wall (where the rate would be exceedingly high, as the wall can act as a third-body), then the atoms could not disappear in less time than they would take to diffuse to the wall. This time is found from the equation $(\overline{x^2})^{1/2} \sim (2Dt)^{1/2}$ where $\overline{x^2}$ is the mean square of the displacement, D the coefficient of diffusion and t the time during which the atoms travel. Taking the coefficient of diffusion of chlorine atoms as 30 cm. sec^{-1} at 1 mm. Hg, at 5 mm. Hg D would be 6. In our case the wall was about 1 cm. away from the centre of the tube, so $t \sim 0{\cdot}1$ sec. Thus since the time t for diffusion to the walls is small compared with the lifetime τ required for recombination in the volume, we deduce that recombination takes place almost entirely on the walls.

§ 7. THE EFFECT OF IRRADIATING DIFFERENT REGIONS OF THE DISCHARGE

To investigate this, a narrow parallel beam of light from a 40-watt bulb was passed through the discharge ($p \sim 10$ mm. Hg) as in Figure 5. No measurable

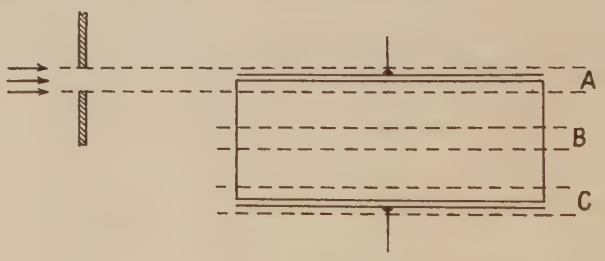

Figure 5. Irradiation with narrow beam applied to different parts of the vessel.

effect on the average pulse height was observed when the central portion B of the vessel was irradiated. When the region A near the wall was irradiated the average heights of the pulses in one half cycle only were reduced, and when the wall C was illuminated pulses in the other half cycle decreased. Further it was found that the illumination of the gas near the wall reduced those pulses which occurred in the half cycle in which the external electrode at that wall was negative. This means that the height of a pulse was reduced when the region from which the electrons started was irradiated.

As the heights of the pulses in two successive half cycles were unequal, the shorter pulses must either have been greater in number or of longer duration

because the net total charge transferred across the vessel in two half cycles has to be zero. We did not observe an increase in number of the pulses and the sensitivity of our apparatus was not great enough to show any increase in their duration.

Light falling on the central portion of the gas dissociates the chlorine molecules into atoms. Now the probability of attachment of electrons to atoms is high for small and low for high energies. Thus few electrons are lost from the avalanche near the centre, because they are too fast. Electrons have small velocities only near the wall at which they start, and here the probability of attachment is high. The removal of a few electrons here reduces the multiplication and hence the peak current considerably.

Although in the central portion of the tube atoms are formed which diffuse to the wall and few recombine in the gas, no reduction in pulse height was observed. This suggests that the conditions near the wall are more favourable for the attachment of electrons to atoms. This leads to the assumption of a gas layer adsorbed on the wall as distinct from the boundary layer consisting of ions and excited molecules as suggested before (Joshi 1946).

The likelihood of electrons becoming attached to excited atoms is small (Massey 1950) because of the Auger effect; the excited ion would be stable if the excitation energy were smaller than the affinity, which is rarely the case.

§ 8. INFLUENCE OF ADSORBED GAS LAYERS ON THE PULSE

There is little doubt that gas molecules and atoms can become adsorbed on glass walls where they form one or more layers. The atoms will adhere mainly by an adsorption process described by Langmuir (Miller 1949) whereby the adsorbed atom can be regarded as being held on the glass by a chemical bond. The molecules on the other hand are held by van der Waals forces. Thus the atoms are much more firmly held, their energy of adsorption being twenty or more times larger than the link produced by van der Waals forces. An atom coming from the gas which strikes an adsorbed atom will recombine in approximately 10^{-13} sec., i.e. the time of oscillation of a diatomic molecule, and the molecule so formed will return to the gas. The likelihood of this process taking place is large because the recombining energy balances the energy of atomic adsorption, any excess energy being transferred to the wall which acts as a third body.

Though there are no measurements available about adsorption of chlorine on glass at room temperature, one can deduce from the experimental evidence with other gases and walls that in equilibrium there will be a sparsely distributed population of atoms on the glass with molecules on adjacent sites, and on top of the whole several layers of molecules (Miller 1949). In this system of layers the density is high; it resembles a phase which is more akin to a liquid than a gas. Chlorine atoms from the gas can recombine on the surface of these layers without penetrating to the wall surface.

When the vessel is irradiated, light is strongly absorbed in the adsorbed gas layers where the concentration of molecules is high, and hence a large number of atoms is formed. An equilibrium process is set up in the adsorbed layers of molecules dissociating and atoms recombining, and an equilibrium concentration of atoms is established. Thus secondary electrons released from the glass walls have a good chance of becoming attached to these atoms, because near the wall the electron energy is low and, moreover, the energy of electron affinity can be

dissipated easily in such densely populated layers because a 'third body' is always present.

In addition to external irradiation, light pulses are emitted from the discharge producing photo-dissociation. Again electrons of sufficient speed can dissociate molecules by collision. The atoms so formed diffuse towards the walls where they recombine quickly; the increase in the number of atoms in the adsorbed phase is expected to be very small for the reasons given below. Hence there will be only an inappreciable change in the number of negative chlorine ions and in the average pulse height.

We have estimated the light produced by the discharge on the basis that up to ten times more quanta are emitted per pulse then there are electrons. With the largest value of the pulse height and number of pulses per second, we found that the number of active quanta produced by the discharge is several orders of magnitude smaller than that from external irradiation.

§ 9. REDUCTION IN THE PULSE HEIGHT BY THE PRECEDING PULSE

It has been pointed out earlier that at higher voltages and in the absence of irradiation the height of the pulses in a group decreased gradually (Figure 2 (*d*)). It was also found that the first pulse of a group remained large up to the highest applied voltages, and was only reduced in height when the vessel was externally irradiated. The explanation is that at increasing voltages the interval between two successive pulses becomes shorter. It is evident that the basic factor is the time interval at which the influence of one pulse on the following one becomes apparent. This was estimated (Figure 2) to be of the order of 10^{-4} second. We must therefore look for a process which remains active for that time. It could not influence the first pulse of a group because the interval between the last pulse of one group and the first of the rest was greater than ten times this (Figure 2), even at the highest applied voltage.

The light emitted from the previous pulse cannot be effective, as it would reach the wall almost instantaneously and any atoms formed would recombine in 10^{-13} second. Again the effect cannot be due to positive ions: these positive ions would be those few from a previous pulse which during 10^{-4} sec. would have moved to the region of the next pulse under the influence of lateral electric fields which are due to the non-uniform distribution of wall charges; further, positive ions might increase the electron emission from the wall, because they have sufficient kinetic energy to penetrate the gas layers: this would make the pulse larger and not smaller.

One mechanism which seems to explain the above facts is associated with metastable atoms. Chlorine atoms have not only a metastable level at about 0·1 ev. above the ground state, but also one at about 8 ev., just below the resonance level suggested by H. Kuhn from the term scheme. These metastable atoms are produced by electron collision in the gas. They could release further electrons from the glass unless a layer of gas was present, adsorbed to the wall. The energy of the metastable atoms is used to dissociate molecules in this layer into atoms (dissociation energy less than 2·5 ev. which is the dissociation energy of the free molecule), to which any secondary electrons released from the wall can become attached. As the lifetime of metastable chlorine atoms at these pressures is probably of the order of 10^{-4} second or more, they would continue to arrive at the wall for this time after any pulse had ceased. Hence dissociation of

molecules into atoms could continue for this length of time and thus a reduction of any pulse occur sufficiently soon after a previous one.

A similar argument would also apply to resonance radiation which is emitted from excited gas atoms. This radiation diffuses through the gas being emitted from one atom, reabsorbed by another and so on, until it reaches the dense molecular phase adsorbed on the glass walls in which it dissociates molecules.

Either of these two processes would satisfy the condition that it increases the concentration of atoms on the wall and continues to do so for an interval of 10^{-4} sec. or more.

It can now be seen why at higher voltages external irradiation has practically no effect on the pulse height. Since the pulses follow each other very closely, a large number of metastable atoms and resonance quanta and a large concentration of unexcited atoms is available in the adsorbed layers at the instant of the next pulse. As the irradiation reduces the height of the first pulse to about that of the next, yet does not further reduce the following ones, one has to conclude that with a given light source the concentration of atoms in the adsorbed layer cannot exceed a saturation value. Hence at large voltage the heights of the pulses remain unchanged when irradiation is applied (apart from the first pulse of a group). Other workers have found that the change in r.m.s. current due to irradiation became smaller the higher the voltage.

§ 10. EFFECT OF TEMPERATURE

It has been shown (Joshi and Deshmukh 1941, Visvanathan and Kuppuswamy 1950) that increase of temperature decreases the change of the average current due to irradiation. This may be so because an increase of temperature would reduce the number of molecules in the adsorbed layer on the wall, on which the reduction of pulse height seems to depend.

ACKNOWLEDGMENTS

We should like to thank Professor Lord Cherwell for extending to us the facilities of the Clarendon Laboratory, Drs. E. J. Bowen and A. R. Miller for stimulating discussions, and Dr. R. W. Lunt for advice and for the loan of papers previously published on this subject.

REFERENCES

Austen, A. E. W., and Whitehead, S., 1941, *J. Instn. Elect. Engrs.*, Part II, **88,** 88.
Bodenstein, M., and Lütkemeyer, H., 1924, *Z. Phys. Chem.*, **114,** 208.
Bowen, E. J., 1946, *Chemical Aspects of Light*, 2nd Ed. (Oxford : University Press).
Deo, P. G., 1944, *Proc. Indian Acad. Sci.* A., **19,** 117.
von Engel, A., and Steenbeck, M., 1932, *Elektrische Gasentladungen*, **1** (Berlin : Springer), p. 106.
Gross, B., 1950, *Brit. J. Appl. Phys.*, **1,** 259.
von Halban, H., and Siedentopf, K., 1922, *Z. Phys. Chem.*, **103,** 84.
Joshi, S. S., 1944, *Nature, Lond.*, **154,** 147 ; 1946, *Proc. Indian Sci. Cong.*, III.
Joshi, S. S., and Deo, P. G., 1943, *Nature, Lond.*, **151,** 561 ; 1944, *Ibid.*, **153,** 434.
Joshi, S. S., and Deshmukh, G. S., 1941, *Nature, Lond.*, **147,** 806.
Loeb, L. B., 1939, *Fundamental Processes of Electrical Discharges in Gases* (New York : Wiley).
Mason, J. H. 1951, *Proc. Instn. Elect. Engrs.*, Part I, **98,** 44.
Massey, H. S. W., 1950, *Negative Ions*, 2nd Ed. (Cambridge : University Press).
Miller, A. R., 1949, *The Adsorption of Gases on Solids* (Cambridge : University Press), p. 100.
Noyes, W. A., and Leighton, P. A., 1947, *Photochemistry of Gases* (New York : Reinhold).
Thornton, W. M. 1939, *Phil. Mag.*, **28,** 666.
Townsend, J. S., 1915, *Electricity in Gases* (Oxford : University Press).
Visvanathan, K. S., and Kuppuswamy, K., 1950, *Indian J. Phys.* **24,** 13.
Whitehead S,, 1950, *Dielectric Breakdown of Solids* (Oxford : University Press), chap. IV.

LETTERS TO THE EDITOR

The Saturation Magneto-Resistance of Iron–Aluminium Alloys

In a recent publication (Parker 1951) the author suggested that the magneto-resistance coefficient at technical saturation magnetization of iron alloys containing up to 9·5% silicon can be considered to depend upon two distinct terms ; these are associated with the temperature-dependent and independent scattering of conduction electrons by the crystal lattice of the alloy. Based upon this hypothesis, the following equation was derived :

$$\Delta\rho/\rho=[\Delta\rho_S/\rho_S+(\Delta\rho_F/\rho_F)\rho_0(1+\beta t)/\rho_S]/[1+\rho_0(1+\beta t)/\rho_S], \qquad \ldots\ldots(1)$$

where $\Delta\rho/\rho$ and $\Delta\rho_F/\rho_F$ are the saturation magneto-resistance coefficients of the alloy and of pure iron respectively, $\Delta\rho_S/\rho_S$ is a quantity characteristic of the silicon atoms present in the alloy, $\rho_0(1+\beta t)$ the resistivity of iron at t°c., and ρ_S the temperature-independent contribution to the resistivity of the silicon solid solution. It was further postulated that $\Delta\rho_F/\rho_F$ and $\Delta\rho_S/\rho_S$ were proportional to the square of the spontaneous magnetization of the alloy. Values for $(\Delta\rho/\rho)_{\parallel}$, the longitudinal saturation magneto-resistance coefficient (magnetization parallel to the direction of current flow) calculated from equation (1), are in good agreement with experimental results reported by Shirakawa (1939) if the value of $(\Delta\rho_S/\rho_S)_{\parallel}$ at low temperatures is chosen as $-1{\cdot}34\times10^{-3}$.

Measurements of resistivity and saturation magneto-resistance have now been made on two samples of iron containing 2·68% and 3·60% aluminium respectively, in the temperature range from −78°c. to +300°c., a range in which a comparison with equation (1) can most readily be made. The chemical analyses of the samples were respectively : Al 2·68%, Si 0·06%, S 0·027%, P 0·03%, C 0·07%, Mn 0·08%, Ni 0·085%, Cu 0·18%, Fe balance, and Al 3·60%, Si 0·15%, P 0·028%, C 0·013%, Mn 0·10%, Ni 0·08%, Cu 0·15%, Fe balance. The measured values of the resistivities of the samples are in good agreement with those already reported for iron–aluminium alloys by Yensen and Gatward (1917) and Masumoto (1936). The new values of $(\Delta\rho/\rho)_{\parallel}$ are recorded in Figure 1 together with the curves calculated from equation (1) in the same manner as

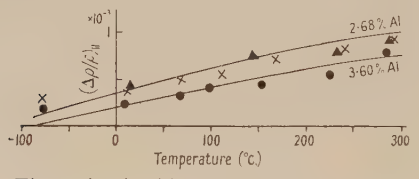

Figure 1. $(\Delta\rho/\rho)_{\parallel}$ for 3·60% Al iron ●, and for two different specimens of 2·68% Al iron × and ▲; curves, calculated from equation (1).

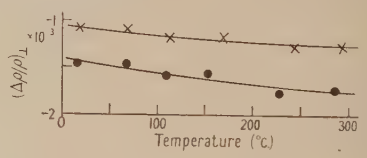

Figure 2. $(\Delta\rho/\rho)_{\perp}$ for 3·60% Al iron ●, and for 2·68% Al iron ×.

was previously done for iron–silicon alloys. The value of $(\Delta\rho_S/\rho_S)_{\parallel}$ at low temperatures, calculated from $(\Delta\rho/\rho)_{\parallel}$ at 10° c., is $-0{\cdot}41\times10^{-3}$. Agreement between the experimental and calculated values of $(\Delta\rho/\rho)_{\parallel}$ for both samples is about the same as that reported for iron–silicon alloys. It is well within the limits of accuracy expected, due to the uncertainty in choosing the correct value of $(\Delta\rho_F/\rho_F)_{\parallel}$, the contribution to $(\Delta\rho/\rho)_{\parallel}$ of the impurities, and the difficulty in correcting the experimental results for the variation of resistivity with spontaneous magnetization.

The transverse saturation magneto-resistance coefficient, $(\Delta\rho/\rho)_{\perp}$ (magnetization perpendicular to the direction of current flow), of the samples was measured between 15°c. and 300°c., the result being recorded in Figure 2. Unfortunately, direct comparison with equation (1) is here not possible owing to the lack of data of $(\Delta\rho_F/\rho_F)_{\perp}$ for pure iron, thus virtually resulting in two unknown parameters in the equation. It is almost certain, however (Webster 1927), that the latter lies between $-0{\cdot}3\times10^{-3}$ and $-1{\cdot}6\times10^{-3}$ at room temperature ; assuming any value within this range, a calculation analogous to the one for the longitudinal coefficient predicts a variation of $(\Delta\rho/\rho)_{\perp}$ between 10°c. and 300°c. of less than $0{\cdot}3\times10^{-3}$ for both samples. It can be seen from Figure 2 that this is the case.

It may be concluded from the above measurements that the longitudinal and transverse magneto-resistance coefficients at technical saturation of both samples obey equation (1) to within the expected limits of accuracy.

The author's thanks are due to Professor L. F. Bates and to Dr. R. Street for their interest in this work.

Department of Physics, R. Parker.
The University, Nottingham.
13th July 1951.

Masumoto, H., 1936, *Sci. Rep. Tohoku Imp. Univ.*, K. Honda Anniv. Vol., 388.
Parker, R., 1951, *Proc. Phys. Soc.* A, **64**, 447.
Shirakawa, Y., 1939, *Sci. Rep. Tohoku Imp. Univ.*, **27**, 255.
Webster, L. W., 1927, *Proc. Roy. Soc.* A, **114**, 611.
Yensen, T. D., and Gatward, W. A., 1917, *Univ. of Illinois Eng. Exper. Station*, Bulletin 95.

The Magnetic Properties of α-Ferric Oxide

In a comprehensive survey, presented at the Grenoble Colloquy last year, of the observed magnetic properties of the various forms, both natural and synthetic, of rhombohedral ferric oxide α-Fe_2O_3, Chevallier (1951) justifiably contends that the theory due to Néel (1949) to account for the weak ferromagnetism often observed in this substance cannot hold when the conditions of chemical formation, or subsequent prolonged annealing in oxygen at 1,100° c. or above, preclude the existence of any ferrous ions in the structure.

The essence of Néel's theory is that the ferromagnetism is due to an 'impurity' in the form of localized thin layers of what is sensibly magnetite, but with a somewhat deformed (cubic to rhombohedral) lattice, the ternary axes of both structures being coincident, as are the common planes of close-packed oxygen atoms normal to this common axis. In the discussion at Grenoble, as well as in an earlier published note (1950), Snoek made the alternative suggestion that the underlying cause might merely be slight lattice displacements, leading to local lack of balance of electron spins; such lattice distortions would be expected to be in part relieved by prolonged heating at high temperature, leading to the reduction in observed magnetic moment which Néel attributed to transformation of magnetite by oxidation.

There would appear to be a fairly obvious way of combining these two basic theories, although so far no reference to such a compromise has been seen. Suppose that the local dislocations suggested by Snoek were such as to lead to localized thin layers, not of quasi-magnetite, but of quasi-cubic ferric oxide γ-Fe_2O_3. The unstrained oxygen lattice of the latter is almost identical with that of magnetite, but of slightly smaller dimensions ($a \simeq 8{\cdot}3$ A. compared with 8·39 A.). Hence the distance between oxygen nearest neighbours in the (111) cubic plane for γ-ferric oxide is at most 2·94 A., compared with 2·97 A. for magnetite. The amount of distortion required to make this plane coincide with the (0001) rhombohedral plane of α-ferric oxide, in which the oxygen nearest neighbours are 2·90 A. apart, is thus only one half of that needed to bring about the conjunction with magnetite envisaged by Néel.

In this hypothetical picture there are no unwanted ferrous ions, and we have a basic close-packed oxygen lattice, the packing being mainly hexagonal but locally changing towards cubic in thin transition zones, a type of varying structure which is already well known in pure metallic cobalt after suitable treatment (Lipson and Edwards 1942). The saturation magnetization per unit volume of γ-ferric oxide being $\simeq 0{\cdot}8$ times that of magnetite, the conditions for ferromagnetism are much the same as in Néel's theory. Furthermore, the temperature at which γ-ferric oxide transforms to the α form is $\simeq 650°$ c., so that it is less surprising that the ferromagnetic Curie point found for weakly ferromagnetic α-ferric oxide should apparently coincide with the antiferromagnetic transition point 675° c. On heating to 1,100° c. or above, the reduction of lattice strains suggested by Snoek would lead to the partial destruction of the γ-ferric oxide 'islands'; but it is possible that carrying out this

annealing in oxygen impels a tendency to acquire surplus oxygen, with some consequent diffusion of ferric ions to a distribution more nearly of the γ type than of the α, and that this may be the most stable arrangement after cooling, so that the ferromagnetism has not been wholly destroyed, as noted by Chevallier. If this is indeed so, a similar building up of oxygen on a lattice heavily dislocated by grinding may also be a major cause of the marked increase in magnetic properties on heating in oxygen at 1,100° C., also noted by Chevallier for a powder subjected to such treatment.

Magnetic Tapes Division,
Minnesota Mining and Manufacturing Company, Ltd.,
Slough, Bucks.
26th July 1951.

W. P. Osmond.

Chevallier, R., 1951, *J. Phys. Radium*, **12**, 172.
Lipson, H., and Edwards, O., 1942, *Proc. Roy. Soc.* A, **180**, 268.
Néel, L., 1949, *Ann. Phys., Paris*, **4**, 249.
Snoek, J. L., 1950, *Physica*, **16**, 333.

REVIEWS OF BOOKS

An Introduction to Laboratory Technique, by A. J. Ansley. Pp. xv + 288. 2nd Edition. (London : Macmillan, 1950.) 16*s*.

This is a second edition of a book first published in 1938, and written for the guidance of laboratory stewards and for those teachers of physics who lack trained laboratory assistants. The author, an experienced technical laboratory steward at a university college, has added new material to this edition, e.g. the properties of some plastics, the use of the epidiascope and film projectors, etc., in an endeavour to bring the volume up to date. The chapter headings and much of the contents, however, remain the same as in the first edition, and it is a pity that the opportunity was not taken to omit certain parts of the old text to allow the inclusion of more useful information. For instance, the description of the Kelvin method of measuring the resistance of a galvanometer occupies half a page and yet no mention is made of any modern universal measuring instrument.

In many ways the author does not appear to have kept up with the rapid advance in laboratory techniques and apparatus of recent years, e.g. copper-oxide rectifiers are mentioned with no reference to the selenium variety, and one looks in vain for such important items of modern laboratory apparatus as the cathode-ray oscillograph, the power pack, the photocell, gas discharge lamps, the thermocouple, etc. Again, the references to vacuum techniques are rather scanty, and although no detailed information can be expected in a book of this size, modern developments in laboratory techniques such as electrolytic polishing might at least be recorded, with the sources of further information.

Several useful tables are included, although the author appears to have missed again a point raised with regard to the first edition, viz. the absence of units as in Table V, and no indication is given of the temperature scale in quoting linear coefficient of expansion in Table XX. The book is well produced, but would be the better for the omission of certain illustrations which have little instructive value, e.g. Figure 40. R. W. B. S.

Einführung in das Studium der Physik, by W. Finkelnburg. Pp. 128. (Heidelberg : Carl Winter, 1950.) DM 4.50; bound in cloth DM 6.30.

This interesting booklet is meant to be a guide for prospective German physicists. It contains a little of everything : the aims and problems in physics, the history of physical thought, the methods of research, the University syllabus, the main sections in physics and the type of person likely to be an ideal physicist. There is a chapter on the physicist in various professions which is, alas, the weakest chapter of all. It contains contributions by several sub-authors about the physicist as academic and school teacher, industrial researcher,

employee in the electrical and chemical industries and about women physicists. A chapter is included on physical literature listing textbooks, handbooks and periodicals, and giving an introduction into the international decimal classification. Finally there are some notes about the German learned societies and professional bodies.

In Germany physicists are trained at universities and technical academies. During the first two years (=4 semesters) 14 to 18 hours per week are spent on lectures on compulsory subjects and about three hours on optional subjects apart from the time for practical work and seminars. At the end of that period a preliminary diploma examination is taken. During the following two years the number of lectures is reduced and the time for practical and seminar work increased. At the end of this period the diploma examination (or teaching examination) is taken; this requires a miniature thesis but not original research. A further two years spent on original research are necessary to complete a dissertation and after an examination in the form of our *viva*, the degree of Dr.Phil. or Dr.Ing. is awarded

One cannot help feeling that in those chapters in which the author ' advises ' his future colleagues, the dogmatic element becomes sometimes so strongly pronounced that it makes rather amusing reading; for example he says, " anyone who wants to stick to fixed working hours and wants to be left alone in the evenings or spend his spare time on a hobby, should abandon the idea of ever becoming a good physicist ". The author's only support for this opinion is that of a well-known mathematician who once said that " modern physics is actually much too difficult for physicists ".

May I suggest that the author mentions in a future edition the value of personal contact by attending meetings at home and abroad, of a knowledge of foreign languages, and last but not least, the need of a revival of the travelling scholar. A. VON ENGEL.

The Industrial Applications of Gas-filled Triodes (*Thyratrons*), by R. C. WALKER. Pp. ix+325. (London: Chapman and Hall, 1950.) 40*s*.

This book is an introduction to the many applications of gas triodes and similar valves. It commences with a chapter giving a clear and detailed account of the fundamental characteristics of the hot-cathode gas-filled valve without entering the realm of fundamental theoretical physics. The practical aspects such as cathode temperature, gas pressure, ionization and de-ionization times, grid current, etc., are explained so that the reader will appreciate the technical problems when they are discussed in the later portions of the book. Following this first chapter is a brief chapter on the gas tetrode explaining the improved characteristics that have been obtained compared with the triode. Here the author could with advantage have given some details of the type 2D21 valve which has become, in recent years, a very popular valve for small electronic devices. This valve, although illustrated in a manner which does not indicate its small size, is not mentioned in the text.

The third chapter deals with the basic principles of control circuits in which A.C., D.C. and pulses are applied to the grid combined with A.C. and D.C. on the anode, while the next chapter deals with typical examples of simple switching circuits and their applications to a wide range of devices such as oscilloscopes, counting circuits, thermostats, printing machinery, and control mechanisms employing a photocell to provide the controlling potential.

The fifth chapter deals with heavier current devices such as are used for controlling the heating time in electric welding and for the automatic stabilization of the frequency of rotary generators, while the following chapter discusses the application of gas valves to the control of current and voltage in generators and motors. This is followed by an account of commutating devices such as current rectifiers and D.C. to A.C. converters.

The concluding chapter contains details of other types of grid-controlled valves such as the ignitron, the cold-cathode triode and the strobotron. Each chapter has its own references and in addition there are comprehensive references to associated subjects not mentioned in the text.

The book is precisely written and at the same time is easy to read, while the diagrams are clear and well explained. It should prove to be a valuable addition to the bookshelves of all physicists and engineers who are not actively engaged in work on the subject, but who encounter various problems of thyratron control in the course of their researches.

G. E. ASHWELL.

CONTENTS FOR SECTION A

ABSTRACTS FOR SECTION A

Experiments on the Production of Very Low Temperatures by Two-Stage Demagnetization, by J. DARBY, J. HATTON, B. V. ROLLIN, E. F. W. SEYMOUR and H. B. SILSBEE.

ABSTRACT. A two-stage demagnetization apparatus employing a superconducting wire as the thermal switch between the stages is described. Temperatures in the region of 0·003° K. have been obtained using a magnetic field of only 4,200 gauss. The problem of thermal insulation was investigated and the residual heat inflow after demagnetization was reduced to one erg/min. The possibility of employing a superconducting switch in cyclical magnetic cooling systems and in nuclear demagnetization is discussed.

A Note on Fröhlich's Theory of Superconductivity, by KUN HUANG.

ABSTRACT. It is shown that the physical mechanisms underlying the two energy terms E_1 and E_2 in Fröhlich's theory are very different: E_1 is largely the energy change due to a modification of the lattice vibration frequencies caused by the adiabatic deformation of the electrons; E_2 is on the other hand a dynamical term, representing the energy change due to virtual collisions between lattice oscillations and electrons. A proof is given that certain inadmissible consequences of the theory, pointed out recently by Wentzel, derive from the energy term E_1; the superconductive behaviour discussed by Fröhlich arises however entirely from the term E_2. Although both terms follow from the same perturbation treatment, the analysis given makes it seem not unlikely that whatever mechanism actually inhibits E_1 will leave the superconductive behaviour deduced from E_2 not substantially affected.

Scintillations from Organic Crystals: Specific Fluorescence and Relative Response to Different Radiations, by J. B. BIRKS.

ABSTRACT. The scintillation response S of organic crystals depends on the nature and energy E of the incident ionizing particle, of residual range r. The specific fluorescence dS/dr is not in general proportional to the specific energy loss dE/dr. By considering the quenching effect of the molecules damaged by the particle on the ' excitons ' produced by it, it is shown that $dS/dr=(A\ dE/dr)/(1+kB\ dE/dr)$. A and kB are constants, which have been evaluated for anthracene from observations of S and E, and the range–energy data. Curves are computed for the relative response S of anthracene to electrons, protons, deuterons and α-particles of E up to 15 MEV., and these are shown to agree closely with the available experimental results. The method used for evaluating the relative response is applicable to ionizing particles of any nature or energy, and also to the other organic scintillation crystals.

Effect of the Change in Lattice Parameter on the Width of the Forbidden Energy Zone according to Kronig and Penney's One-Dimensional Lattice Model, by E. BILLIG.

ABSTRACT. The effect of changing the lattice parameter in Kronig and Penney's linear lattice model is investigated theoretically. Möglich and Rompe have predicted a decrease in the width of the forbidden energy zone as the lattice parameter is increased. It is shown that this is true only if the width of the potential troughs is increased whilst the thickness of the barriers is maintained constant. However, the opposite effect, i.e. an increase in the width of the forbidden zone, is expected when the potential troughs are kept constant and the width of the barriers is increased instead. In the intermediate case of a uniform expansion of potential hills and troughs, a small net decrease in the width of the forbidden zone is expected.

Influence of a Black Sphere and of a Black Cylinder upon the Neutron Density in an Infinite Non-Capturing Medium, by B. DAVISON.

ABSTRACT. For a black body inserted into a homogeneous scattering medium, the neutron density at large distances from the body is determined using the perturbation method for the case when the scattering in the scattering medium is assumed elastic and isotropic capture is absent and the following four types of the black body are considered: (i) a sphere of radius small compared with the mean free path in the scattering medium; (ii) a sphere of radius large compared with the mean free path; (iii) an infinitely long cylinder of radius small compared with the mean free path; (iv) an infinitely long cylinder of radius large compared with the mean free path. Combining the results for the above limiting cases with the results obtained by other methods the distribution is also estimated for a sphere and an infinitely long cylinder of intermediate radii.

The Excitation Function for the Production of ^{7}Be by the Bombardment of ^{12}C by Protons, by J. M. DICKSON and T. C. RANDLE.

ABSTRACT. The excitation function for the production of ^{7}Be from ^{12}C has been determined by an activation method, using the internal proton beam of the 110-inch Harwell cyclotron. The threshold energy has been found to be 32 MEV. and the cross section at 156 MEV. is $11{\cdot}0 \pm 1{\cdot}3 \times 10^{-27}$ cm^2.

Gamma-Rays from the Deuteron Bombardment of Boron and the Proton Bombardment of Aluminium, by J. G. RUTHERGLEN, E. R. RAE and R. D. SMITH.

ABSTRACT. The gamma-ray spectra from the nuclear reactions $^{10}B+d$, $^{11}B+d$, and $^{27}Al+p$ have been measured with a pair spectrometer. Lines are found from $^{10}B+d$ at $8{\cdot}88 \pm 0{\cdot}06$ MEV., $6{\cdot}7 \pm 0{\cdot}15$ MEV., $6{\cdot}4 \pm 0{\cdot}15$ MEV., and $4{\cdot}38 \pm 0{\cdot}05$ MEV.; from $^{11}B+d$ at $4{\cdot}44 \pm 0{\cdot}05$ MEV.; and from $^{27}Al+p$ at $12{\cdot}12 \pm 0{\cdot}1$ MEV., $10{\cdot}46 \pm 0{\cdot}07$ MEV., and $7{\cdot}62 \pm 0{\cdot}1$ MEV. The correlation of these gamma-rays with the energy levels of the nuclei involved is discussed.

The Density of the Penetrating Particles in Extensive Cosmic-Ray Air-Showers, by C. B. A. MCCUSKER and D. D. MILLAR.

ABSTRACT. The ratio of penetrating particles to electrons in extensive cosmic-ray showers has been investigated experimentally at sea level. For the great majority of showers this ratio, in agreement with previous results, is found to be 2·5%. A small number of showers was detected in which the proportion of penetrating particles was much greater.

The Diamagnetic Anisotropy of Large Aromatic Systems: III—Structures with Hexagonal Symmetry, by R. MCWEENY.

ABSTRACT. The molecular orbital method is employed in calculations of the diamagnetic anisotropies of a series of highly condensed aromatic systems having hexagonal symmetry and containing up to fifty-four carbon atoms. A new method of calculation is introduced in which the π-electron susceptibility of the whole molecule is determined by an integration, no knowledge of the unperturbed energy levels being necessary: the inclusion of overlap between adjacent atomic orbitals is shown generally to have little effect on the calculations.

The results are compared with those calculated using the method of Pauling: this semi-classical method is found to be quite misleading when applied to large molecules or to molecules possessing stray C–C bonds. Qualitative valence bond considerations are advanced in support of these conclusions, and certain general results are tentatively suggested.

Printed by Taylor & Francis, Ltd., Red Lion Court, Fleet Street, London E.C.4.